

DISS. ETH NO. 20369

**Global and European climate response to
transient forcings since 1870,
as simulated in an atmospheric general circulation model**

A dissertation submitted to

ETH ZURICH

for the degree of

Doctor of Sciences

presented by

ADELINE BICHET

Master of Science, VU Amsterdam

Born September 27, 1983

Citizen of France

accepted on the recommendation of

Prof. Dr. C. Schär, examiner

Prof. Dr. Martin Wild, co-examiner

Prof. Dr. Stefan Brönnimann, co-examiner

2012

Acknowledgements

I first would like to thank my supervisor Christoph Schär for accepting me as a PhD student and giving me the opportunity to work in his research group. His broad scientific knowledge and enthusiasm guided and motivated me throughout my thesis, thanks to numerous discussions and a friendly atmosphere. I also would like to thank him for his generosity as a person as well as financial (conferences, workshops and summer schools).

I then would like to thank my co-supervisor Martin Wild for his great guidance and support, always strait to the point and uncomplicated. I also would like to thank him for the fun part of the supervision and his availability.

My thanks also go to Stefan Brönimann, for accepting to review this thesis and act as a co-examiner for the defence, as well as for his input on Chapter 4.

In addition, this thesis would have not been possible without the helpful and friendly staff of our research group. I therefore would like to thank Doris Folini for her precious help regarding the IT side of this thesis, but also for her guidance throughout my thesis, as well as her friendship, availability and honesty. My thanks also go to Rahel Buri for her great help and kindness, as well as to Daniel Lüthi and Urs Beyerle for the IT support.

Finally, I would like thank all my friends at the IAC for all the fun and the great ambiance, in particular my office mates Peter Brockhaus, Marc Chiacchio, Luka Egloff, Arturo Sanchez-Lorenzo and Nikolina Ban, and our group members Bellprat Omar, Bosshard Thomas, Maria Hakuba, Hanieh Hassanzadeh, Michael Keller, Sven Kotlarski, Wolfgang Langhans, Anna Possner, Jan Rajczak, Jürg Schmidli, and Elias Zubler.

My deepest thanks however go to my family, in particular my parents, brother and boyfriend, for their unconditional support, encouragements and patience throughout these years.

Finally, this thesis was carried out at the Institute for Atmospheric and Climate Science at ETH Zurich, and was partly supported by the NCCR Climate, funded by the Swiss National Science Foundation. The simulations were done on the CRAY at the Swiss National Supercomputing Centre (CSCS) in Manno, Switzerland, and the code of the model was provided by MPI Hamburg with further developments realised at ETH Zurich and the Centre for Climate System Modelling C2SM, in particular by Ulrike Lohmann, Sylvaine Ferrachat, and Grazia Frontosa.

Abstract

Predicting and adapting to climate change is one of the major challenges for the twenty-first century. To better understand the future changes in precipitation associated with climate change on the global and regional scale, this thesis investigates, for the past 140 years, the time-varying impact of the major climate forcings on precipitation. To do so, the global climate is simulated between 1870 and 2005 in a transient mode with the atmospheric general circulation model “ECHAM5-HAM”. The model is forced with observationally based time-varying sea surface temperatures (SSTs) and the major climate forcings, which include total solar irradiance, volcanic optical depth, aerosol emissions (natural and anthropogenic), and greenhouse gas concentrations. Sensitivity experiments, holding one or more of these forcings constant throughout the experiments are then used to identify and quantify their time-varying impacts on the hydrological cycle. In a first step, the thesis aims to identify the main climate forcings driving the decadal variability of global land temperature and precipitation between 1870 and 2005. It then investigates the causes driving the wind stilling observed over land after 1970 in many sites over the globe, due to its potential impact on the hydrological cycle and on industries such as wind powered energy. Finally, the high precipitation anomalies observed in central Europe in the late nineteenth century are also investigated, for their potential contribution to the accumulation of destructive floods recorded at the time in central Europe.

On the global scale, it is shown that when forced with observed SSTs and the major climate forcings mentioned above, ECHAM5-HAM satisfactorily reproduces the decadal variability of global land temperature and precipitation observed since 1870 and 1900, respectively. After 1950 however, the strong response of convective precipitation to increasing anthropogenic aerosol emissions leads to a centennial precipitation trend that is negative in the model (~ -10 mm/year) but positive in the observations ($\sim +10$ mm/year). In addition, the sensitivity results show that whereas transient SSTs (as opposed to climatological ones) drive the decadal variability of global land temperature and precipitation since 1870, the variations in greenhouse gas concentration and anthropogenic aerosol emissions (atmospheric response) drive their long-term trends: After about 1950, the increasing concentration of greenhouse gases increases the global land temperature and precipitation by up to 0.25 °C and 10 mm/year, respectively, whereas after 1930, the increasing emission of anthropogenic aerosols decreases them by up to 0.4 °C and 30 mm/year, respectively (especially in China and the Amazonian region). It is also suggested that between about 1950 and 1970, the impact of anthropogenic aerosols on the hydrological cycle may have been larger than the impact of greenhouse gases, thereby “masking” the precipitation increase expected from the increase in greenhouse gas concentration during this time period (atmospheric-only responses).

Regarding the wind stilling, it is shown that only up to 20% of the decline observed over land in many sites over the globe after 1970 is reproduced by the model. Additional sensitivity experiments performed in this thesis show that in order to reproduce the full extent of the observed wind stilling, the vegetation roughness length (climatological in our model, but believed to have increased in the past decades due to the observed increase in vegetation) is required to increase by a factor of 1.2 to 4.9, depending on the region. However, whereas such an increase in roughness length may not necessarily be realistic everywhere, up to 20% of the observed wind stilling must be explained by the forcings included in the model: In particular, it is found that after 1950, the increase in anthropogenic aerosol emissions decreases the surface land wind speed globally, with larger impacts in summer as well as in Asia and India (up to -0.3 m/s in summer in India). Note that the short-term impacts of increasing greenhouse gas concentrations are found to be relatively small.

In central Europe, it is found that the model satisfactorily reproduces the high summer precipitation anomalies observed in the late nineteenth century. According to the sensitivity experiments, the transient SSTs (as opposed to climatological mean) located in the “El Nino region” between 1875 and 1890 drive these high anomalies, and affect them mostly via their impacts on the atmospheric circulation. In the model, the associated pressure patterns include weaker westerlies, a PNA-like pattern over North America, and reduced pressure over Europe. Note nevertheless that no deterministic link between the ENSO index and the European precipitation was found during this time period. Finally, it is shown that when SSTs are transient in the model, the increase in anthropogenic aerosol emissions further enhances these precipitation anomalies by about 50%.

To conclude, this thesis demonstrates the ability of ECHAM5-HAM to reproduce the global and to some extent the European land precipitation, when forced with time-varying observed SSTs and major climate forcings. On the global scale, the thesis particularly emphasizes the “slow down” of the hydrological cycle triggered by the increase in anthropogenic aerosol emissions after about 1950, whereas on the regional scale, it points out the potential capacity of the Pacific Ocean to trigger heavy precipitation in central Europe.

Résumé

Prédire et s'adapter aux futures changements climatiques font parti des challenges majeures du vingt-et-unième siècle. Pour mieux comprendre les future changements de précipitation liés aux changements climatiques à l'échelle globale et régionale, cette thèse étudie l'impact des principaux forçages climatiques sur la précipitation pendant les 140 dernières années. Pour se faire, le climat global est simulé en mode transitoire avec le modèle atmosphérique de circulation général "ECHAM5-HAM", pour la période 1870-2005. Le modèle est forcé avec les données observationnelles de température de surface des océans (SSTs), ainsi que les majeures forçage climatiques qui incluent l'irradiance solaire totale, l'épaisseur optique provenant des explosions volcaniques, les émissions d'aérosols (naturelles et anthropiques) et les concentrations de gazes à effet de serre. Des études de sensibilité sont ensuite réalisées, qui consistent à garder un ou plusieurs forçage(s) constant pendant la simulation de manière à en identifier les effets sur le climat. Cette thèse est divisée en trois parties: La première partie étudie les variations décennales des températures et précipitations globales pour la période 1870-2005. La deuxième partie étudie les différentes causes qui peuvent être à l'origine de la diminution de la vitesse des vent de surface terrestre observée à l'échelle globale après 1970, et la troisième partie étudie les différentes causes qui peuvent être à l'origine des importantes précipitations observées en Europe centrale à la fin du dix-neuvième siècle.

A l'échelle globale, ECHAM5-HAM reproduit de manière satisfaisante la variabilité décennale des température et précipitations globales observées dans la période 1870-2005. La tendance centennale des précipitations est néanmoins négative dans le modèle (~ -10 mm/an) et positive dans les observations ($\sim +10$ mm/an), due à un effet trop prononcé des aérosols anthropiques sur la précipitation convective après 1950. Les études de sensibilité montrent que depuis 1870, la variation des SSTs détermine les variations décennales de températures et précipitations terrestres globales, alors que la concentration des gazes à effet de serre et les émissions d'aérosols anthropiques en déterminent la tendance à long-terme (réponse atmosphérique uniquement): Dans le modèle, l'augmentation des gazes à effet de serre augmente la température et la précipitation terrestre globale de 0.25 °C et 10 mm/an respectivement, après 1930 (particulièrement en Chine et en Amazonie), alors que l'augmentation des aérosols anthropiques les diminue de 0.4 °C et 30 mm/an respectivement, après 1950. Il est également suggéré qu'entre 1950 et 1970, l'impact des aérosols anthropiques sur le cycle hydrologique est plus important que l'impact des gazes a effet de serres, ce qui aurait "masqué" l'augmentation des précipitations attendue suite à l'augmentation des gazes à effet de serre pendant cette période (réponse atmosphérique uniquement).

En ce qui concerne la diminution de la vitesse des vents de surface après 1970, cette thèse montre que le modèle ne reproduit que jusqu'à 20% des valeurs observées à l'échelle globale, et que dans le modèle, cette diminution est principalement due à l'augmentation des émissions d'aérosols anthropiques (jusqu'à -0.3 m/s en été en Inde). La partie de la diminution du vent qui n'est pas reproduite par le modèle pourrait entre autre être due à l'augmentation de la végétation qui est observée dans l'Hémisphère Nord depuis 1970 mais qui n'est pas prise en compte dans les simulations transitoires réalisées dans le cadre de cette thèse, où cette variable est constante dans le temps. Des études de sensibilité supplémentaire (à l'équilibre) ont donc été réalisées, qui montrent que de manière à reproduire la totalité de la diminution observée, la longueur de rugosité de végétation devrait augmenter d'un facteur allant de 1.2 à 4.9 selon les régions, ce qui n'est pas nécessairement réaliste partout.

En Europe centrale, il est montré que le modèle reproduit de manière satisfaisante les anomalies positives de précipitation estivales observées à la fin du dix-neuvième siècle. D'après les études de sensibilité, ces anomalies sont dues aux variations de SSTs (par rapport aux SST climatologiques) localisées dans la région du El Niño entre 1875 et 1890, qui affectent la circulation atmosphérique globale: Les anomalies de pression associées incluent entre autre de faibles vents dominants d'ouest, un pattern qui ressemble à la PNA en Amérique du Nord, et des basses pressions en Europe. Aucun lien déterministe entre l'index ENSO et les précipitations Européennes n'ont cependant été trouvé pendant cette période. Finalement, les résultats montrent également que quand les SSTs sont transitoires dans le modèle, l'augmentation des aérosols anthropiques augmentent ces anomalies de précipitation d'environ 50%.

Pour conclure, cette thèse démontre la capacité de ECHAM5-HAM à reproduire la précipitation terrestre globale et jusqu'à un certain point Européenne quand le modèle est forcé avec les SST transitoires observées et les majeurs forçages climatiques. Cette thèse montre particulièrement le "ralentissement" du cycle hydrologique à l'échelle globale provoqué par l'augmentation des émissions d'aérosols anthropiques après 1950, ainsi que la capacité potentielle de l'Océan Pacifique à augmenter les précipitations en Europe.

Contents

1. Introduction	1
1.1 Motivation.....	1
1.2 The global energy and water cycles.....	2
1.3 Methodology.....	4
1.4 Climate forcings and their expected impact on the water cycle	5
1.4.1 Natural climate forcings.....	5
1.4.2 Anthropogenic climate forcings.....	6
1.5 Objectives and overview of the thesis.....	10
2. Global precipitation response to changing forcings since 1870	11
2.1 Introduction.....	14
2.2 Methodology.....	14
2.2.1 Model set up and experimental design.....	14
2.2.2 Evolution of the main climate forcings since 1870.....	16
2.2.3 Observational data for temperature and precipitation.....	18
2.3 Results.....	19
2.3.1 Global scale assessment of the model.....	19
2.3.2 Global scale sensitivity of the model to external forcings.....	25
2.4 Discussion.....	28
2.4.1 Origin of water in the global land precipitation.....	28
2.4.2 Role of SSTs.....	30
2.4.3 Role of aerosols and greenhouse gases.....	30
2.5 Conclusions.....	32
3. Causes for decadal variations of wind speed over land: Sensitivity studies with a global climate model	33
3.1 Introduction.....	36
3.2 Methods.....	37
3.3 Sensitivity.....	38
3.3.1 Roughness length.....	38
3.3.2 SSTs, aerosol emissions, and greenhouse gas concentrations.....	41
3.4 Discussion.....	43

3.5 Conclusions.....	44
Supplementary Material.....	45
4. Sensitivity of European precipitation in the late 19th century	47
4.1 Motivation.....	50
4.2 Methods.....	51
4.2.1 Model set up and experimental design.....	51
4.2.2 Observational data.....	53
4.3 Results.....	53
4.3.1 Observed and simulated European precipitation in the late 19 th century....	53
4.3.2 Sensitivity of simulated precipitation to forcings.....	57
4.4 Discussion.....	61
4.5 Conclusions.....	64
5. Conclusions	65
6. Outlook	67
References	69
Curriculum Vitae	81

Chapter 1

Introduction

1.1 Motivation

Predicting and adapting to climate change is one of the major challenges for the twenty-first century. In addition to temperature, future changes in precipitation (amount, intensity, frequency and type) are also particularly relevant: Since the 1970s, droughts have increased in Africa, southern Asia, south-western United States, and the Mediterranean regions (Dai et al., 2004, Trenberth et al., 2007), as a result of precipitation decrease over land. In the mean time, large floods (Milly et al., 2002) and heavy rains (e.g. Easterling et al., 2000, Peterson et al., 2002) have increased in Europe, northern Asia, and America (North and South). Aside from the environmental and societal impacts of such changes, economical sectors can also be affected, such as agriculture, water management, urban planning and tourism. Finally they may also affect the entire climate system, with particularly important implications for the occurrence of heatwaves and temperature extremes (e.g. Schär et al. 2004, Fischer et al. 2007, Fischer and Schär 2010).

Despite these potential important consequences, future changes in precipitation are still subject to large uncertainties (e.g. Douville et al., 2006). This is partly due to the local aspect of precipitation variations (as opposed to temperature for instance), but also because it is part of a more complex system, the hydrological cycle, which involves numerous interactions and feedbacks within its different components (e.g. Trenberth et al., 2006). According to the Fourth Scientific Assessment Report (AR4) of the Intergovernmental Panel on Climate Change (IPCC, 2007), global precipitation is expected to increase in the future, proportionally to the global warming induced by the increase in greenhouse gases (about 1.4 to 2.3 % °C⁻¹ depending on the future climate scenario). Such an increase is however not entirely reproduced by climate models (e.g. Douville et al., 2006), and fails to explain the decadal variations observed in the past century.

In order to better understand the future changes in global precipitation, the different factors influencing the hydrological cycle on the decadal time scale should therefore be identified, and their impacts quantified. Primarily driven by solar heating, the hydrological cycle strongly depends on the Earth's radiative budget, and hence, on climate forcings defined in the IPCC AR1 (1992) as “a perturbation of an initial climate state that leads to a radiative imbalance in the atmosphere and that initiates a climate response”. On the interannual to decadal time scale, natural climate forcings include variations in the total solar irradiance (TSI) and large volcanic eruptions, whereas anthropogenic climate forcings include the release of pollutants into the atmosphere (particles and gases) and the changes in land use. Note that variations in SSTs can also be considered to some

extent as a climate forcing (although they are also affected by the radiative forcings), since they perturb the climate system via changes in the radiative budget (e.g. Liepert 2010).

To understand how the future variations in climate forcings will affect the hydrological cycle on the interannual to decadal scale, it is crucial to understand how they have affected it in the past and why. Most previously studies have focused on the past 40 years only using the ERA-40 reanalysis, and/or quantify the impacts of individual climate forcings as a change between two different equilibrium states. However, in order to fully capture the sensitivity of the hydrological cycle to changing climate forcings, it is important to study a period that covers at least the past 140 years, as it marks the changeover from a climate dominated by natural forcings to one dominated by anthropogenic forcings, and to evaluate the time-varying impact of these climate forcings through time, as individuals, but also as combined. Therefore, this thesis investigates, for the period 1870-2005, the transient response of the hydrological cycle (global and regional scales) to observationally-based, time-varying climate forcings, which include the total solar irradiance (TSI), explosive volcanoes, sea surface temperatures (SSTs), and anthropogenic greenhouse gases and aerosols.

In the following, Section 1.2 illustrates how precipitation is linked to the hydrological cycle and the radiative balance, and Section 1.3 explains the methodology used in the thesis. Section 1.4 briefly describes the climate forcings relevant for the hydrological cycle during the time period 1870-2005, along with their expected impact on precipitation, their evolutions since 1870, and the corresponding datasets used in this thesis. Finally, Section 1.5 outlines the objectives and gives an overview of the thesis.

1.2 The global energy and water cycles

To understand the variations in precipitation, it is important to understand where the water comes from (evaporation from land and sea surface) and why it falls out (condensation and precipitation). Globally, precipitation can be approximated by surface evaporation, since the variability of the atmospheric moisture storage (10^{13} m³/year) is negligible compared to the variability of the fluxes (10^{14} m³/year) (Baumgartner and Reichel, 1975). Therefore, any change in the globally averaged surface evaporation implies an equivalent change in precipitation, and hence, in the intensity of the hydrological cycle. Evaporation requires energy, which is obtained from the surface radiation balance that can be expressed as follows:

$$R_s = SW_n + LW_n = SH + LH (+G) \quad ,$$

where R_s corresponds to the net surface radiation, SW_n to the net short-wave radiation, LW_n to the net long-wave radiation, SH to the sensible heat, LH to the latent heat (evapotranspiration), and G to the ground heat flux (negligible in the annual and longer-term means). Therefore, the surface energy balance depends on the variations in the short- and long-wave radiation, which are part of the radiative balance, described in Figure 1.1.

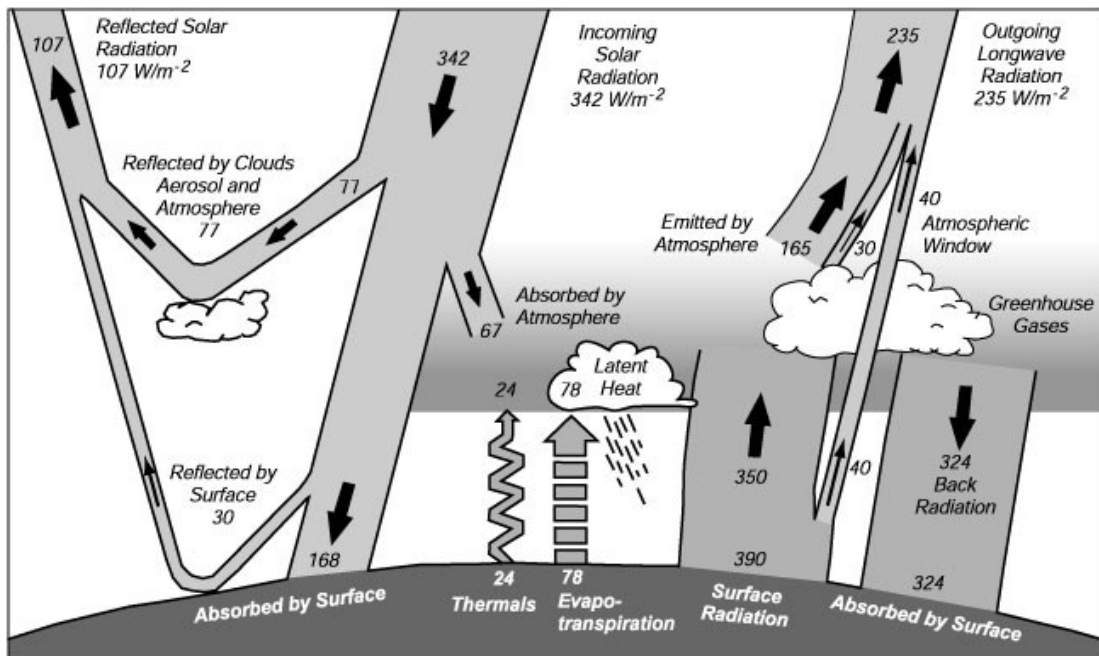


Figure 1.1: The global annual mean Earth's energy budget in W/m^2 (Trenberth et al., 2009)

The radiative balance is primarily driven by the incoming solar radiation at the top of the atmosphere (about $342 W/m^2$). About 30% of this incoming shortwave radiation is reflected back into space by clouds, aerosols and the Earth's surface. The remaining energy is partly absorbed by the atmosphere, but most of it is absorbed by the Earth's surface ($SW_n = 168 W/m^2$). The Earth's surface then re-emits most of this energy as long-wave (thermal) radiation, which is then absorbed by the atmosphere (mostly by greenhouse gases), and re-emitted upward and downward. This radiative balance therefore implies an imbalance between the positive net radiation at the surface ($R_s = 102 W/m^2$) and the negative net radiation in the atmosphere ($= -102 W/m^2$), which is compensated for by the emission of sensible ($SH = 24 W/m^2$) and latent ($LH = 78 W/m^2$) heat fluxes, from the surface to the atmosphere. Since the latent heat flux (energy equivalent of evaporation) dominates the sensible heat flux, the surplus of energy at the surface is thus mainly consumed by evaporation and its subsequent release in the atmosphere. This implies that any change in the radiative balance triggers a change in the hydrological cycle (Wild and Liepert, 2010).

However, evaporation does not depend solely on its energy equivalent (latent heat), but also on the thermodynamical properties of the air and on the soil moisture availability. According to the Penman equation, the potential surface evaporation (E_{pot}) depends primarily on an energy balance term (E_{bal}) and on an air capacity term (E_{air}).

$$E_{pot} = E_{bal} + E_{air} \quad ,$$

with, $E_{bal} = R_s$, and $E_{air} = \rho \cdot C_w \cdot u_a \cdot (q_a^{sat} - q_a)$,

where ρ corresponds to the air density, C_w to the heat capacity and $(q_a^{sat} - q_a)$ to the vapour pressure deficit of the air.

Once in the atmosphere, the condensation of water vapour and the formation of precipitation are determined by dynamical processes and the accompanying lifting (e.g. Mason, 1962). The relevant weather systems include the storm tracks and their associated low-pressure and frontal systems in the middle and high latitudes, as well as the Hadley circulation and the associated convective precipitation systems in the low latitudes. The involved microphysical processes also depend on the presence of cloud condensation nuclei (e.g. aerosols). The ability of the troposphere to radiate away the latent heat released by precipitation is a decisive factor for global mean precipitation, as it strongly affects the intensity of the Hadley circulation (e.g. Trenberth et al, 2009, Held and Soden 2000, Figure 1.1).

1.3 Methodology

In order to understand the variations in the hydrological cycle between 1870 and 2005, one can analyse the observational datasets available, as two datasets cover the global land precipitation since 1900, one at 0.5 degree resolution for the time period 1901-2002 (Mitchell and Jones, 2005), and one at 5 degree resolution for the time period 1900-2009. Datasets including temperature (e.g. Brohan et al., 2006) and surface radiation (e.g. Gilgen et al., 1998) at different time and spatial scales are also available, and can be used to complete the analysis. More details about observational datasets and their uncertainties can be found throughout the thesis.

Reanalysis are also very useful, as they allow a more “in depth” analysis of the climate system than observational dataset. The ECMWF ERA-40 reanalysis are traditionally used, as they cover the globe at 2.5 degree resolution for the time period 1957-2002. In the future however, the recently released NCEP-NCAR 20CR reanalysis (Compo et al., 2011) could also be used, as it covers the globe at 2 degree resolution for the period 1871-2010. More details about the NCEP-NCAR 20CR reanalysis can be found in Chapter 4.

Finally, climate models are also powerful tools, as they provide a numerical representation of the climate system: Atmospheric general circulation models (GCMs) incorporate the basic physical laws and equations that govern the circulation of the Earth’s atmosphere, and interactively calculate prognostic (e.g. vorticity, divergence, temperature and surface pressure) and diagnostic variables for each time step. They are forced with boundary conditions at the Earth’s surface, usually taken from observational datasets, and provide a three-dimensional representation of the Earth’s surface and atmosphere, represented by individual grid boxes. Whereas equilibrium experiments are usually used to assess the overall changes between a perturbed steady state and the initial unperturbed state (e.g. Liepert et al., 2004, Feichter et al., 2004, Koch et al., 2009), transient experiments allow the analysis of time-varying changes (e.g. Roeckner et al., 1998, Boer et al., 2000, Meehl et al., 2004). Furthermore, whereas most modelling studies use a simple treatment of aerosol (bulk modelling based on aerosol mass), the non-linearity of the global aerosol system (Stier et al., 2006b), along with the complexity of its impact on the hydrological cycle (e.g. Ramanathan et al., 2001, Lohmann and Feichter, 2005) justify the use of a more complex treatment of aerosols.

In this thesis, the version of the GCM “ECHAM5” (Roeckner et al., 2003) is coupled to the fully interactive aerosol module “HAM” (Stier et al., 2005 and Lohmann et al., 2007). The double-moment cloud microphysical scheme (Lohmann et al. 2007) of “ECHAM5” includes prognostic equations for the mass mixing ratios of the cloud liquid water and ice (Lohmann and Roeckner, 1996) and for the number concentrations of cloud droplets and ice crystals (Lohmann et al., 1999; Lohmann, 2002; Lohmann and Diehl, 2006). The development of this double-moment cloud microphysical scheme led to major advances in the climate community and allows the coupling with the size-resolved aerosol scheme of the module “HAM”, which predicts the evolution of seven micro-physically interacting, internally and externally mixed lognormal aerosol modes. The major aerosol categories include sulphate, black carbon, particulate organic matter, sea salt and mineral dust (Stier et al., 2005). For the purpose of this thesis, 149 transient experiments are performed with “ECHAM5-HAM” at resolution T42: 45 experiments are clustered in 5 ensembles and cover the time period 1870-2005, whereas 104 experiments are clustered in 8 ensembles and cover the time period 1870-1900. The different ensembles correspond to sensitivity experiments.

1.4 Climate forcings and their expected impact on the water cycle

This section describes the impact on precipitation of the main climate forcings discussed in this thesis, as well as their time evolution since 1870, and the datasets used to force ECHAM5-HAM in this thesis (a more detailed description of the datasets can be found in Chapter 3).

1.4.1 Natural climate forcings

Total solar irradiance (TSI). As the primary driving force of the radiative balance, TSI has a direct impact on evaporation and precipitation (see Section 1.2 and Figure 1.1). Since 1870, the main changes in TSI include the 11-year solar cycle and an increase of about 4 W/m^2 during the time period 1900-1950 ($\sim 0.7 \text{ W/m}^2$ in the absorption on the Earth’s sphere). According to previous studies however, the 11-year solar cycle has no significant impact on the hydrological cycle (e.g. Labitzke and Matthes, 2003), and the recent changes in TSI are too weak to explain the climate changes after 1970 (e.g. Solanki and Krivova, 2003; Foukal et al., 2006). For the purpose of this thesis, ECHAM5-HAM is forced with the time-varying monthly means TSI reconstruction from Solanki and Krivova (2003).

Volcanoes. Large volcanoes can affect the hydrological cycle via their injection of sulphur gases into the stratosphere, which convert into sulphate aerosols with a residence time of about 1 year (Robock, 2000). Such a residence time allows the particles to spread globally and affect the climate on a global scale. In the stratosphere, volcanic aerosols scatter some solar radiation back into space, thereby cooling the Earth’s surface, and absorb solar and terrestrial radiation, thereby warming the aerosol layer. Both effects perturb the radiative balance and hence, precipitation. Finally, note that volcanoes can also affect the hydrological cycle via their impact on the atmospheric circulation (e.g. Robock, 2000; Fischer et al., 2007).

Large volcanic eruptions were frequent between 1870 to 1920 and between 1960 to 2005, but rare between the two periods (e.g. Sato et al., 1993). Since 1870, the major volcanoes include

Krakatau (1883), Santa Maria (1902), Agung (1963), El Chichon (1982), and Mount Pinatubo (1991) (Sato et al., 1993). However, because satellite derived precipitation data are not available on the global scale prior to 1979, only the impact of Mount Pinatubo have been investigated in details (e.g. Trenberth and Dai, 2004). According to Trenberth and Dai (2004), the year following the Pinatubo eruption was dry and led to widespread droughts in many places. For the purpose of this thesis, ECHAM5-HAM is forced with the annual stratospheric optical depth resulting from explosive volcanoes, reconstructed by Sato et al. (1993).

Seas-surface temperatures (SSTs). In the real world, SSTs are part of the coupled atmospheric / oceanic system. However, in uncoupled atmospheric GCMs, SSTs are prescribed as a boundary condition, and hence, cause a perturbation of the climate system (instead of varying interactively), acting in that sense as a climate forcing. Variations in SSTs are important for precipitation because they are a major source for evaporation, but also because they strongly affect the atmospheric circulation (e.g. Gu et al., 2007) and the radiative budget via their impacts on the thermodynamical properties of the air (Hoerling et al., 2008; Compo and Sardeshmukh, 2009; Findell et al., 2009).

Globally, SSTs have increase by about 0.4 °C from 1870 to 2005, with stable values observed in the 1870-1900 and 1940-1970 time periods (Rayner et al., 2003). In the past century however, the best known examples of SSTs impact on the hydrological cycle include the variations of the El Nino Southern Oscillation (ENSO): These interannual variations in the eastern tropical Pacific SSTs perturb the tropical atmospheric circulation, and trigger changes in the global (Gu et al., 2007; Trenberth and Dai, 2007) and regional precipitation (e.g. Trenberth and Caron, 2000). Whereas the most affected regions are located in the tropics (e.g. Diaz and Markgraf, 2000), European precipitation can also be affected, but in a non-deterministic way (e.g. Brönnimann et al., 2007). In particular, variations in the ENSO profoundly affect the distribution and timing of floods and droughts in the tropics and over much of the mid-latitudes of the Pacific-rim countries (Diaz and Markgraf, 2000), as illustrated by the 1988 drought and 1993 floods in North America (Trenberth and Guillemot, 1996). Finally, SSTs in other regions may also be influence precipitation on longer time scales, as it was shown for instance that the recent drying in Sahel was linked to changes in tropical SST patterns located in the Pacific, Indian and Atlantic Ocean (Giannini et al., 2003, Hoerling et al., 2006). In this thesis, ECHAM5-HAM is forced with monthly mean observed SSTs and sea-ice concentrations taken from Rayner et al. (2003).

1.4.2 Anthropogenic climate forcings

Greenhouse gases. In the troposphere, greenhouse gases absorb upward long-wave radiation and re-emit most of it back to the surface. This increases the downward long-wave radiation, and hence, the amount of energy absorbed at the surface (e.g. Mitchell, 1989). In turn, this increases the outgoing long-wave radiation along with the sensible and latent heat fluxes (Figure 1.1), and hence, the surface temperature and evaporation.

Since 1870, the main anthropogenic greenhouse gases include carbon dioxide and methane, mostly emitted from fossil fuels burning. On a country level, the emissions are dominated by China (17% of the total emissions in 2005), the United States (16% of total emission in 2005) and Europe

(11% of total emissions) (IPCC, 2007). Globally, the total concentration of greenhouse gases in the atmosphere has increased from about 280 to 380 ppm in the past century (e.g. IPCC, 2007), and is expected to increase by a further 25 to 90% from 2000 to 2030 (Rogner et al., 2007). Greenhouse gases have an atmospheric residence time ranging from a decade (e.g. methane) to tens of thousands years (e.g. sulphur hexafluoride), which allows them to spread globally and affect the climate on the global scale. Note that greenhouse gases are also emitted from natural sources (e.g. decomposition), but their quantities are relatively small compared to anthropogenic emissions.

Numerous studies attribute the global warming observed in the past century to the recent increase in anthropogenic greenhouse gas concentrations (e.g. Hansen et al., 1981). This global warming is expected to intensify the hydrological cycle due to the resulting increase in evaporation (e.g. Yu and Weller, 2007), but also because this is expected to increase the air moisture holding capacity (e.g. Held and Soden 2000, Huntington et al 2006), as given by the Clausius-Clapeyron equation for the saturation vapour pressure:

$$\frac{d \ln(es)}{dt} = \frac{L}{RT^2} = \alpha(T)$$

where es corresponds to the saturation of vapour pressure, L to the latent heat of vaporization, R to the gas constant for air, and T to the temperature. At tropospheric temperatures, the saturation vapour pressure increases by about $7\% \text{ K}^{-1}$ ($\alpha \sim 0.07 \text{ K}^{-1}$).

However, whereas the global land precipitation observed in the past two decades seems to follow the Clausius-Clapeyron rate (Wentz et al., 2007), this is not necessarily the case in other time periods (e.g. Gu et al., 2007, Adler et al., 2008 and Huffman et al., 2009). In addition, whereas the Clausius-Clapeyron relation may apply to the precipitation trend of the past century (global land precipitation increase by about 10 mm/yr since 1900), it fails to explain the large decadal variability (up to 50 mm/year) observed in the global land precipitation since 1900.

In this thesis, ECHAM5-HAM is forced with time-varying annual mean, greenhouse gas concentrations taken from observations until 2000 and from the IPCC A1B scenario for 2001-2005. It includes the concentrations of carbon dioxide, methane, nitrous oxide, ozone and chlorofluorocarbons.

Tropospheric aerosols. In the troposphere, anthropogenic aerosols scatter and absorb short-wave radiation, which reduces the amount of solar radiation absorbed at the surface (Angström 1962, McCormic and Ludwig, 1967, Haywood and Boucher, 2000). Less energy absorbed at the surface reduces the amount of outgoing long-wave radiation, sensible and latent heat fluxes (Figure 1.1), and hence, reduces the surface temperature and evaporation. These reflective and absorbing effects of aerosols are referred to as direct radiative effects. In addition to these direct effects, aerosols also act as cloud and ice condensation nuclei (e.g. Haywood and Boucher, 2000; Lohmann and Feichter, 2005). Increasing the aerosol emissions therefore also increases the cloud droplet number concentration, and in turn, enhances the reflection of solar radiation back into space, which further reduces the amount of energy absorbed at the surface (first indirect radiative forcing)

(Twomey, 1977). If the condensed moisture inside the cloud is not affected by the aerosols increase, this is expected to decrease the droplet radius, and hence, precipitation (e.g. Twomey, 1959, Haywood and Boucher, 2000, Givati and Rosenfeld, 2004). This is also expected to increase the cloud life time, and further reflect the solar radiation back into space (second indirect radiative effect) (e.g. Albrecht, 1989). Finally, the heating of the aerosol layers due to absorption can also dissolve the clouds (semi-direct radiative effect) (e.g. Ackerman et al., 2000). Overall, the reduction of solar energy absorbed at the surface, together with the precipitation suppression induced from increasing aerosols are expected to slow down the hydrological cycle (e.g. Ramanathan et al., 2001). Additional feedbacks inferred from increasing aerosol emissions include the potential reduction of the temperature gradient between the surface (cooling) and the atmosphere (warming), which is expected to increase the atmospheric stability (e.g. Ramanathan et al., 2005), with potential consequences for convective precipitation and wind speed.

Since 1870, the main anthropogenic aerosols include sulphur dioxide (SO₂), black carbon and organic carbon, mostly emitted by fossil fuel burning and wildfire, and in majority by China, the eastern United States, and Europe (Dentener et al., 2006, Roeckner et al., 2006, Stier et al., 2006 and Nozawa et al., 2006). Globally, the total emissions of SO₂, black carbon and organic carbon have increased between 1860 and 2000 from about 20 to 90 Tg(S)/year, 2 to 15 Tg/year and 30 to 130 Tg/year, respectively (Stier et al., 2006). Based on the A1B scenario from the IPCC AR4 (2007), global emissions of SO₂ are expected to reach 120 Tg(S)/year in 2020 and decrease to 45 Tg(S)/year in 2100, whereas global emissions of black and organic carbon are expected to reach 30 and 190 Tg/year in 2070 and decrease only slightly until 2100. The residence-time of aerosols in the atmosphere depends on the species, but vary from about 4-5 days for sulphate and mineral dust aerosols (e.g. Feichter et al., 1996, Stier et al., 2005), to 5-7 days for black and organic carbon (e.g. Lohmann et al., 1999, Stier et al., 2005). This short residence-time limits their geographical spread, and thus, aerosols accumulate close to their emission sources and affect the climate mostly on regional scale. Note that natural sources of aerosol emissions such as sea salt and dust also affect the climate system, but their emissions are relatively stable through time (Stier et al., 2005 and 2006a).

To assess the impact of aerosols on the hydrological cycle in the past century, one can look at the variations in surface solar radiation absorbed at the surface. According to observations, the solar radiation absorbed over land has decreased by up to 7 W/m² between about 1950 and 1980 (e.g. Liepert, 2002; Stanhill and Cohen, 2001, Wild 2009) in numerous sites around the globe, before partly recovering (Liepert et al., 2002, Wild et al., 2005). These two periods are referred to as the global dimming and brightening, and have been attributed, at least partly, to the temporal variations in global aerosol emissions (Wild 2009, Streets et al., 2009). According to Wild and Liepert (2010), observations may even show an early-brightening phase prior to 1950. These decadal variations in absorbed solar radiation surprisingly resemble the decadal variations in observed global land precipitation (Wild and Liepert, 2010), and suggest a strong link between the two variables.

In this thesis, ECHAM5-HAM is forced by the emissions of SO₂, black carbon, and particulate organic matter taken from the Japanese National Institute for Environmental Sciences (NIES) (Roeckner et al., 2006; Stier et al., 2006a; Nozawa et al., 2008). They include geographically resolved time varying annual mean emissions from wildfires (considered nowadays as human induced), agricultural burning and domestic fuel-wood consumption, as well as time varying annual mean emissions from fossil fuel consumption.

Combined effects of increasing aerosols and greenhouse gases since 1870. Because the increase in greenhouse gas concentration and aerosol emissions affects precipitation in opposite ways, it is crucial to understand how they affect precipitation when combined. According to their respective radiative forcing, previous studies (Allen and Ingram 2002, Feichter et al., 2004, Andrews et al., 2009, Liepert and Previdi, 2009 and 2010, Wild and Liepert, 2010) find that aerosols may have more impact on the hydrological cycle than greenhouse gases: Whereas the former affects evaporation directly via its instant impact on the incoming solar radiation, the latter affects precipitation in an more “indirect way”, by primarily changing the temperature. According to previous studies (e.g. Ohmura 2009, Wild and Liepert, 2010), this is observed in the net surface radiation datasets, which suggest that between 1960 and 1990, the net surface radiation was more affected by the increase of aerosols than the one of greenhouse gases. Therefore, even though the increase in greenhouse gas concentrations is expected to intensify the hydrological cycle on the long-term, short-term variations seem to be more sensitive to changes in aerosol emissions. Based on equilibrium climate simulations including greenhouse gas forcing and a complex treatment of aerosols, Liepert et al. (2004) even suggest that the hydrological cycle can slow down despite a warmer climate. According to the authors, their model shows that the decrease in incoming solar radiation is only partly offset by enhanced downward long-wave radiation, and that this leads to a decrease in the sensible and latent fluxes (via the decrease in incoming shortwave radiation), but an increase in temperature (via the increase in outgoing long-wave radiation).

Land use. Land use changes affect primarily the surface albedo, with direct impacts on net surface radiation (e.g. Copeland et al., 1996, Bonan, 1999). However, changes in soil types can also affect the surface hydrology and the vegetation transpiration characteristics, with potential consequences on the partitioning into latent and sensible heat fluxes (e.g. Feddema et al., 2005). Finally, the vegetation structure can also affect the surface roughness, thereby altering momentum and heat transport (e.g. Vautard et al., 2010).

Since 1870, the main changes in land use include the global increase in crop and grazing lands, mostly at the expense of forests and natural grasslands, respectively (Ramankutty and Foley, 1998, Klein Goldewijk, 2001, Goldewijk and Ramankutty, 2004). Historical changes in land use are however not typically included in transient climate simulations, and the biogeophysical processes described above are therefore not usually accounted for in numerical simulations. Nevertheless, the potential impact of land use changes on the hydrological cycle has been assessed in various sensitivity experiments (e.g. Werth and Avissar, 2001; Pielke 2005; Feddema et al., 2005). Many studies focus for instance on the impact of deforestation in the Amazonian region, and find that it triggers a drying of the Amazon basin throughout the 20th century (Werth and Avissar, 2001; Pielke 2005; Avissar and Werth, 2005 and therein) with possible extratropical impacts (e.g. Avissar and Werth, 2005), but have no impact on the global scale (e.g. Zhao et al., 2001).

Finally, the Earth's surface also acts as a source for aerosol emissions, and as a source and sink for greenhouse gases. It was shown that since 1870, land use changes have released almost half as much carbon as that from fossil fuel emissions (Houghton, 1999). In this thesis, ECHAM5-HAM is forced with climatological fields of land use, taken from Hagemann (2002).

1.5 Objectives and overview of the thesis

As outlined in the previous section, important changes in climate forcings occurred since 1870, with reported consequences for the hydrological cycle. Numerous questions remain however open, especially regarding the transient impact of these climate forcings on the hydrological cycle through time, as individuals and as combined (e.g. Liepert et al., 2004; Wild and Liepert, 2010). On the global scale, the thesis focuses on the impacts of these forcings on the decadal variability of global land precipitation and wind speed since 1870, whereas on the regional scale, it focusses on the high summer precipitation anomalies observed in the late nineteenth century in central Europe (e.g. Pfister 1999; Casty et al., 2007). These questions are addressed in three scientific papers which constitute the three following chapters of the thesis.

Chapter 2 identifies the main forcings that drive the decadal variability of global land temperature and precipitation since 1870, and quantifies their impacts. As a first step, the capacity of ECHAM5-HAM to reproduce the observed global land temperature and precipitation anomalies in the time period 1870-2005 is evaluated. Then, the sensitivity studies investigate how the climate forcings affect the hydrological cycle through time, with a focus on the impacts of SSTs, anthropogenic aerosol emissions, and greenhouse gas concentrations.

Chapter 3 investigates the potential causes that triggered the wind stilling observed globally over land after 1970. First, the global impact of uniformly increasing vegetation roughness length is quantified, as a first step to understand how the reported recent increase in vegetation (e.g. Ciais et al., 2008) may have influenced the surface land wind speed. Then, the global impact of realistic changes in climate forcings is assessed, with a focus on anthropogenic aerosol emissions.

Chapter 4 aims to identify the main forcings that drive the high precipitation anomalies observed in central Europe in the summers of the late nineteenth century. First, the capacity of ECHAM5-HAM to reproduce these anomalies is evaluated. Then, the impact of the time-varying climate forcings on these anomalies is assessed, with a focus on the SSTs and the contribution from individual oceanic basins.

Finally, Chapter 5 concludes the thesis and Chapter 6 gives an outlook on the future work that would be needed to enhance our understanding of the hydrological cycle sensitivity to time-varying climate forcings.

Chapter 2

Global precipitation response to changing forcings since 1870

Global precipitation response to changing forcings since 1870*

A. Bichet¹, M. Wild¹, D. Folini¹, and C. Schär¹

Abstract

Predicting and adapting to changes in the hydrological cycle is one of the major challenges for the twenty-first century. To better estimate how it will respond to future changes in climate forcings, it is crucial to understand how the hydrological cycle has evolved in the past and why. In our study, we use an atmospheric global climate model with prescribed sea surface temperatures (SSTs) to investigate how, in the period 1870-2005, changing climate forcings have affected the global land temperature and precipitation.

We show that between 1870 and 2005, prescribed SSTs (encapsulating other forcings and internal variability) determine the decadal and interannual variabilities of the global land temperature and precipitation, mostly via their influence in the tropics (25°S-25°N). In addition, using simulations with prescribed SSTs and considering the atmospheric response alone, we find that between 1930 and 2005 increasing aerosol emissions have reduced the global land temperature and precipitation by up to 0.4 °C and 30 mm/year, respectively, and that between about 1950 and 2005 increasing greenhouse gas concentrations have increased them by up to 0.25 °C and 10 mm/year, respectively. Finally, we suggest that between about 1950 and 1970, increasing aerosol emissions had a larger impact on the hydrological cycle than increasing greenhouse gas concentrations.

* *Atmospheric Chemistry and Physics*, 2011, Volume 11, page 9961-9970 (doi:10.5194/acp-11-9961-2011).

¹ Institute for Atmospheric and Climate Sciences, ETH Zürich, Switzerland

2.1 Introduction

Global and regional variations in temperature and precipitation are key parameters affecting our economy and ecosystems. To better predict their changes under future climate conditions, it is essential to understand their sensitivity to the relevant climate forcings, and how this sensitivity evolves through time. Based on observations, previous studies (e.g. Allen and Ingram, 2002; Wild et al., 2008; Wild and Liepert, 2010) show the crucial role of the radiation balance in driving the hydrological cycle, and point out the important role of aerosol and greenhouse gas concentrations. On the one hand, increasing aerosol concentrations in the atmosphere is expected to cool the Earth's surface and reduce precipitation (e.g. Ramanathan et al., 2001; Liepert et al., 2004; Wild et al., 2005; Wild and Liepert, 2010). On the other hand, increasing greenhouse gas concentrations in the atmosphere is expected to warm the Earth's surface and increase precipitation (e.g. Trenberth, 1990; Boer, 1993; IPCC AR4, 2007; Trenberth, 2010). Recent studies (e.g. Wild et al., 2007 and 2008; Wild and Liepert, 2010) suggest that between about 1960 and 1980, increasing aerosol concentrations had a larger impact on the global land temperature and precipitation than increasing greenhouse gas concentrations, whereas the opposite is true after about 1980.

The atmospheric forcings addressed affect the coupled climate system in intricate ways. Changes in radiative forcings will instantaneously affect local land and sea-surface temperatures, and these changes may operate on and feed back to the atmosphere on longer (daily to decadal) time scales. The oceans are particularly essential in driving the hydrological cycle (e.g. Mitchell, 1983). Sea surface temperatures (SSTs) are strongly coupled to both global land temperatures (e.g. Hoerling et al., 2008; Compo et al., 2009) and precipitation (e.g. Koster and Suarez, 1995). Many modelling studies have focused on the climatic response of the fully coupled system to changing carbon dioxide (CO₂) and aerosol concentrations, but only few examine the transient climatic response to time varying emissions of pollutants. In our paper, we use an atmospheric general circulation model (GCM) forced with prescribed SSTs, to quantify the transient response of the hydrological cycle to changing climate forcings in the period 1870-2005.

The layout of the paper is as follows: Section 2.2 describes the methodology, Section 2.3 shows the results, and Sections 2.4 and 2.5 discuss and concludes the study, respectively.

2.2 Methodology

In this section, we first explain the model set up and experiments (Section 2.2.1), we then show the evolution of the main climate forcings since 1870 (Section 2.2.2), and finally we describe the observational datasets used to validate our simulations (Section 2.2.3).

2.2.1 Model set up and experimental design

We perform climate simulations using the fifth generation of the atmospheric GCM, ECHAM (Roeckner et al., 2003). The basic prognostic variables, vorticity, divergence, temperature and surface pressure are represented by spherical harmonics with triangular truncation, in our case at wave number 42 (T42), which implies a horizontal grid spacing of approximately 2.8 degree. Non-

linear processes and physical parametrization are solved on a corresponding Gaussian grid. Tracers are advected using the scheme by Lin and Rood (1996). In the vertical, 19 hybrid sigma-pressure levels are used, with the uppermost level at 10 hPa (Roeckner et al., 2003). Since direct and indirect aerosol effects significantly affect the global temperature and precipitation (e.g., Ramanathan et al., 2001; Stier et al., 2006), we use a version of ECHAM5 that is coupled to a fully interactive aerosol module, the Hamburg Aerosol Model (HAM) (Stier et al., 2005). This module predicts the evolution of microphysically interacting internally and externally mixed aerosol populations. The major global aerosol categories, sulphate, black carbon (BC), particulate organic matter (POM), sea salt and mineral dust are included (Stier et al., 2005).

Hagemann et al. (2006) investigated the impact of model resolution on the hydrological cycle with ECHAM5 for the time period 1978-1999. They found that increasing the vertical resolution is more beneficial than increasing the horizontal resolution due to the improved moisture transport. They used horizontal resolutions going from T21 to T106, vertical resolutions going from 19 to 31 atmospheric layers, and forced ECHAM5 with prescribed SSTs and sea-ice dataset specifically constructed for the AMIP experiments by the NOAA Climate Analysis Centre (Gates, 1992).

In our study, we use ECHAM5-HAM at resolution T42 for the time period 1870-2005, and conduct a series of experiments driven by prescribed SSTs and accounting for different atmospheric forcings. The forcings used include the time varying monthly mean of the total solar irradiance (TSI) (Solanki and Krivova, 2003), time varying annually stratospheric optical depth due to aerosols from explosive volcanoes (Sato et al., 1993), and time varying annual mean of greenhouse gas concentrations taken from observations until 2000 and from the Intergovernmental Panel on Climate Change (IPCC) A1B scenario for 2001-2005 (CO₂, methane, nitrous oxide, ozone and chlorofluorocarbons). Emissions of sulphur dioxide (SO₂), BC and POM are taken from the Japanese National Institute for Environmental Sciences (NIES) (Roeckner et al., 2006; Stier et al., 2006; Nozawa et al., 2007). They include geographically resolved time varying monthly mean emissions from wildfires, agricultural burning and domestic fuel-wood consumption, as well as time varying annual mean emissions from fossil fuel consumption. To reduce the source of uncertainty coming from atmosphere-ocean coupling, we force our model with monthly mean observed SSTs and sea-ice concentrations, using gridded data from Rayner et al. (2003). It was assembled by the Hadley Centre for Climatic Prediction and Research and consists of monthly observed sea ice and SSTs from 1870 to present. It covers the global sea surface at 1 degree resolution, and uses a two-stage reduced-space optimal interpolation procedure, followed by superposition of quality-improved gridded observations onto the reconstructions to restore local detail. SSTs near sea ice are estimated using statistical relationships between SST and sea ice concentration (Rayner et al., 2003).

We perform twenty-seven transient experiments, listed in Table 2.1 All the experiments run from 1870 to present and use a spin-up time ranging from several months to several years. The twenty-seven experiments are divided into four ensembles: Fourteen simulations correspond to the control runs (referred to as CTRL, “all forcings run”), for which all the forcings are time varying (e.g. TSI, greenhouse gases, aerosols and SSTs), four simulations are identical to CTRL except that aerosol emissions (anthropogenic and natural) are held constant at their 1870 level (referred to as AEC), six simulations are identical to CTRL except that SSTs are held constant at their 1871-1900 climatological values (referred to as SSTC), and three experiments are identical to CTRL except that both, SSTs and aerosol emissions (anthropogenic and natural) are held constant (referred to as AESSTC). Note that in AESSTC, the only remaining forcings expected to affect the climate at

decadal scale are the greenhouse gases and the TSI. AESSTC can therefore be used to evaluate the impact of these two forcings, knowing that the TSI cannot be a dominant factor influencing the climate after 1970 (Solanki and Krivova, 2003).

Name of ensemble mean	Number of experiments	SSTs	Aerosol emissions
CTRL	14	Time-varying since 1870	Time-varying since 1870
AEC	4	Time-varying since 1870	Constant to 1870 value
SSTC	6	Climatology averaged over 1871-1900	Time-varying since 1870
AESSTC	3	Climatology averaged over 1871-1900	Constant to 1870 value

Table 2.1: Summary of the different simulations. All the simulations cover the period 1870 to 2005 and are forced with time-varying greenhouse gas concentrations since 1870.

To suppress the “noise” from individual simulations and assess their natural variability, we calculate ensemble means and quantify their uncertainties via the computation of their standard deviation (assuming a normal distribution). We also carried out tests with different ensemble sizes (not shown), and use at least three members ensembles to estimate the ensemble spread. In our sensitivity studies, we do not separate the explosive volcanic aerosols from other aerosols (e.g. anthropogenic), since no significant difference was found, in the 11-years running means, between the global land temperature and precipitation anomalies simulated with, and without explosive volcanic emissions (not shown). This lack of differentiation may come from the prescribed SSTs. Therefore, “aerosol emissions” in our paper always refer to anthropogenic and natural (including explosive volcanic) aerosols.

2.2.2 Evolution of the main climate forcings since 1870

Figure 2.1a-c shows the global annual mean emissions of SO_2 , BC and OC (from NIES), Figure 2.1d shows the stratospheric aerosol optical depth due to explosive volcanoes (Sato et al., 1993), and Figure 2.1e shows the global seasonal SST anomalies relative to the 1870-2000 mean (Rayner et al., 2003). Aerosol emissions from fossil fuel (Figure 2.1a-c, red curves) increase slightly from 1870 to 1910, stabilize until 1930, increase strongly until 1990 and then stabilize. On the other hand, aerosol emissions from biofuel (black curves) and wildfires (green curves), together with the greenhouse gas concentrations (not shown), increase slightly from 1870 to the 1950s and strongly after this date. Emissions of SO_2 from fossil fuel (Figure 2.1a, red curve) and BC and OC from wildfires (Figure 2.1b-c, green curve) exhibit the strongest increase since 1870. In addition, large volcanoes are very active between 1870 and 1920 as well as between 1960 and 2000, but almost absent between 1920 and 1960 (Figure 2.1d). Finally, global SST anomalies are relatively stable from 1870 to 1910, increase until 1940, stabilize until 1970 and then increase (Figure 2.1e).

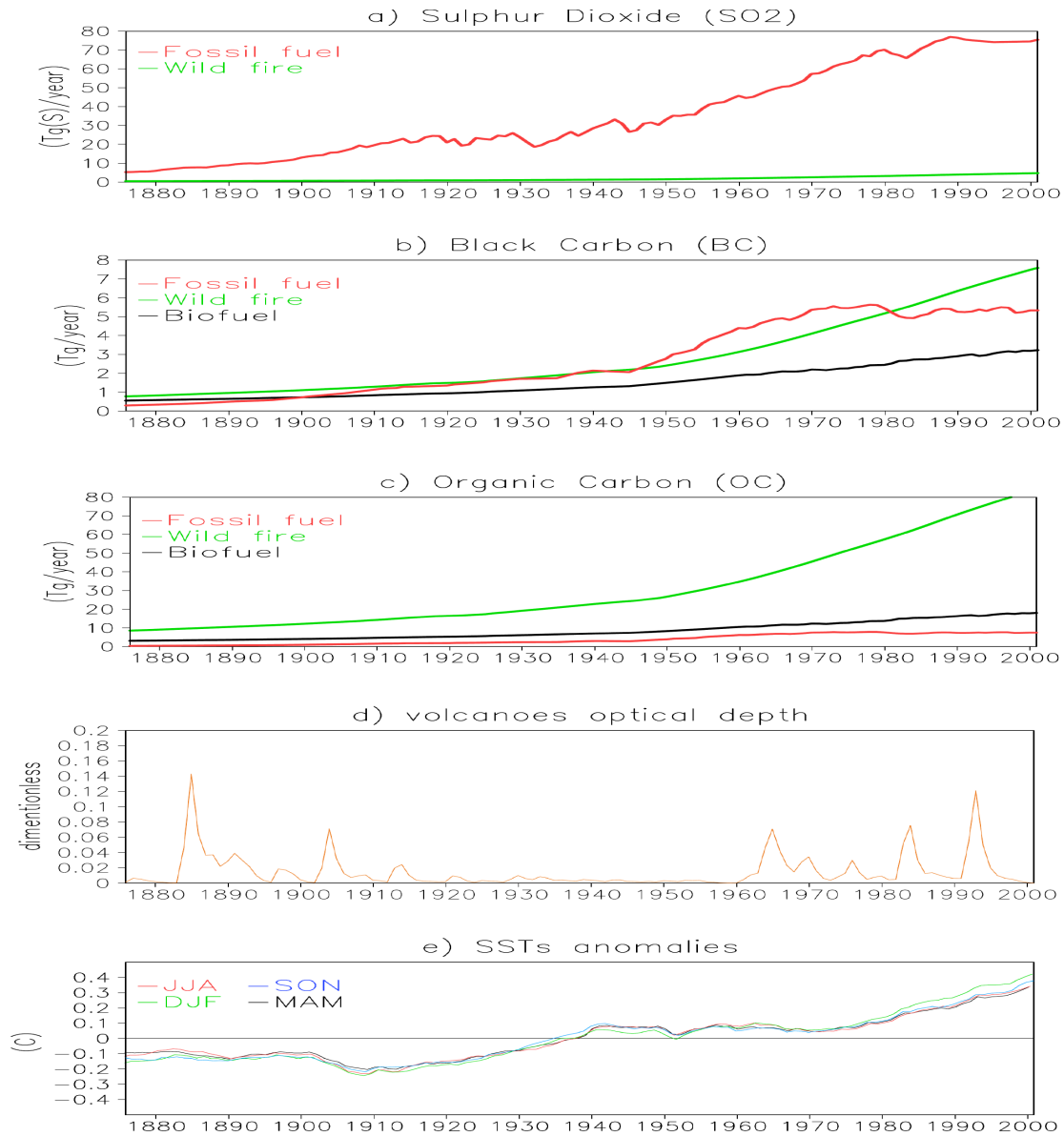


Figure 2.1: Global annual time series of anthropogenic aerosol emissions (a-c) and stratospheric optical depth due to explosive volcanoes (d), and global seasonal time series of SST anomalies shown as 11-years running means (e). The SST anomalies are in °C and correspond to the SST global mean value for each year, minus the global mean of the reference period (1870-2000).

2.2.3 Observational data for temperature and precipitation

To make full use of our results, we validate our simulations against observed temperature and precipitation datasets covering the globe since 1870. Because historic observational data are scarce over the oceans, we limit our analysis to the land.

We first look at temperature. At least four datasets cover the global land temperature since 1880 (Hansen et al., 2001; Lugina et al., 2005; Smith and Reynolds, 2005; Brohan et al., 2006), one of them even starts in 1850 (Brohan et al., 2006). Since the global land annual means of these four datasets are in good agreement since 1880 (IPCC AR4, 2007), we validate our simulated temperatures against one single dataset, “CRUTEM3”, starting in 1850 (Brohan et al., 2006). It has been assembled by the Climate Research Unit of the University of East Anglia (CRU) and consists of monthly observed two meters air temperatures from 1850 to present. It is based on 4,349 stations and covers the global land surface at 5 degree resolution. It uses an interpolation method such that each grid box value is the mean of all available station anomaly values excluding the station outliers in excess of five standard deviations. Missing values are not spatially infilled and most gaps are found in the tropics and the southern hemisphere (particularly Antarctica), as well as during the nineteenth century and the two world wars (Brohan et al., 2006). When comparing observed against simulated temperatures, we change the grid of the simulated temperatures each year according to the data coverage.

We validate our simulated precipitation against two observational datasets. The first one, “CRU TS 2.1” (Mitchell and Jones, 2005), has been assembled by the CRU, and consists of monthly observed precipitation going from 1901 to 2002. It covers the global land surface at 0.5 degree resolution and includes oceanic islands but excludes Antarctica. The interpolation is done directly from station observations and uses the angular distance-weighting method. Because this dataset has not been corrected for gauge biases, it may undercatch solid precipitation in colder areas (New et al., 2000). Note that for the two datasets assembled by the CRU, namely “CRUTEM3” and “CRU TS 2.1”, the station data values are first transformed into anomalies relative to a standard normal period prior to interpolation (New et al., 2001). The second precipitation dataset, “GHCN” (Peterson and Vose, 1997), has been assembled by the National Oceanic and Atmospheric Administration (NOAA) and consists of monthly observed precipitation calculated from the “GHCN V2” dataset going from 1900 to 2009. It comprises stations with varying temporal coverage going from 5,500 in 1900 to 16,500 in 1966, and covers the global land surface at 5 degree resolution (New et al., 2001).

Although no quantified uncertainties are given with these precipitation datasets, most uncertainties, due to poor spatial coverage, are located in the high latitudes, arid regions and parts of the tropics (New et al., 2001). Additional uncertainties can come from errors and biases in the gauge measurements as well as inhomogeneity arising from several sources (New et al., 2000 and 2001). Finally, since both precipitation datasets (“CRU” and “GHCN”) have been spatially infilled by interpolation (Mitchell and Jones, 2005; New et al., 2001), there is no need to change the grid of the simulated precipitation according to the data coverage as it was done for temperature.

2.3 Results

This section first evaluates the capacity of ECHAM5-HAM to reproduce the observations (Section 2.3.1). It then describes the results from the sensitivity experiments (Section 2.3.2). All the time series are shown as 11-years running mean anomalies, with a reference period varying according to the analysis. We first calculate the anomalies, then the global means, and finally the running means.

2.3.1 Global scale assessment of the model

Observed (dashed curves) and simulated (CTRL, solid curves) global land temperature anomalies are shown in Figure 2.2, relative to the 1960-1990 mean. Note that whereas observed temperatures correspond to the two meters temperatures, simulated temperatures refer to the surface “skin” temperatures. Qualitatively, simulated and observed anomalies are in good agreement since 1870, particularly in the June-July-August (JJA) and September-October-November (SON) averages (Figure 2.2). In line with the IPCC AR4 (2007), global land annual anomalies show two warming periods of about 0.5 °C each, one from 1910 to 1940, and a second one after about 1980. According to Figure 2.2, this is the case in all seasons.

Two warm biases occur in the global land annual averages: One in the late nineteenth century (0.2°C on average) and a second one in the 1940s and 1950s (0.1°C on average). Both are particularly pronounced in the December-January-February (DJF) and March-April-May (MAM) averages. Figure 2.3 shows that the warm bias in the late nineteenth century is mostly located in Siberia. Interior of continents such as Siberia are more likely to have biases in our experiments since they are the least constrained by SSTs. On the other hand, the warm bias in the 1940s and 1950s falls into a period with a general underestimation of SSTs due to changes in observational practice (Thompson et al., 2008). The cold biases contained in the driving SSTs should thus trigger cold biases in the simulated land temperatures, which is opposite to our results (Figure 2.2). This means that the simulated warm bias in the 1940s and 1950s might actually be somewhat larger than indicated in Figure 2.2.

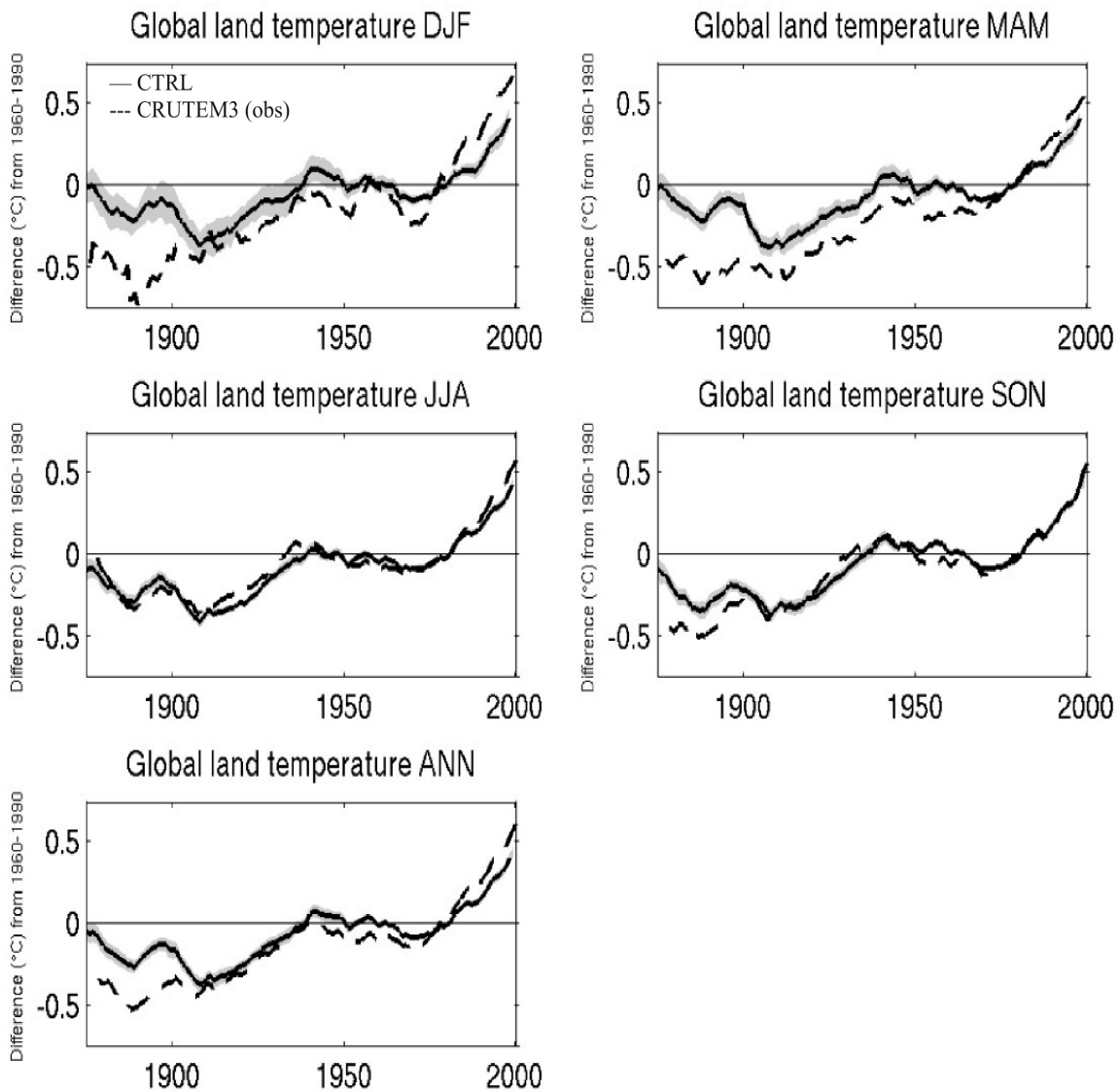


Figure 2.2: Simulated (CTRL, solid) and observed (CRUTEM3, dashed) annual and seasonal global land temperature anomalies ($^{\circ}\text{C}$), relative to the 1960-1990 mean, shown as 11-years running means. Gray shaded area corresponds to the ± 1 sigma spread of the ensemble CTRL.

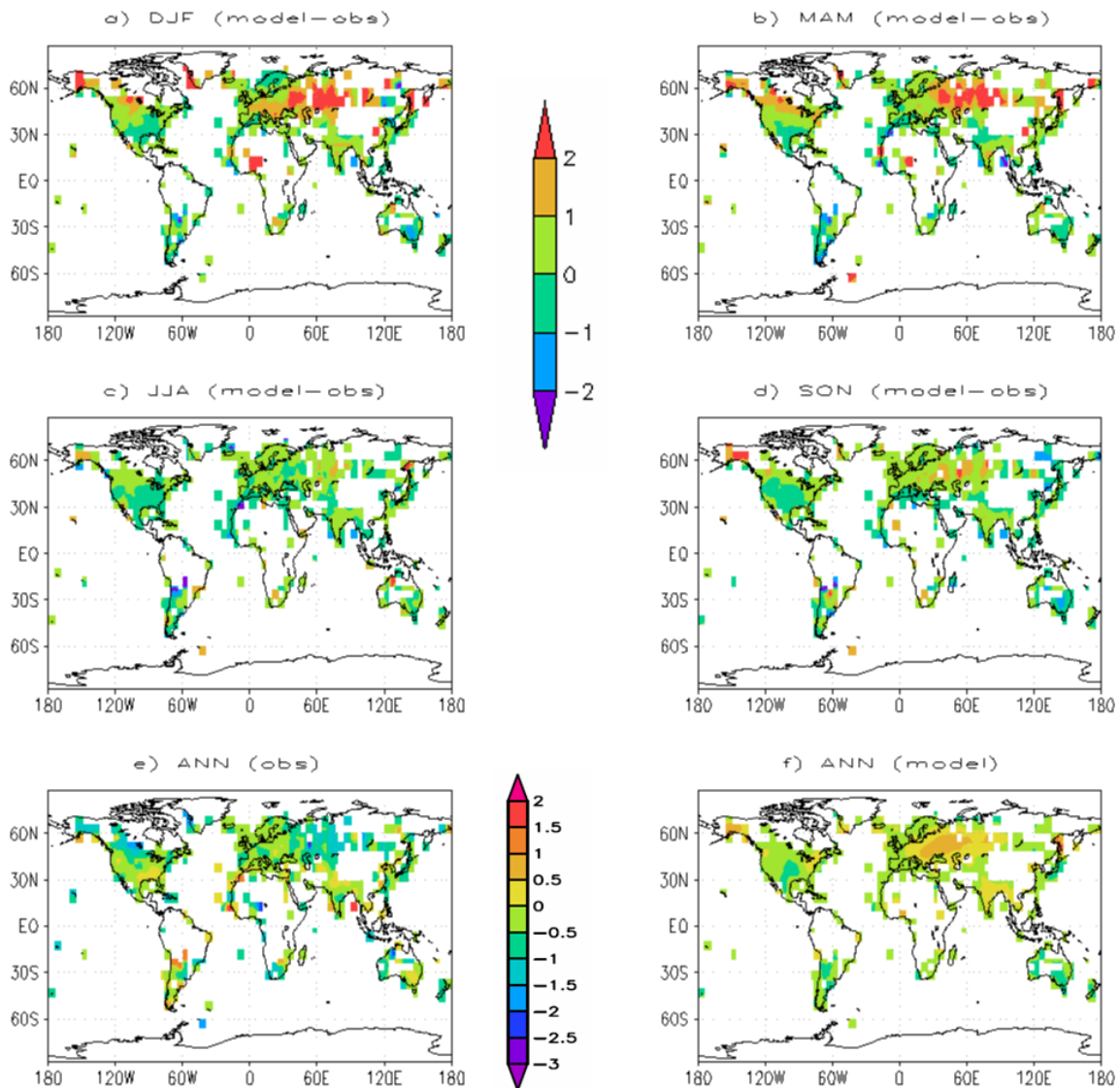


Figure 2.3: Maps of seasonal land temperature biases ($^{\circ}\text{C}$) averaged over the time period 1890-1900 (a-d). The maps correspond to the difference between the temperature anomalies from the CTRL ensemble mean and from observations (CRUTEM3), remapped on a T42 grid. The annual temperature maps ($^{\circ}\text{C}$) are shown as observed (e) and simulated (f) anomalies, averaged over the time period 1890-1900. Here, the reference period 1960-1990 has been used.

The global land precipitation anomalies relative to the 1901-2000 mean are shown in Figure 2.4. Despite a wet bias in the 1930s and a dry bias in the 1970s, both located in China and in northern South America (not shown), simulated (solid curves) and observed (dashed curves) global land precipitation anomalies are in reasonable agreement since 1901 (Figure 2.4): Both exhibit an increase during the first half of the 20th century, a decline until the early 1990s and then recover (New et al., 2001; IPCC AR4, 2007). However, the magnitude and timing of the associated decadal variations is not well captured. Note that the centennial trends are relatively small compared to decadal variations.

Figure 2.5b-c shows the simulated (solid curves) and observed (“CRU”, dashed curves) land precipitation anomalies relative to the 1901-2000 mean with yearly resolution. In the tropics, interannual and decadal variations are surprisingly well reproduced (Figure 2.5c), while on a global scale there are considerable discrepancies (Figure 2.5b). In addition, Figure 2.5b-c shows that observed and simulated land precipitation anomalies decrease after large tropical volcanic eruptions (blue vertical lines) as well as during El Nino events (green vertical lines), and increase during La Nina events (magenta vertical lines). These atmospheric responses, more pronounced in the tropics (Figure 2.5c), are in line with previous studies (Gu et al., 2007; Trenberth and Dai, 2007), and suggest, in agreement with Hagemann et al. (2006), that ECHAM5-HAM produces a realistic response of land precipitation to changes in external forcings and SSTs.

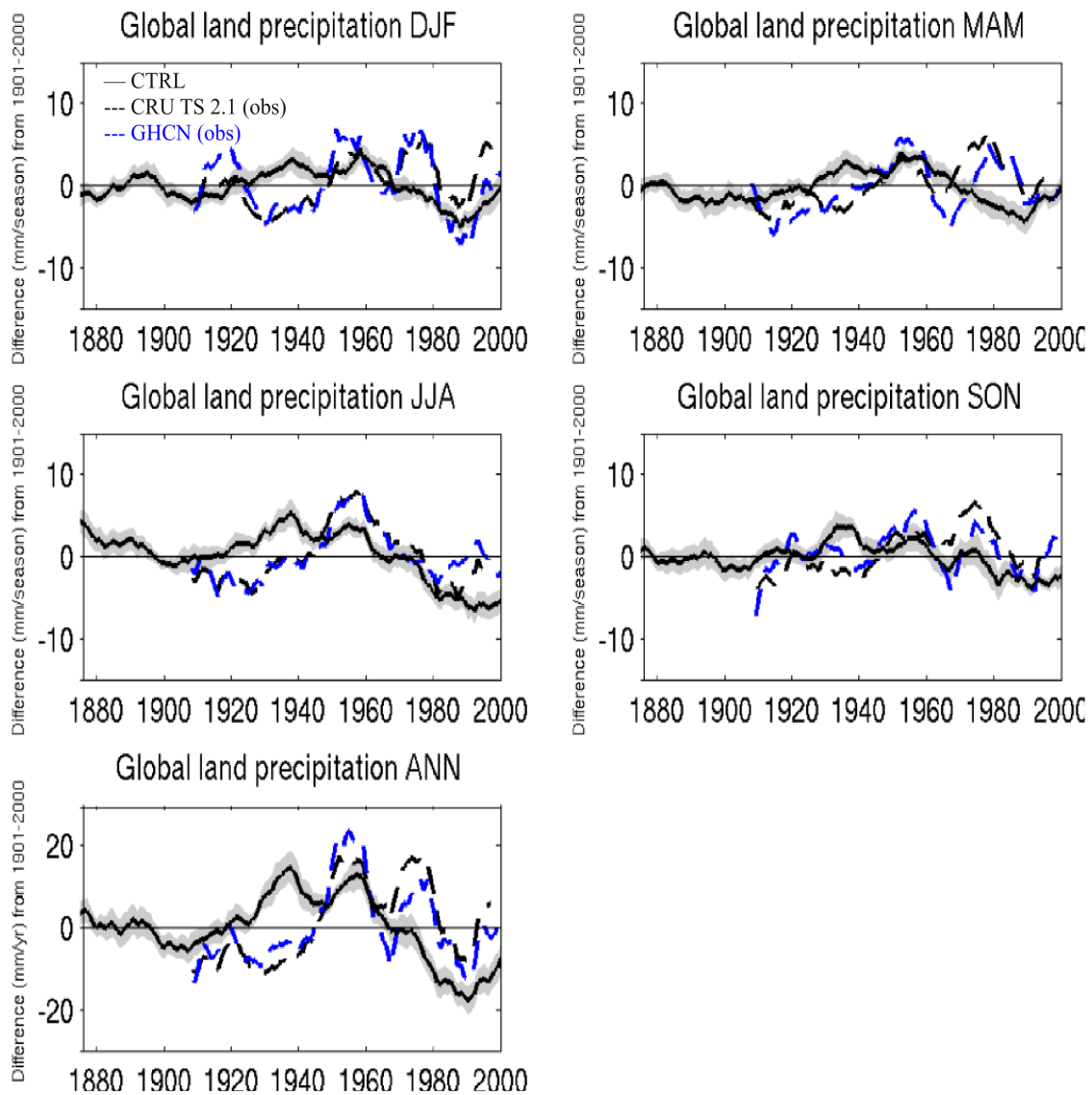


Figure 2.4: Simulated (CTRL, solid) and observed (CRU, black dashed; GHCN, blue dashed) annual and seasonal global land precipitation anomalies (mm/season and mm/year, respectively), relative to the 1901-2000 mean, shown as 11-years running means. Gray shaded area corresponds to the ± 1 sigma spread of the ensemble CTRL.

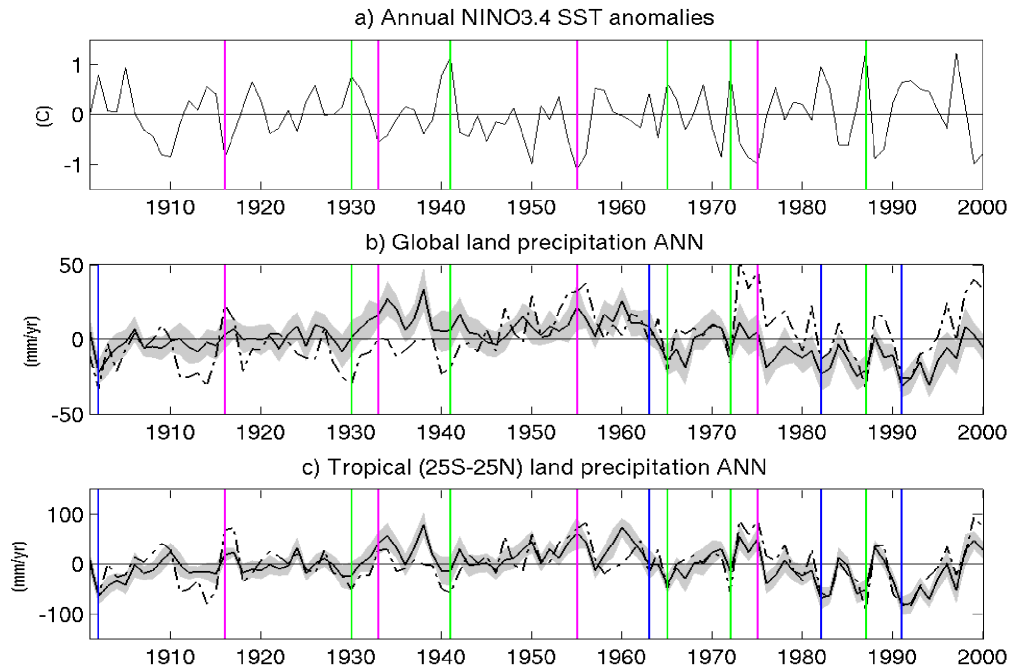


Figure 2.5: Annual NINO3.4 index anomalies calculated from observed SSTs (Rayner et al., 2003) (a). Simulated (CTRL, solid curves) and observed (CRU, dashed curves) global (a) and tropical (b, 25°S-25°N) land precipitation anomalies, plotted with yearly resolution. Here, the reference period 1901-2000 has been used. El Niño (green lines), La Niña (magenta lines) and large tropical volcanic eruptions (blue lines) years.

2.3.2 Global scale sensitivity of the model to external forcings

Figures 2.6 and 2.7 show the global land temperature and precipitation anomalies, respectively, relative to the 1870-1880 mean. Both figures show the ensemble means simulated in CTRL (black curve), SSTC (blue curve), AEC (red curve) and AESSTC (green curve) (see Table 2.1 and Section 2.2.1). According to Figures 2.6 and 2.7, the different ensemble means, corresponding to different forcings, significantly depart from each other. Since at least qualitatively, annual and seasonal global land temperature and precipitation anomalies are similar to each other, we focus our discussion on annual means only.

According to Figure 2.6, the global land temperature anomalies simulated in CTRL (black curve) show a clear decadal variability since 1870, which is suppressed in the anomalies simulated with climatological SSTs (SSTC and AESSTC): Not present in the SSTC and AESSTC simulations are in particular, the two temperature increases from 1910 to 1940 and 1980 to 2000. Instead, the anomalies simulated in SSTC (blue curve) are constant until 1950, decrease by about 0.2 °C from 1950 to 1990 and then recover, whereas the anomalies simulated in AESSTC (green curve) are constant until about 1950 and increase by about 0.25 °C from 1950 to 2000. In addition, although the anomalies simulated in AEC (red curve) show a similar decadal variability than the ones simulated in CTRL (black curve), they exhibit a larger trend after about 1930 (up to 0.4 °C warmer in 2000).

According to Figure 2.7, the global land precipitation anomalies simulated in CTRL (black curve) also show a clear decadal variability since 1870, which is suppressed in the anomalies simulated with climatological SSTs (SSTC and AESSTC): Not present in the SSTC and AESSTC simulations are in particular, the two precipitation maxima in the late 1930s and late 1950s. Instead, the anomalies simulated in SSTC (blue curve) are constant until 1930, decrease by about 20 mm/year between 1930 and 1970 and then stabilize, whereas the anomalies simulated in AESSTC (green curve) are constant until about 1930 and increase by about 10 mm/year from 1930 to 2000. In addition, although the anomalies simulated in AEC (red curve) show a similar decadal variability than the ones simulated in CTRL (black curve), the former exhibit almost no trend after 1930, whereas after this date, the latter decrease by about 10 mm/year. This implies that the global land precipitation centennial trend (1900-2000) is negative with transient aerosol emissions (CTRL and SSTC) but positive with constant aerosol emissions (AEC and AESSTC).

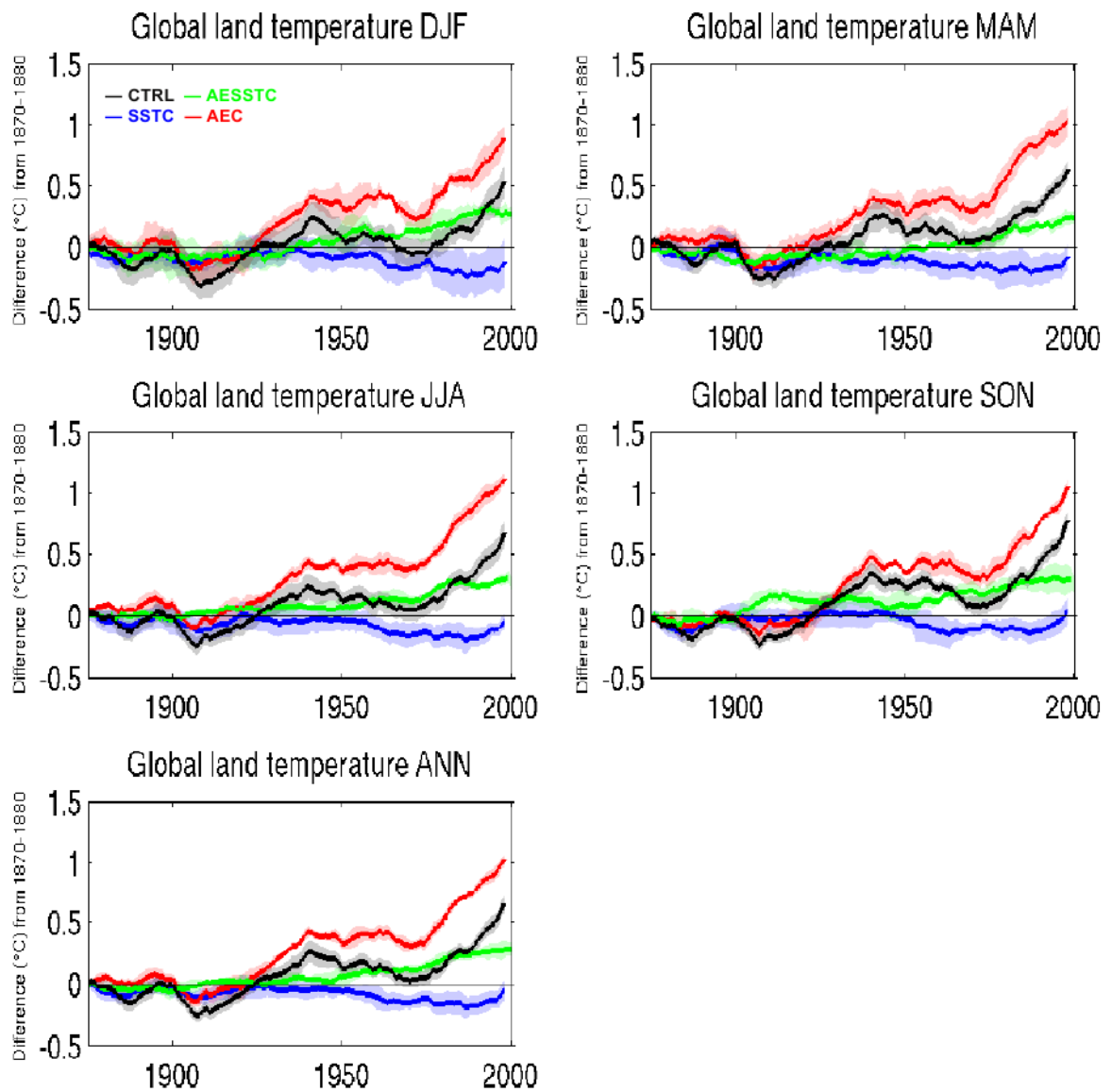


Figure 2.6: Simulated annual and seasonal global land temperature anomalies ($^{\circ}\text{C}$), relative to the 1870-1880 mean, shown as 11-years running means. Shaded areas correspond to the ± 1 sigma spread of each ensemble.

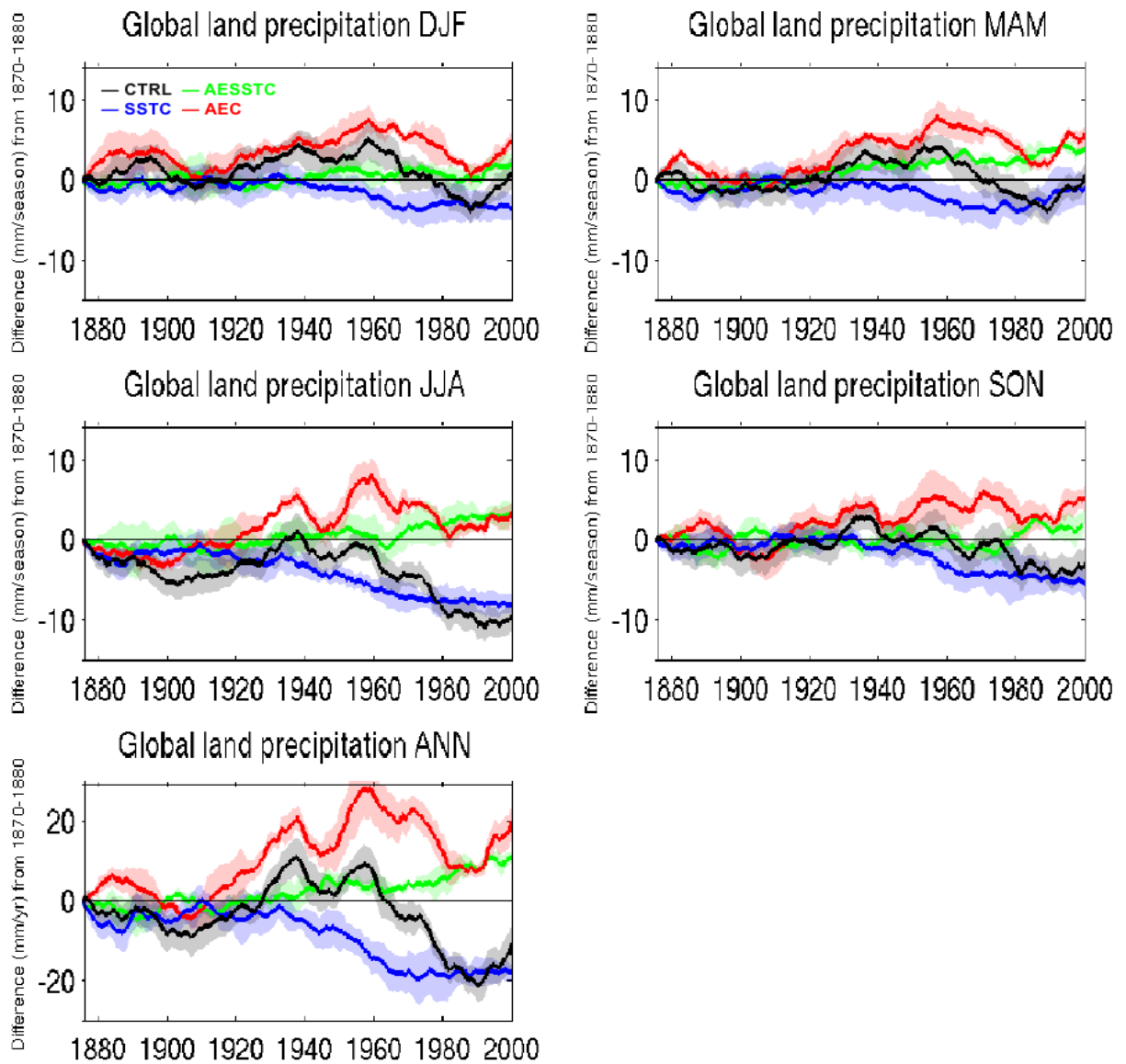


Figure 2.7: Simulated annual and seasonal global land precipitation anomalies (mm/season and mm/year, respectively), relative to the 1870-1880 mean, shown as 11-years running means. Shaded areas correspond to the ± 1 sigma spread of each ensemble.

2.4 Discussion

In the following section, we investigate the physical processes behind these sensitivities, focusing on the hydrological cycle. Section 2.4.1 explains where, at global scale, the water falling on land comes from. Sections 2.4.2 and 2.4.3 discuss the sensitivity of this water cycle to SSTs and external forcings, respectively. All the time series are shown as 11-years running means.

2.4.1 Origin of water in the global land precipitation

The global land precipitation has two sources: The land evaporation and the advection of moisture from the oceans. According to Figure 2.8a (black curve), the global land surfaces evaporate about 500 mm of water per year. Because the global land precipitation amounts to about 760 mm/year (not shown), we conclude, in agreement with previous studies (e.g. Wild et al., 2008), that at least 35 % (260 mm/year) of the global land precipitation must come from the oceans (Figure 2.8b, black curve). According to Van der Ent et al. (2010) however, the water recycling on land is about 57%. Therefore, out of the 65% global land precipitation, only 57% falls back on land. This implies that about 40% of the global land precipitation actually comes from land evaporation and thus, 60% is advected from the oceans. Nevertheless, our results show that in the 11 years running mean time series, the global land precipitation trend (-0.92 mm/decade) and variability are more highly correlated with the trend (-0.77 mm/decade) and variability of the global land evaporation ($r^2 = 0.81$), than with the ones of global oceanic evaporation (trend: -0.15 mm/decade, $r^2 = 0.36$).

Over the oceans, our modelling framework implies that the evaporation directly depends on the prescribed SSTs. Over land however, evaporation depends on the energy balance (governed by the net surface radiation) and on the air moisture holding capacity (governed by the Clausius-Clapeyron relation) (e.g. Penman, 1950; Hartmann, 1994). Note that changes in land evapotranspiration will in addition depend upon changes in the availability of water (soil moisture). According to our 11 years running mean time series, about 76% of the global land evaporation (Figure 2.8a, black curve) is directly explained by the global land net surface radiation (Figure 2.8c, black curve, $r^2=0.76$). This implies that changes in air moisture holding capacity and/or soil moisture, both being also under the influence of the net surface radiation, explain the remaining 24%.

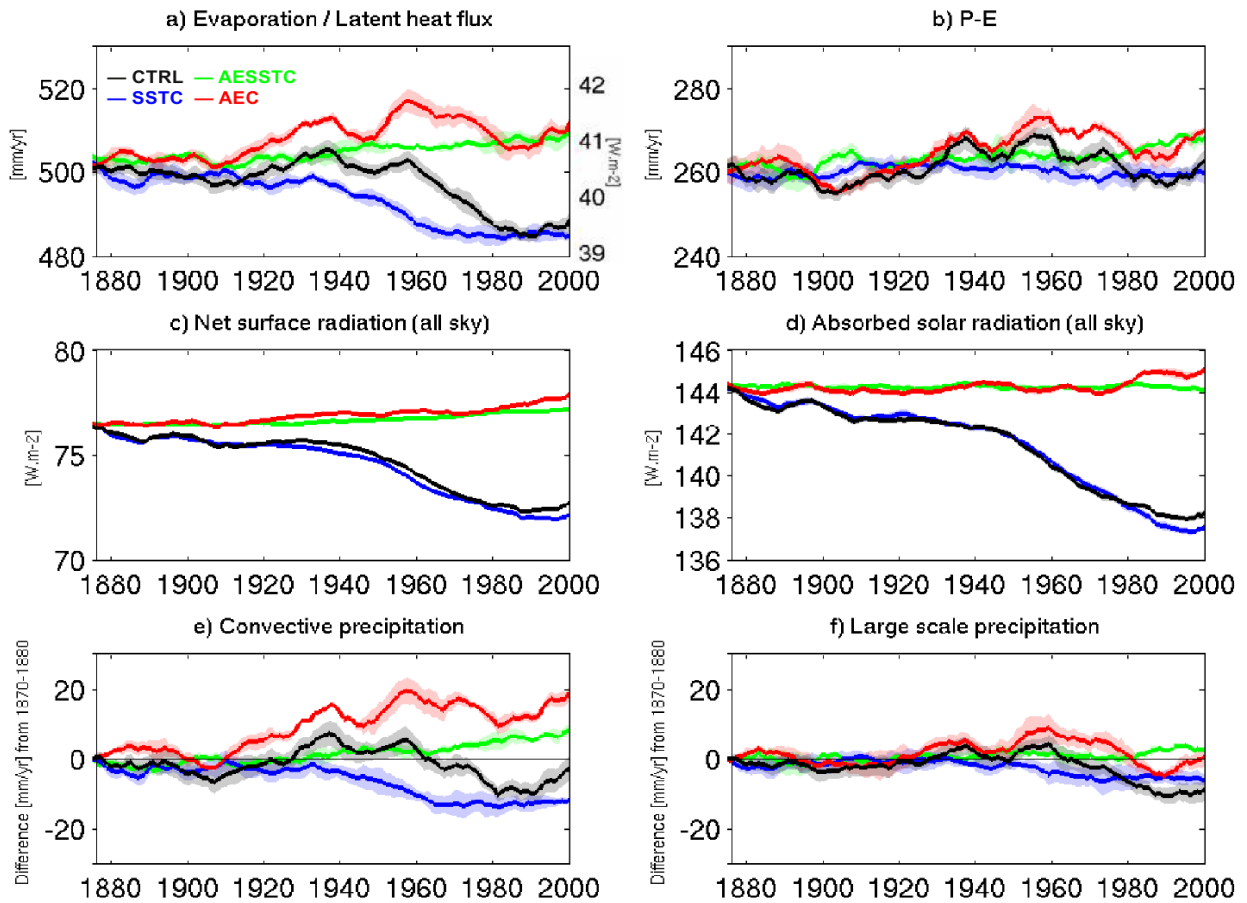


Figure 2.8: Simulated annual global land absolute values of evaporation (left hand side axis, mm/year) and latent heat flux (right hand side axis, W/m^2) (a), precipitation minus evaporation (P-E, mm/year) (b), net surface radiation all sky (W/m^2) (c) and absorbed solar radiation all sky (W/m^2) (d), as well as anomalies of convective (e) and large scale precipitation (f) (mm/year; ref: 1870-1880). All the time series are shown as 11-years running means. Shaded areas correspond to the ± 1 sigma spread of each ensemble.

2.4.2 Role of SSTs

Our results show that since 1870, SSTs determine the decadal and interannual variabilities of the global land temperature and precipitation (Section 2.3.2): Compared with fully transient simulations, simulations with climatological SSTs show hardly any decadal variability in these variables (Figures 2.6 and 2.7).

On the one hand, the high correlation coefficient between the 11 years running mean time series of the global annual SSTs and land temperatures simulated in CTRL ($r^2 = 0.85$), indicates, in line with previous studies (e.g. Hoerling et al., 2008; Compo and Sardeshmukh, 2009; Findell et al., 2009), that the two variables are strongly coupled: Warmer SSTs increase land temperatures primarily via moistening and warming of the air over land, which then increase the downward longwave radiation at the surface (Compo and Sardeshmukh, 2009).

On the other hand, while we see that the decadal variation of the global land precipitation is determined by the SSTs (Figure 2.7), the relation is not trivial: The red curve (AEC) from Figure 2.7 shows that SSTs increase the global land precipitation before 1960, decrease it between 1960 and 1990 and increase it after 1990. However, Figure 2.1e shows that global SSTs increase from 1910 to 1940, stabilize from 1940 to 1980 and increase after 1980. In line with previous studies (e.g. Gu et al., 2007; Trenberth and Dai, 2007), Figure 2.5a-b suggests that El Nino and La Nina events affect the global land precipitation, a negative (positive) El Nino Southern Oscillation (ENSO) index being associated with high (low) global land precipitation. The NINO3.4 index shown in Figure 2.5a is reconstructed from observed SSTs (Rayner et al., 2003) and defined as the average (5°S - 5°N ; 170 - 120°W) of Pacific SST anomalies (e.g. Trenberth, 1997). Since the ENSO index is negative between 1940 and 1960 and increases after 1960 (Figure 2.5a), it provides some evidence that after 1960, the increasing frequency of El Nino events may have reduced the global land precipitation via their associated changes in atmospheric circulation. Note that changes in air moisture holding capacity may also influence the impact of SSTs on global land precipitation. Consistent with the above argumentation, Figure 2.9a shows that SSTs affect mostly the tropical precipitation, especially in the regions strongly related with ENSO (south-east Asia, India and South America). In addition, further analyses (not shown) show that the decadal and interannual variabilities of the global land precipitation are dominated by the tropics (25°S - 25°N).

2.4.3 Role of aerosols and greenhouse gases

Because in our simulations (prescribed SSTs) the ocean cannot respond to the changing external forcings applied in the sensitivity experiments, the sensitivities discussed in the following section refer to atmospheric processes only.

We first compare the ensemble means from CTRL (black curves) and AEC (red curves), which differ from each other only by their aerosol emissions. According to Figure 2.8d, at global land scale, increasing aerosol emissions decrease the solar radiation absorbed at the surface, after about 1930, by up to 6.2 W/m^2 . In turn, this decreases the net surface radiation by up to 5.4 W/m^2 (Figure 2.8c), the latent heat flux by up to 2 W/m^2 (equivalent to about 23 mm/year in evaporation, Figure 2.8a), and the P-E by up to 10 mm/year (Figure 2.8b). The reduced land evaporation

combined with the reduced advection of moisture from the oceans thus decreases the global land precipitation, after about 1930, by up to 30 mm/year (Figure 2.7). About two third of this global land precipitation decrease is in the form of convection (Figure 2.8e-f), mostly located in northern South America and in China (Figure 2.9b). In addition, especially absorbing aerosols higher up in the troposphere can reduce the convection via their impact on stability (Koch and Del Genio, 2010). Finally, indirect aerosol effects are also expected to decrease the global land precipitation (Ramanathan et al., 2001). However, even though the associated processes are taken into account in our simulations, our experimental set up does not allow to quantify their impacts separately from the other aerosols impacts.

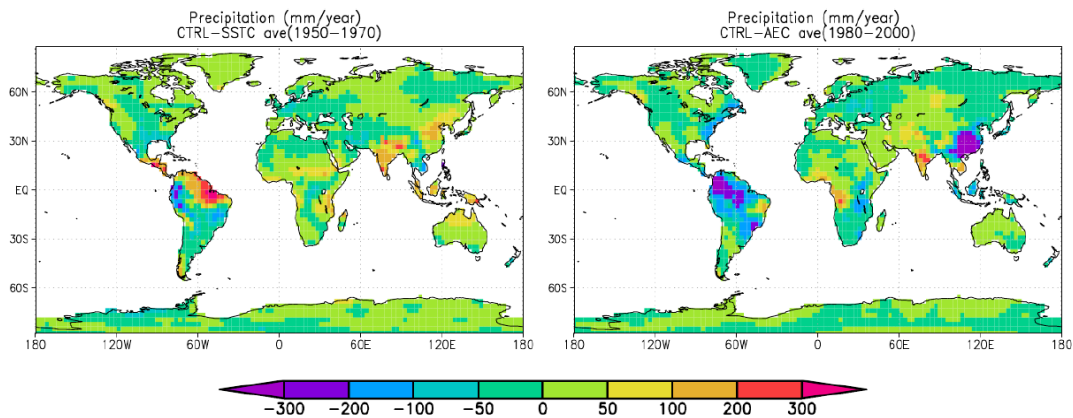


Figure 2.9: Maps of annual land precipitation (mm/year) differences between the anomalies from the CTRL and the SSTC ensemble means, averaged over the time period 1950-1960 (a), and between the anomalies from the CTRL and the AEC ensemble means, averaged over the time period 1990-2000 (b). Here, the reference period 1870-1880 has been used.

We now look at the AESSTC ensemble mean (green curves), which corresponds to the simulations where greenhouse gases and TSI constitute the only transient forcings. According to Figure 2.8c, at global land scale, increasing the greenhouse gas concentrations increases the net surface radiation, after about 1950, by up to 1 W/m^2 , which increases the latent heat flux by up to 0.4 W/m^2 (equivalent to about 5 mm/year of evaporation) (Figure 2.8a) and the P-E by up to 5 mm/year (Figure 2.8b). The enhanced land evaporation combined with the enhanced advection of moisture from the oceans thus increase the global land precipitation, after about 1950, by up to 10 mm/year (Figure 2.7). About two third of this global land precipitation increase is in the form of convection (Figure 2.8e-f).

The combined atmosphere-only effect of aerosols and greenhouse gases is apparent in the SSTC ensemble mean (blue curves). Our results suggest, in agreement with previous studies (e.g. Wild et al., 2007; Wild and Liepert, 2010), that the aerosol effects dominate between about 1950 and 1970, as both, global land temperature and precipitation decrease during this time period (Figures 2.6 and 2.7, blue curves). After about 1970 however, the greenhouse gases start to dominate, as

there is no further decrease in either temperature or precipitation.

Finally, our results show that since 1870, increasing aerosols emissions decreases the global oceanic net surface radiation by up to 3 W/m^2 (not shown). In the real world, this is expected to cool the SSTs, which is in turn expected to decrease the global land temperature and precipitation. Because this process cannot be simulated in our modelling framework (prescribed SSTs), we suggest that the atmosphere-only sensitivities discussed in this section are rather minimum estimates, and could be larger if the full system (including the ocean feedback) was taken into account. This also applies to the greenhouse gas concentrations response.

2.5 Conclusions

Our study shows that ECHAM5-HAM, forced with prescribed SSTs and transient greenhouse gas and aerosol emissions, is able to very satisfactorily reproduce the observed tropical land temperature and precipitation variations since the early 20th century, while it has substantial biases in terms of extratropical precipitation variations. Sensitivity studies show that in our framework, SSTs (encapsulating other forcings and internal variability) determine the decadal and interannual variabilities of the global land temperature and precipitation since 1870, which is mostly due to the large impact of SSTs in the tropics (25°S - 25°N). In addition, we find that between about 1930 and 2005, the atmosphere-only response to increasing aerosol emissions is a reduction in global land temperature and precipitation by up to $0.4 \text{ }^{\circ}\text{C}$ and 30 mm/year , respectively. Similarly, between about 1950 and 2005, the atmosphere-only response to increasing greenhouse gas concentrations is an increase in global land temperature and precipitation by up to $0.25 \text{ }^{\circ}\text{C}$ and 10 mm/year , respectively. Finally, in agreement with previous studies (e.g. Wild et al., 2007 and 2008; Wild and Liepert, 2010), we suggest that between about 1950 and 1970, aerosols have “masked” the greenhouse gas impact on the hydrological cycle.

Acknowledgements

The authors thank the MPI Hamburg for providing access to the ECHAM5-HAM code and colleagues at ETH Zürich who contributed to model development, in particular Ulrike Lohmann. This research has partly been supported by the NCCR Climate funded by the Swiss National Science Foundation. The simulations were done on the CRAY XT-5 at the Swiss National Supercomputing Centre (CSCS) in Manno, Switzerland.

Chapter 3

Causes for decadal variations of wind speed over land: Sensitivity studies with a global climate model

Causes for decadal variations of wind speed over land: Sensitivity studies with a global climate model*

A. Bichet¹, M. Wild¹, D. Folini¹, and C. Schär¹

Abstract

Over the past 30 years, observations indicate a decline of about -0.3 m/s in the northern mid-latitudes land surface wind speed. The picture is less conclusive for the Southern Hemisphere and over the oceans. Such a stilling can affect surface evaporation and climate feedback processes, and may impact technical applications such as wind power. Using an atmospheric global climate model, we perform sensitivity experiments for the period 1870-2005 to assess the role of changing roughness length, aerosol emissions, sea surface temperature, and greenhouse gas concentrations in surface wind speed changes.

The wind speed trends simulated by the model generally underestimate the observed trends (land and ocean). Over land, the model can reproduce the observed stilling by increasing the roughness length by a factor of 1.2 to 4.9, depending on region. The other forcings examined can also decrease the 10m wind speeds (up to 15% of observed values in Europe), particularly those related to increasing aerosol emissions (up to -0.2 m/s in India). Compared to observations, the simulated impact of climate forcings on global wind speeds over land and ocean is however small and not always significant

* *Geophysical Research Letter*, 2012, Volume 39, L11701 (doi:10.1029/2012GL051685).

¹Institute for Atmospheric and Climate Sciences, ETH Zürich, Switzerland

3.1 Introduction

Observations indicate that the annual land 10 meter (10m) wind speed has decreased in numerous sites around the globe during the past few decades (e.g. Klink, 1999; Pirazzoli and Tomasin, 2003; Tuller, 2004; Smits et al., 2005; Xu et al., 2006; Roderick et al., 2007; McVicar et al., 2008; Brazdil et al., 2009; Pryor et al., 2009; Vautard et al., 2010, Guo et al., 2011; McVicar et al., 2012). The notion of wind “stilling” was first introduced by Roderick et al. (2007), who have also shown that measurement artefacts are not responsible for the observed trends. Recently, the stilling was acknowledged to be a widespread phenomenon (Vautard et al., 2010; McVicar et al., 2012). This is potentially important for basic climate processes such as evapotranspiration and land-surface atmosphere feedback processes, but also for diverse applications such as wind-power generation and air pollution dispersion (McVicar and Roderick, 2010). In order to better estimate the future trends in surface wind speed, it is essential to understand the causes and patterns of this stilling.

According to Vautard et al. (2010), 25 to 60% of the northern mid-latitude stilling in the past 30 years may be attributed to a recent increase in vegetation cover (e.g. Kauppi et al., 2006; Ciais et al., 2008) and associated changes in roughness length, whereas up to 50% may be attributed to atmospheric circulation changes. The recent increase in vegetation cover observed in the Northern Hemisphere is mostly due to improved silvicultural practices and enhanced fertility (e.g. Kauppi et al., 2006; Ciais et al., 2008). However, given the lack of objective information on past changes in the Northern Hemisphere’s roughness length, Vautard et al. (2010) base their conclusions on regional sensitivity studies for Eurasia (20°-80°E, 30-70°N). In addition, only few studies investigate the contribution from atmospheric circulation changes: Most of them focus on China and stress the dominant role of sea-surface temperatures (SSTs) in controlling the surface wind speed, in particular the land-sea temperature gradient, itself sensitive to aerosol and greenhouse gas concentrations (e.g. Xu et al., 2006; Li et al., 2008; Guo et al., 2011). For the US, Klink (1999) also suggests that a reduced meridional temperature gradient in response to global warming could partly explain the observed wind stilling. Other possible causes for the wind stilling have also been mentioned (e.g. Section 2.4 from McVicar et al., 2012), such as the recent increase in urbanization (Xu et al., 2006), but no dataset covering the roughness increase due to urbanization is currently available to further investigate the issue. In addition, the increasing trend in available soil water (e.g. driven by changes in precipitation and irrigation), which potentially increases the latent heat flux and decreases the sensible heat flux, has also been mentioned (Shuttleworth et al., 2009), but is not discussed in this study.

In our paper, we extend previous sensitivity studies to the global scale, investigating the response of the 10m wind speed to friction changes (roughness length from vegetation) on the one hand, and to changes in atmospheric forcings (sea surface temperatures, aerosol emissions, and greenhouse gas concentrations) on the other hand.

3.2 Methods

We perform climate simulations using the fifth generation of the atmospheric global climate model (GCM) ECHAM5 (Roeckner et al., 2003), at horizontal resolution T42. The methodology follows Bichet et al. (2011) and Folini and Wild (2011). We use a version of ECHAM5 that is coupled to the fully interactive Hamburg Aerosol Module (HAM) (Stier et al., 2005), which predicts the evolution of seven interacting, internally and externally mixed lognormal aerosol modes. A double-moment cloud microphysics scheme is used (Lohmann et al., 2007) that couples to the size-resolved aerosol scheme of HAM and predicts the mass mixing ratios and number concentrations of cloud droplets and ice crystals.

We conduct a series of experiments driven by monthly mean observed SSTs and sea-ice concentrations (Rayner et al., 2003), accounting for different atmospheric forcings. Other forcings used include time varying monthly means of the total solar irradiance (TSI) (Solanki and Krivova, 2003) and of stratospheric optical depth due to aerosols from explosive volcanoes (Sato et al., 1993), as well as time varying annual mean greenhouse gas concentrations taken from observations until 2000 and from the IPCC A1B scenario for 2001-2005 (carbon dioxide, methane, nitrous oxide, ozone, and chlorofluorocarbons). Aerosol emissions of sulphur dioxide, black carbon, and particulate organic matter are taken from the Japanese National Institute for Environmental Studies (NIES) (Roeckner et al., 2006; Stier et al., 2006; Nozawa et al., 2007). They include geographically resolved, time varying monthly mean emissions from wildfires, agricultural burning, and domestic fuel-wood consumption, as well as time varying annual mean emissions from fossil fuel consumption. Stratospheric ozone and land use are both kept at climatological values.

We perform thirty transient experiments running from 1870 to 2005. Thirteen experiments correspond to the control runs (CTRL, “all forcings runs”), for which all the forcings are time varying except for the roughness length which is held constant. Ten experiments are identical to CTRL except that aerosol emissions (anthropogenic and natural, including explosive volcanoes) are held constant at their 1870 values (referred to as AEC), four are identical to CTRL except that SSTs are held constant at their climatological values averaged over the time period 1870-1900 (referred to as SSTC), and three are identical to CTRL except that both, SSTs and aerosol emissions are held constant (referred to as AESSTC). To suppress the “noise” from individual simulations and assess their natural variability, we calculate ensemble means and quantify their uncertainties via the computation of standard deviations. We also compute the 10m wind speed trends and assess their statistical significance.

The sensitivity to increasing roughness length is assessed by conducting 40 years long simulations (using climatological SSTs and climatological aerosol emissions for the period 1860-1900) with the same model configuration, where the monthly climatological values of the land surface roughness (vegetation only) prescribed in the model are multiplied by a factor of 1.5, 2 and 4, respectively. We analyse the last 30 years mean. These simulations are a first step to understand the impact of increasing roughness length, even though the changes in roughness length in the “real world” are both geographically and time dependent. The simple approach is justified as the current knowledge on historic roughness length changes appears too vague to justify transient simulations.

3.3 Sensitivity

3.3.1 Roughness length

The response of the 10m wind speed to a uniform doubling of the vegetation roughness length over land shows strong regional differences, as can be taken from Figure 3.1. As listed in Table 3.1 (columns 4-6), globally increasing the vegetation roughness length in ECHAM5-HAM by a factor of 1.5, 2 and 4 decreases the global land annual 10m wind speed on average by -0.15, -0.26 and -0.55 m/s, respectively. Within this range, the relation is approximately linear at global scale as well as in the selected regions. Assuming this linear approximation and based on the results obtained with roughness length multiplied by 2 (Table 3.1, column 5), we find that in order to reproduce the observed wind stilling (Table 3.1, column 3) by modifying the roughness length only, this latter should increase by a factor of 1.2 to 4.9 over the past 30 years, depending on the region under consideration (Table 3.1, column 7).

These results confirm the results by Vautard et al. (2010) as obtained with a regional climate model and extend their findings to further regions and the global scale.

Consistent with boundary layer theory, most of the impacts of roughness length changes will be local, i.e. occur in the same region as the roughness length changes. Regional changes in vegetation should thus imply a corresponding pattern of wind-speed changes, modulated by the regionally varying response (Figure 3.1). While observations indicate a recent vegetation increase (and associated increase in roughness length) in most of the Northern Hemisphere (e.g. Kauppi et al., 2006; Ciais et al., 2008), it appears unlikely that roughness length changes alone are able to explain the observed wind stilling in all the regions (Table 3.1, column 7). Other forcings may therefore also play a role (see Section 2.4 from McVicar et al., 2012), which could include changes in SSTs, aerosol emissions, and greenhouse gas concentrations.

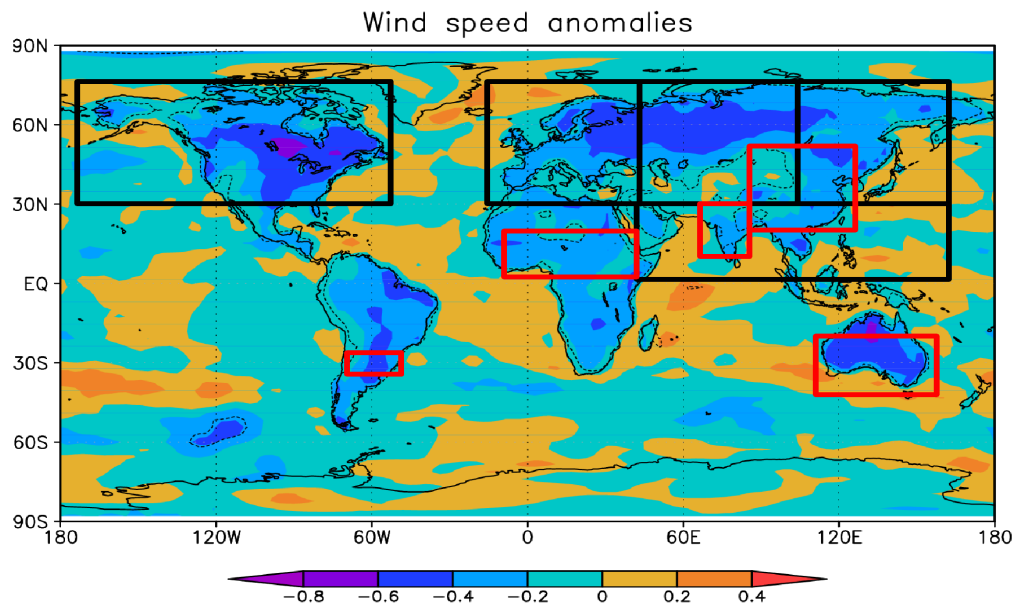


Figure 3.1: Wind speed anomalies (m/s) averaged over 30 years as simulated by ECHAM5-HAM, associated with a doubling of roughness length (vegetation only). The dashed contour lines delimit the areas where anomalies are significant at 99.9% confidence level. The area boundaries for the regions of focus are: Europe 20°W-40°E, 30°-75°N, Central Asia 40°-100°E, 30°-75°N, Eastern Asia 100°-160°E, 30°-75°N, North America 170°-50°W, 30°-75°N and South Asia 40°-160°E, 0°-30°N (as in Vautard et al., 2010, black boxes), and China 90°-130°E, 20°-50°N, India 70°-90°E, 10°-30°N, Sub-Sahara 10°W-40°E, 0°-20°N, Australia 112°-155°E, 45°-20°S, and Argentina 69°-56°W, 26°-35°S (red boxes).

	Wind speed trends (m/s in 30 years)		Wind speed anomalies (m/s)			Factor needed to increase Z0 in ECHAM5-HAM to match observations	Wind speed trend differences (m/s in 30 yrs)	
	CTRL	Obs	(1.5xZ0 - Z0)	(2xZ0 - Z0)	(4xZ0 - Z0)		CTRL-AEC	CTRL-SSTC
Global ocean (4)	0.03	0.24	-	-	-	-	-0.03	0.05
Tropical ocean (4)	0.025	0.12	-	-	-	-	-0.04	0.05
Global land	-0.01	-	-0.15	-0.26	-0.55	-	-0.02	0
North Hemisphere land (1)	-0.01	-0.33	-0.15	-0.26	-0.57	2.5	-0.03	0
Europe (1)	-0.04	-0.27	-0.19	-0.32	-0.73	1.7	-0.05	-0.02
Central Asia (1)	-0.015	-0.48	-0.13	-0.24	-0.53	4	-0.02	0
Eastern Asia (1)	-0.04	-0.36	-0.16	-0.3	-0.62	2.4	-0.02	-0.02
North America (1)	0.01	-0.21	-0.23	-0.36	-0.76	1.2	-0.015	-0.01
South Asia (1)	0	-0.24	-0.14	-0.23	-0.51	2	-0.06	0.03
China (2)	-0.06	-0.54	-0.15	-0.24	-0.5	4.5	-0.025	-0.02
India	0.04	-	-0.15	-0.25	-0.57	-	-0.13	0.08
Sub-Sahara (6)	-0.02	-0.24	-0.15	-0.25	-0.59	1.9	-0.05	0.01
South Hemisphere land	0	-	-0.13	-0.24	-0.48	-	0	0.01
Australia (3,5,6,7,8)	0.07	-0.22*	-0.28	-0.46	-0.92	1	0.05	0.05
Argentina (1,8)	0.06	-0.69	-0.15	-0.28	-0.57	4.9	0.03	0.06

Table 3.1: Wind speed trends and anomalies (m/s in 30 years). Columns 2 and 3 compare the annual trends in 10m wind speed as simulated in the CTRL ensemble mean (30 years trend over the time period 1975-2005) and as observed (30 years trend over or scaled to the time period 1975-2005). Columns 4-6 show wind speed anomalies (averaged over 30 years) between the simulations with increased roughness length (Z0x1.5, Z0x2 and Z0x4) and the simulations with climatological roughness length (Z0). Column 7 estimates the factor by which roughness length needs to increase in order to reach the observed stilling, assuming a linear approximation and based on the results obtained with roughness length multiplied by 2 (column 5). Columns 8-9 show the differences between wind speed trends (1975-2005) simulated in the CTRL and the AEC and SSTC ensemble means, respectively. The values indicated in “bold” are statistically significant at 80%. The area boundaries for the regions of focus are described in Figure 3.1. Observations are from Vautard et al. (2010) (1), Guo et al. (2011) (2), Roderick et al. (2007) (3), Wentz et al. (2007) (4), McVicar et al. (2008) (5), Donohue et al. (2010) (6), Troccoli et al. (2011) (7), McVicar et al. (2012) (8), and Oguntunde et al. (2011) (9).

* Average over the observed 2m wind speed trends (instead of 10m) due to conflicting results between observed 2m and 10m wind speed trends in Australia (Troccoli et al., 2011 and McVicar et al., 2012).

3.3.2 SSTs, aerosol emissions, and greenhouse gas concentrations

SSTs, aerosol emissions, and greenhouse gas concentrations can affect the atmospheric circulation and stability, and thereby surface wind speeds (e.g. Ramanathan et al., 2001; Meehl et al., 2007). In our modelling framework, these factors are assessed using simulations with prescribed SSTs. Therefore, these sensitivity experiments evaluate the atmosphere-only impact of greenhouse gases and aerosols on wind speed. Note also that in this set-up, the effects of previous greenhouse gas and aerosol emissions may partly be encapsulated in the transient SST evolution.

Since 1870, the CTRL ensemble mean (using all time-varying forcings but climatological roughness length) exhibits considerable decadal variations in annual-mean 10m wind speed (Figure 3.2, black curves). In addition, it also exhibits long-term wind trends after the 1950s, which are either negative (e.g. Southern Hemisphere land and China) or positive (e.g. India). Over the past 30 years, these trends are generally smaller than indicated by observations (Table 3.1, column 2-3), but statistically significant at 80% in Central Eurasia, China and Sub-Sahara (Table 3.1, column 2, “bold” entries, and Figure 3.1 from the Supplementary Material). Note that these trends are roughly 5 to 15 times smaller in all regions when compared to observations, so that the effect of SST variability, as well as aerosols and greenhouse gases may only explain a minor part of the observed wind speed trends at global scale.

Based on the sensitivity experiments with varying (CTRL, black curves) and constant (SSTC, blue curves) SSTs, Figure 3.2 shows that transient SSTs explain a considerable fraction of the decadal variations since 1870, but not the long-term trends. In the past 30 years, the difference between their respective linear trends (Table 3.1, column 9) shows that transient SSTs, as compared to constant SSTs, either increase (e.g. 0.08 m/s in the past 30 years in India) or decrease (e.g. -0.02 m/s in the past 30 years in Europe) the annual land 10m wind speed, depending on the region. These trend anomalies, however, are significant at 80% only in small areas located mostly in Eurasia and Sub-Sahara (Table 3.1, column 9, “bold” entries, and Figure 3.2b from the Supplementary Material).

Based on the sensitivity experiments with varying (CTRL, black curves) and constant (AEC, red curves) aerosol emissions, Figure 3.2 shows that in most regions, the atmosphere-only response of the annual 10m wind speed to variable aerosol emissions is a decrease of up to -0.15, -0.1 and -0.08 m/s in India, Sub-Sahara and China, respectively, after about 1950. Over the past 30 years, the respective linear trends (Table 3.1, column 8) show that in most regions, the atmosphere-only response of the annual 10m wind speed to aerosol emissions is a wind speed reduction of -0.13, -0.05 and -0.03 m/s in India, Sub-Sahara and China, respectively (average linear trends, Table 3.1, column 8). These trend anomalies are significant at 80% only in small areas located in Eurasia and Sub-Sahara (Table 3.1, column 8, “bold” entries, and Figure 3.2a from Supplementary Material). In most regions, aerosols have a larger impact in summer, decreasing the surface wind speeds by a maximum of -0.3 and -0.25 m/s in India since 1950 and 1975, respectively (not shown).

Based on the sensitivity experiments with constant SSTs and constant aerosol emissions (AESSTC, green curves), Figure 3.2 shows that after about 1950, the atmosphere-only response to the remaining external forcings (i.e. increasing greenhouse gas concentrations and TSI variations) is an increase in the 10m wind speed. However, their impacts are relatively small after 1950 and almost negligible after 1975 (maximum impact of +0.03 m/s after 1975), suggesting that greenhouse

gases combined with TSI have only a small atmosphere-only impact on the 10m wind speed, and act mostly through the SSTs feedbacks. This result was expected since there is no oceanic feedback in these simulations.

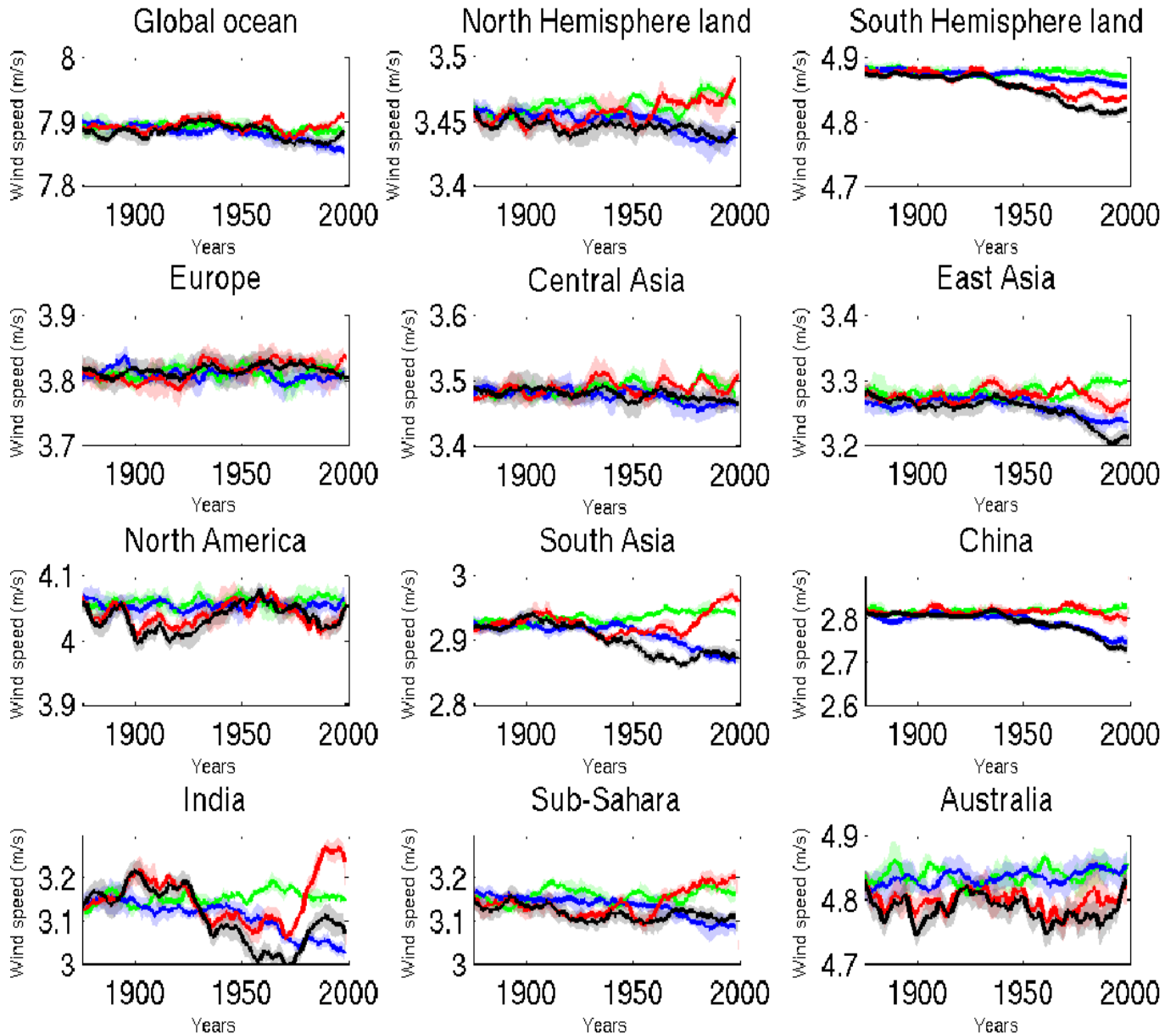


Figure 3.2: Mean annual wind speed over the land portion of selected areas (m/s), as simulated with transient solar, greenhouse gas, aerosol and SST forcings (CTRL, black) in comparison to selected sensitivity experiments: Constant aerosol emissions (AEC, red), constant SSTs (SSTC, blue) and constant aerosol emissions and SSTs (AESSTC, green). The bold lines show the respective ensemble means, the shaded region the standard deviation of the simulations.

3.4 Discussion

Our study shows that over land, increasing the roughness length clearly reduces the annual 10m wind speed over most parts of the globe, with amplitudes that depend on the region (Table 3.1, column 4-6, and Figure 3.1). However, the changes in roughness length required to reproduce the observations of the past 30 years are not necessarily realistic everywhere (Table 3.1, column 7), and other factors may have to be taken into account. The existence of such factors is illustrated by the black curves in Figure 3.2, showing that the 10m wind speed simulated in the CTRL ensemble mean decreases after about 1950 in most of the northern hemispheric lands, despite being forced by climatological roughness length. According to Table 3.1 (column 2-3), the wind stilling trends simulated (CTRL) over the past 30 years represents 12% (ratio of the CTRL ensemble mean (Table 3.1, column 2) over observations (Table 3.1, column 3)) of the wind speed trend observed over the global oceans, and 3% of the wind speed trend observed over the northern hemispheric lands. However, regionally, this ratio reaches substantially higher values such as 20% in the tropical ocean, 15% in Europe, and 11% in China and Eastern Asia. Note that in China, this ratio reaches up to 20% in the summer averages (Guo et al., 2011).

In our simulations, we find that over land, the factors decreasing the 10m wind speed depend upon the region (Figure 3.2) and season (not shown) under consideration. For instance, whereas past SST variations are a dominant factor (aside from potential roughness length changes) in North America and Australia (compare black and blue curves in Figure 3.2), they have almost no impact in China. Similarly, aerosol emissions reduce the land 10m wind speed over most of the globe, but with a magnitude that depends on the region (compare black and red curves in Figure 3.2). Some regions are also strongly affected by both forcings, such as in India, where SSTs increase the annual 10m wind speed in the past few decades but aerosols “slow down” this increase (Figure 3.2). Note that over the ocean, the increasing 10m wind speed trend (global and tropical) is also “slowed down” by the aerosol emissions (Figure 3.2).

This regionally diverse response is consistent with the fact that SST-induced circulation changes have a regional character and can decrease or increase the 10m wind speeds. In contrast, higher aerosol concentrations appear to generally reduce the 10m wind speeds (land and ocean). This rather uniform response could be related to the role of atmospheric aerosols upon the stratification of the atmosphere. Whereas increasing aerosol emissions cool the surface, especially carbonaceous aerosols also warm the aerosol layer in the troposphere. This will increase the atmospheric density gradient between the surface and the troposphere, and thus slow down the atmospheric circulation (e.g. Ramanathan et al., 2005). In essence, increases in stratification have a tendency to decouple the planetary boundary layer from the atmospheric layers aloft, thereby reducing the influence of the upper-level winds at the surface. Our results show that the atmospheric stability simulated in the CTRL ensemble mean has increased since 1950 mostly in eastern Asia, Africa, Middle East, south-eastern North America, and South America. In eastern Asia and Africa, this is largely due to aerosols (Figure 3.3 from Supplementary Material). Simulated trends at different altitudes also suggest that aerosols decrease the global land and oceanic wind speed trends up to 850hPa, which supports this hypothesis (Figure 3.4 from Supplementary Material).

In addition, our results illustrate the land/ocean contrast, showing an increasing (+0.03 m/s in 30 years) and decreasing (-0.01 m/s in 30 years) trend in the global oceanic and land 10m wind

speed, respectively. According to our results, the increase in oceanic 10m wind speed is mostly due to the impact of SST variations in the tropics and the Southern Hemisphere (see Figures 3.1 and 3.2b in Supplementary Material). As previously noted, this increasing trend over the global ocean would be more pronounced without the aerosol emissions.

Finally, the latitudinal dependence pointed out by McVicar et al. (2012), showing decreasing and increasing trends in the mid and high latitudes ($\sim > 70^\circ$), respectively, is reproduced in our experiments in the Northern Hemisphere, although the results are not statistically significant (Figure 3.1 from Supplementary Material).

3.5 Conclusions

In line with Vautard et al. (2010), we find that over land, the recent increases in roughness length, for instance caused by increasing vegetation (e.g. Kauppi et al., 2006; Ciais et al., 2008), could well explain a significant fraction of the decrease in the terrestrial 10m wind speed observed globally. This stresses the need for a better analysis of roughness length changes over the past decades, and motivates scenarios of such changes in the future. In addition to roughness length changes, we find that changes in other climate forcings contribute to the land wind stilling after 1950, by a magnitude representing up to 15% of the observed trends. In particular, we find increasing aerosol emissions to generally reduce the land 10m wind speed, especially in summer. The simulated aerosol impacts are larger in Asia where the trends of aerosol emissions are particularly large, and where the simulated decrease in summer wind speeds amounts to up to 0.3 m/s after 1950. Over the oceans, we find that aerosol emissions “slow down” the simulated increasing trend of the 10m wind speed. Nevertheless, the simulated response to variables SSTs and aerosol emissions remain a factor of 5 to 15 smaller than observed wind speed trends.

Acknowledgements

The authors thank the MPI Hamburg for providing access to the ECHAM5-HAM code, colleagues at ETH Zürich and the Centre for Climate System Modelling C2SM who contributed to model development, in particular Ulrike Lohmann, Sylvaine Ferrachat, and Grazia Frontosa, as well as Tanja Stanelle for extensive discussions on roughness lengths. This research has partly been supported by the NCCR Climate funded by the Swiss National Science Foundation. The simulations were done on the CRAY at the Swiss National Supercomputing Centre (CSCS) in Manno, Switzerland.

Supplementary Material

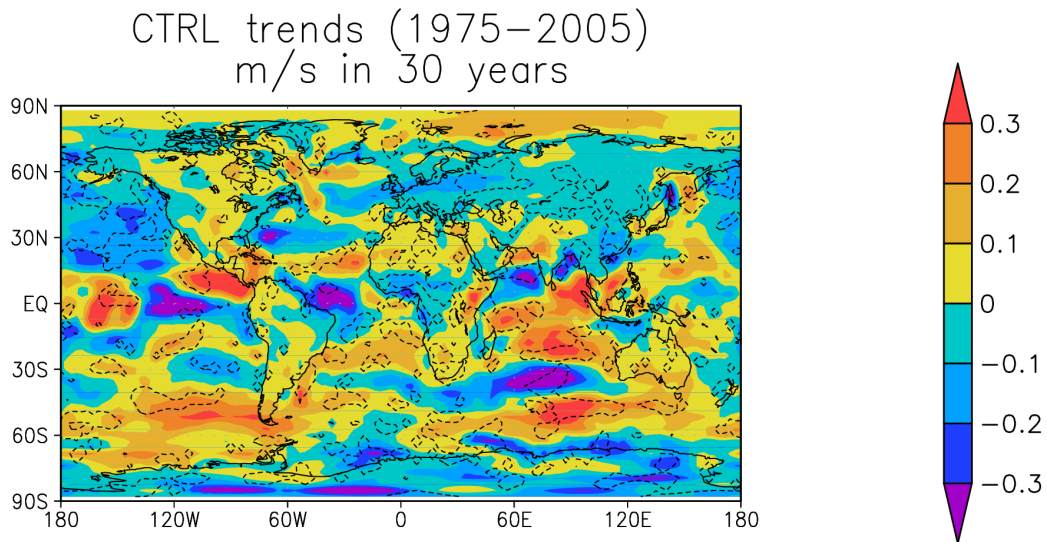


Figure 3.3: 10m wind speed trends (1975–2005) in m/s in 30 years, as simulated in the CTRL ensemble mean. Dashed contour lines delimit the areas where trends are significant at the 80% confidence level.

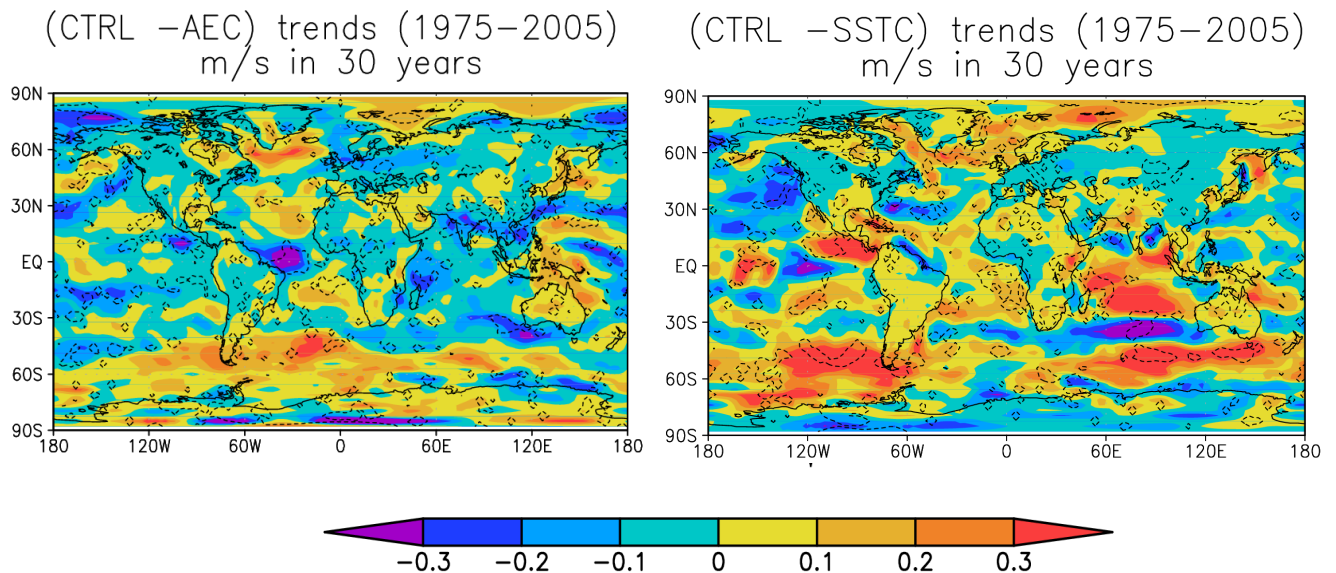


Figure 3.4: Anomalies (CTRL–AEC and CTRL–SSTC) of 10m wind speed trends (1975–2005), in m/s in 30 years. Dashed contour lines delimit the areas where trends are significant at the 80% confidence level.

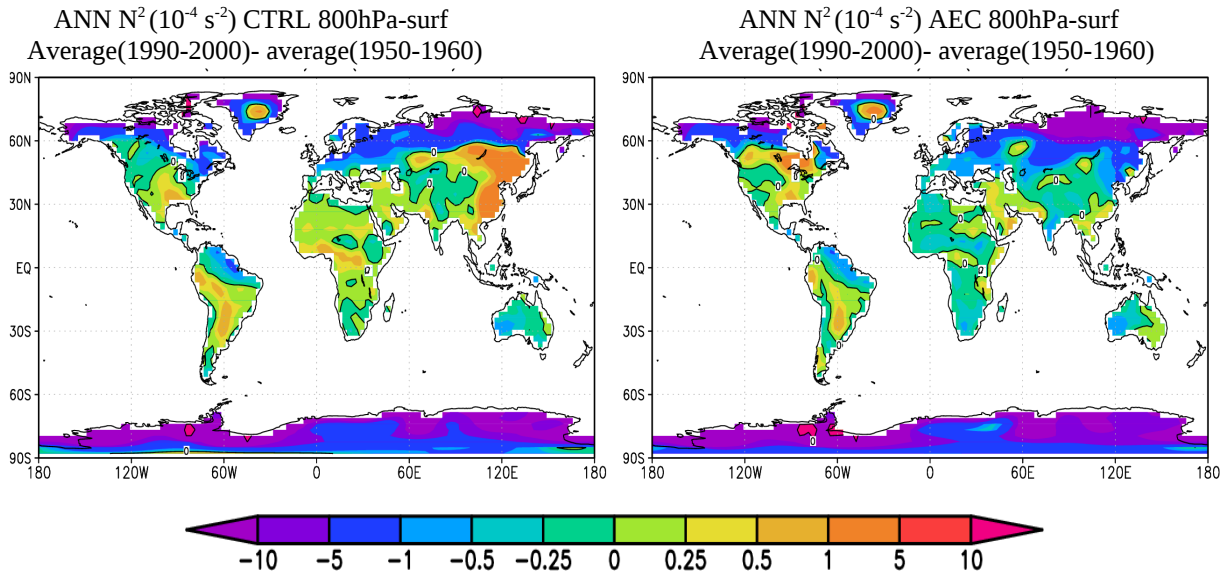


Figure 3.5: Anomalies (average(1990-2000)-average(1950-1960)) of the N^2 (Brunt-Vaisala frequency) (10^{-4} s^{-2}), as simulated in the CTRL (a) and AEC (b) ensemble means.

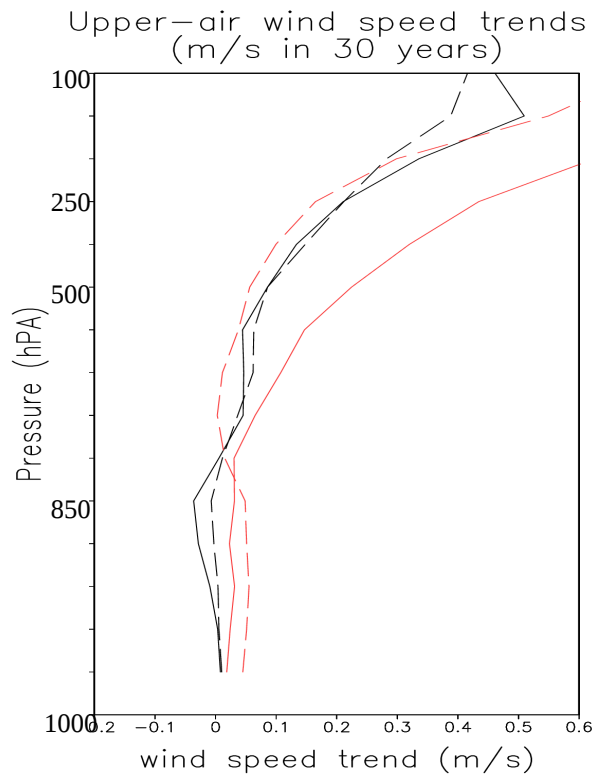


Figure 3.6: Mean vertical profile of wind speed trends, as simulated in the CTRL (solid curve) and AEC (dashed curves) ensemble means, globally averaged over land (black curves) and ocean (red curves).

Chapter 4

Sensitivity of European precipitation in the late 19th century

Sensitivity of European precipitation in the late 19th century*

A. Bichet¹, D. Folini¹, M. Wild¹, and C. Schär¹

Abstract

In central Europe, an unusually large number of floods was recorded in the summers and autumns of the late nineteenth century, causing important damages. Different factors contributing to the occurrence of these floods have been discussed in the literature, including the unusually high precipitation anomalies recorded at the time. Based on the frequency and spatial pattern of these floods, previous studies suggest that changes in the large-scale circulation may have played a relevant role. Here, we use an atmospheric global climate model forced with observed sea surface temperatures and all atmospheric forcings to test this hypothesis and identify causes for the associated atmospheric circulation pattern.

We find that our model is able to reproduce the high summer precipitation anomalies observed in central Europe in the 1880s. We show that between 1875 and 1890, transient sea surface temperatures, as opposed to climatological ones, are the primary driver for this precipitation increase. Using a series of numerical experiments, we find more specifically that the SST variability in the tropical Pacific associated with the El Niño /Southern Oscillation is the main reason behind the central European precipitation anomaly from 1875 to 1890. The atmospheric circulation anomalies associated with wet summers show a PNA-like pattern over North America, a substantially weakened mid-troposphere westerly flow over Europe and the North Atlantic, and reduced pressure over Europe. In addition, we find that increasing anthropogenic aerosol emissions further enhanced the late nineteenth century central European precipitation by about 50%.

* Submitted to Quarterly Journal of the Royal Meteorological Society (May 10, 2012)

¹ Institute for Atmospheric and Climate Sciences, ETH Zürich, Switzerland

4.1 Motivation

An unusually large number of floods were recorded in Switzerland (e.g. Pfister, 1999, Schmocker-Fackel and Naef, 2010a) in the summers and autumns of the late nineteenth century, leading to important life losses and large material damages. For the event of autumn 1868 alone, reported damages amounted to between 1.4 and 4 billion inflation-adjusted Swiss Francs (Pfister, 2003 and 2009).

In June 1876, the city of Basel was severely flooded as the Rhine River reached a maximum peak runoff of about $5700 \text{ m}^3 \text{ s}^{-1}$ (compared to long-term mean annual peak flows of $2330 \text{ m}^3 \text{ s}^{-1}$) (Glaser, 2010; Wetter et al., 2011). According to Röhlisberger (1991), the floods were triggered by “long lasting excessive rainfall and intense thunderstorms on saturated soils” along the northern slopes of the Alps. Besides the Basel areas, also parts of the Swiss Plateau, the canton of Uri, and the Grison were flooded. In 1882, Basel was flooded again in late December (25 to 27), when the mean daily discharge of the Rhine reached $4371 \text{ m}^3 \text{ s}^{-1}$ at the station Basel Rheinhalle, which is the 5th highest value in the station history. Damages were reported from western to northern parts of Switzerland (Röhlisberger, 1991). Already the autumn 1882 had been fairly wet along the northern slopes of the Alps, and after a dry early December, heavy precipitation and snowfall were again observed along the northern slopes on the Alps in late December. Röhlisberger (1991) reported “sudden snowmelt and extraordinary rainfall” as triggering factor for the flood. Severe floods and landslides were also recorded in eastern Switzerland and Ticino in August 1890, partly due to heavy rainfall over the canton of Ticino and in the Rhine valley (120 mm at Bad Ragaz on 24 August 1890). The Rhine dams even broke in Vorarlberg (eastern Austria), which led to the flooding of the Alpine Rhine valley. Lake Constance rose by 1.5 meters from 24 August to 2 September 1890, and Lake Walensee by 2 meters between 28 and 31 August 1890.

Similar floods were observed in most of the Alpine Arch and manifested in the lowlands of western and central Europe (including the Po Valley). In December 1880, the Meuse River flooded after the water rose by 4 meters above its usual level, reaching the highest level of the century (Nienhuis, 2008). In September 1890, extended rainfall in southern Bohemia triggered large floods in Czech Republic along the Elbe (Mudelsee et al., 2004) and the Vltava (Brazdil et al., 2005) Rivers. While the former river reached a maximum peak runoff of $4450 \text{ m}^3 \text{ s}^{-1}$ (compared to a mean discharge of $312 \text{ m}^3 \text{ s}^{-1}$), the latter rose by 2 meters above its usual level, and swept away three arches of the Charles Bridge (Prague). In Prague, this flood was described as one of the worst floods of all time (Brazdil et al., 2005). Two months later, due to long-lasting rainfall, exceptionally strong floods occurred in Germany along the Werra River, with maximum peak discharge reaching $300 \text{ m}^3 \text{ s}^{-1}$ in Meiningen, and $1248 \text{ m}^3 \text{ s}^{-1}$ in Hann Munden (Mudelsee et al., 2006).

At the time, deforestation in the Alpine region was seen as the main cause for these floods, which led to a series of “reforestation laws”, successively established in France (1860), Switzerland (1876), Italy (1877) and Austria (1884) (e.g. Pfister, 2003). However, high precipitation anomalies were also observed in central Europe in the summers and autumns of the late nineteenth century (Hegg and Vogt, 1997; Pfister, 1999, 2003; Benito et al., 2003; Bader and Bantle, 2004; Brazdil et al., 2006; Pauling et al., 2006; Casty et al., 2007), and suggest that climate variations may have been a primary cause. This is also evident from the early precipitation observations in Switzerland (Begert et al., 2005).

Previous attempts to connect the changes in the late nineteenth century flood frequency with external parameters such as solar activity (e.g. Pauling and Paeth, 2007), North Atlantic Oscillation (NAO) (Frei et al., 2000; Casty et al., 2005; Schmocker-Fackel and Naef 2010b), and mean air temperature (e.g. Schmocker-Fackel and Naef, 2010b), have not been conclusive. Nevertheless, even though individual flood events across Europe do not match, the reoccurrence of their spatial patterns through time suggests that the changes in flood frequency are most likely due to changes in the atmospheric circulation patterns on decadal time scale (Schmocker-Fackel and Naef, 2010a and 2010b). Previous studies link these historical floods to changes in the large scale circulation over the North-Atlantic-European region (e.g. Wanner et al., 2004), and in particular to the patterns of the “Vb cyclone tracks” (e.g. Jacobeit et al., 2004, Kundzewicz et al., 2005, Schmocker-Fackel and Naef 2010b), which appear to have been especially relevant in the late nineteenth century (Jacobeit et al., 2004, Schmocker-Fackel and Naef, 2010b). The “Vb cyclone tracks” are associated with cyclogenesis in the Gulf of Genoa, followed by the propagation of the cyclone over the Eastern Alps towards southern Germany, Czech Republic and Poland. This type of weather pattern is well-known for its potential for severe flooding to the north of the Alps (e.g. Medelsee et al., 2004), and has also played a crucial role in recent extreme flood events such as the Elbe/Vltava flood in 2002 (Sodemann et al., 2009) or the Alpine flood in August 2005 (Hohenegger et al., 2008).

As the storm track changes with the large-scale flow, changes in the large-scale atmospheric circulation also affect European precipitation. In particular, previous studies show that the El Nino/Southern Oscillation (ENSO) can affect the European precipitation, even though the link is not stationary through time and it is expected to affect precipitation mostly in winter and spring (e.g. Brönnimann, 2007 Brönnimann et al., 2007, Bulic and Brankovic, 2007). Previous studies (Dettinger et al., 2000a and 2000b) nevertheless find that the runoff of European rivers in summer increases after El Nino events.

In our study, we aim to investigate the role of precipitation as a main cause leading to the late nineteenth century floods in Europe, by studying the sensitivity of European precipitation and associated circulation patterns to different climate forcings for the period 1870-1900, using an atmospheric Global Climate Model (GCM) forced with prescribed, observation based Sea Surface Temperatures (SSTs).

4.2 Methods

4.2.1 Model set up and experimental design

We perform climate simulations using the atmospheric GCM ECHAM5 (Roeckner et al., 2006), at horizontal resolution T42. The methodology follows Bichet et al. (2011) and Folini and Wild (2011). We use a version of ECHAM5 that is coupled to the fully interactive Hamburg Aerosol Module (HAM) (Stier et al., 2005), which predicts the evolution of seven interacting, internally and externally mixed log-normal aerosol modes. A double-moment cloud microphysics scheme is used (Lohmann et al., 2007), which couples to the size-resolved aerosol scheme of HAM and predicts the mass mixing ratios and number concentrations of cloud droplets and ice crystals. We conduct a series of experiments driven by monthly mean observed SSTs and sea-ice concentrations (Hadley Enter, Rayner et al., 2003), and accounting for the following time-varying atmospheric forcings:

monthly mean total solar irradiance (Solanki and Krivova, 2003), stratospheric optical depth due to aerosols from explosive volcanoes (Sato et al., 1993), greenhouse gas concentrations taken from observations until 2000 and from the IPCC A1B scenario afterwards, and aerosol emissions from the Japanese National Institute for Environmental Studies (NIES) (Roeckner et al., 2006, Stier et al., 2006, Nozawa et al., 2007).

We perform 104 transient experiments grouped in 8 ensembles of 13 members, as listed in Table 4.1. All simulations start in 1870, after a spin-up phase of typically 10 years (3 months only in a few cases), which allows the soil moisture to reach equilibrium. The control ensemble (CTRL) is forced with all the time-varying forcings mentioned above, and covers the time period 1870-2005. The seven sensitivity ensembles cover the time period 1870-1900 only. Each of the sensitivity ensembles is identical to CTRL except for one particular aspect, namely (Table 4.1): Aerosol emissions (anthropogenic and volcanic) are held constant at their 1870 level throughout the experiments (AEC); Anthropogenic aerosol emissions only are held constant at their 1870 level throughout the experiments (AECVT); Climatological mean SSTs (defined by the period 1870-1900) are used throughout the experiments (SSTC); Climatological mean SSTs are used in the North Atlantic ($\sim 90^{\circ}\text{W}$ - 60°E ; 0° - 90°N) only, transient SSTs elsewhere (AOC); Transient SSTs are used in the North Atlantic only, climatological mean SSTs elsewhere (AOT); Climatological mean SSTs are used in the Pacific Ocean (120°E - 75°W ; 90°S - 90°N) only, transient SSTs elsewhere (POC); Climatological mean SSTs are used in the “El Nino region” (170°E - 75°W ; 30°S - 20°N) only, transient SSTs elsewhere (NINOC). The SST climatology is taken over the 1870-1900 time period to have a similar SST mean values when using “transient” and “climatological” SSTs.

Name of ensemble mean	Time-period	SSTs	Aerosol emissions
CTRL	1870-2005	Transient SSTs	Time-varying since 1870
SSTC	1870-1900	Climatological SSTs	Time-varying since 1870
AEC	1870-1900	Transient SSTs	Constant at 1870 value
AECVT	1870-1900	Transient SSTs	Anthropogenic: Constant at 1870 value Volcanic: Time-varying since 1870
AOC	1870-1900	Atlantic Ocean: Climatological SSTs Other: Transient SSTs	Time-varying since 1870
AOT	1870-1900	Atlantic Ocean: Transient SSTs Other: Climatological SSTs	Time-varying since 1870
NINOC	1870-1900	NINO region: Climatological SSTs Other: Transient SSTs	Time-varying since 1870
POC	1870-1900	Pacific Ocean: Climatological SSTs Other: Transient SSTs	Time-varying since 1870

Table 4.1: Summary of the different simulations. All experiments are forced with time-varying greenhouse gas concentrations since 1870. Each ensemble contains 13 experiments. The “transient SSTs” correspond to the transient SSTs values taken from observations (Rayner et al., 2003), and the “climatological SSTs” correspond to the climatological mean of these transient SSTs, averaged over the time period 1870-1900.

Throughout this study, we suppress the “noise” from individual simulations by computing ensemble means, and evaluate the ensemble spread via the computation of the standard deviation. Note that the ensemble spread is conditional on several aspects such as the model physics, biases, and the climate internal variability. Inspecting observed precipitation data for individual (Casty et al., 2007) months suggests that anomalously wet months in the late nineteenth century occurred preferentially from June to October (JJASO). In the following, we therefore focus on the five months period JJASO, and refer to this period as “summer”.

4.2.2 Observational data

Gridded, reconstructed precipitation datasets by Pauling et al. (2006) and Casty et al. (2007) both go back prior to 1900, and cover the European land area at a resolution of 0.5 degree. The two datasets use different reconstruction methods, but both use the reanalysis “CRU TS 2.1” (CRU, from Mitchell and Jones, 2005) for calibration purposes, via the principle component regression technique. One dataset (Casty et al., 2007) covers the area 50°W-40°E, 30°-80°N since 1766, the other one (Pauling et al., 2006) covers the area 30°W-40°E, 30°-71°N since 1500. The dataset from Pauling et al. (2006) is only available as seasonal means, so the individual months cannot be isolated, and hence cannot be used in our study. We checked however, that the seasonal time series from both datasets (Pauling et al., 2006 and Casty et al., 2007) are very similar (not shown). The CRU dataset is based on historical measurements and was assembled by the Climate Research Unit of the University of East Anglia. It covers the global land area between 1901 and 2002 at a monthly resolution, on a 0.5 degree grid. Finally, we also consider the reanalysis product by Compo et al. (2011), which contains global precipitation since 1871 on a 2 degree grid. The reanalysis is based on the method of Whitaker and Hamil (2002) and assimilates observed surface pressure and sea level pressure every 6 hours.

4.3 Results

4.3.1 Observed and simulated European precipitation in the late 19th century

Figure 4.1 shows the 11-year running mean summer (JJASO) land precipitation anomalies (ref=1901-2000) in central Europe (2-30°E; 44°-55°N), as simulated (CTRL, black curve) and observed (CRU, red curve; Casty et al., 2007, green curve, and the reanalysis from Compo et al. 2011, blue curve). According to Figure 4.1, the central European land precipitation anomalies from the two observational datasets (CRU and Casty et al., 2007) are in good agreement after 1900. The reanalysis (blue curve) reproduces the high precipitation anomalies in central Europe in the late nineteenth century, but also shows another phase of increased precipitation around 1910, which is not present in observations.

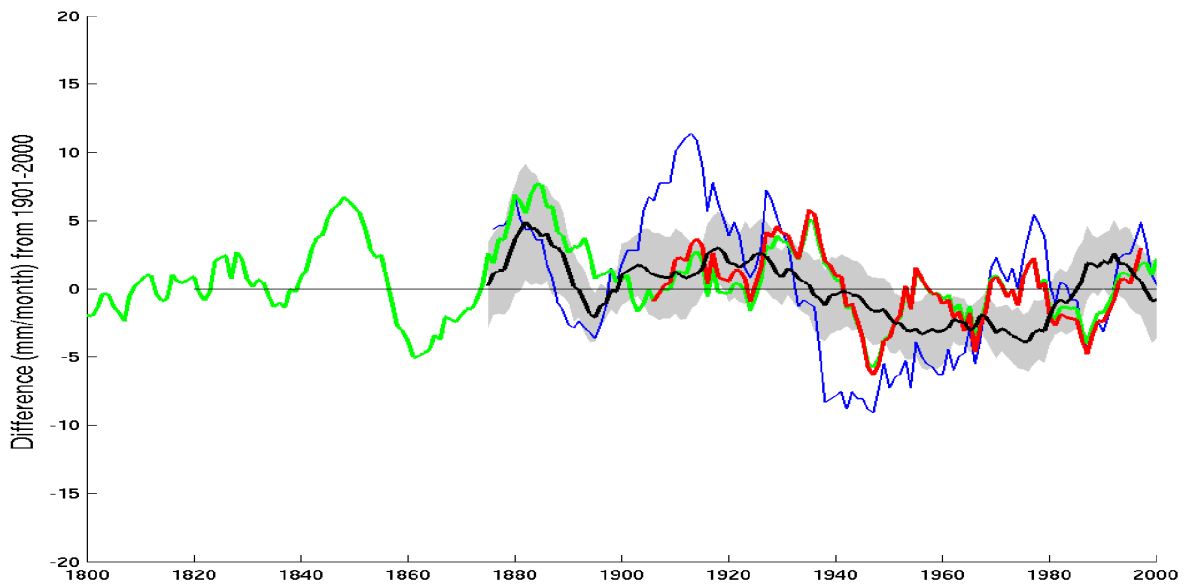


Figure 4.1: Summer (JJASO) land precipitation anomalies (ref= 1901-2000) observed and simulated in central Europe (2° - 30° E, 44° - 55° N) between 1800 and 2000, shown as 11-year running means (mm/month). Shown are the historical measurements from Mitchel et al. (2005, CRU, red curve), the reconstructions from Casty et al. (2007, green curve), the reanalysis from Compo et al. (2011, blue curve), and the simulations from the CTRL ensemble mean (black curve). The shaded area corresponds to ± 1 sigma from the simulated precipitation anomalies.

The CTRL ensemble mean (black curve) captures the high precipitation anomalies in the 1880s, and qualitatively follows the observations in the twentieth century (slightly wet until the 1940s and drier afterwards, until about the 1990s). Note, however, the large ensemble spread of the CTRL ensemble between about 1875 and 1890. According to Figure 4.2, the ensemble even contains some anomalously dry summers. The reproducibility of the observed wet summers is thus probabilistic, rather than deterministic. Nevertheless, a Mann-Whitney test (p-value < 0.05) confirms that average precipitation was high in the 1880s as compared to the long term mean 1870-2005, both in observations and CTRL.

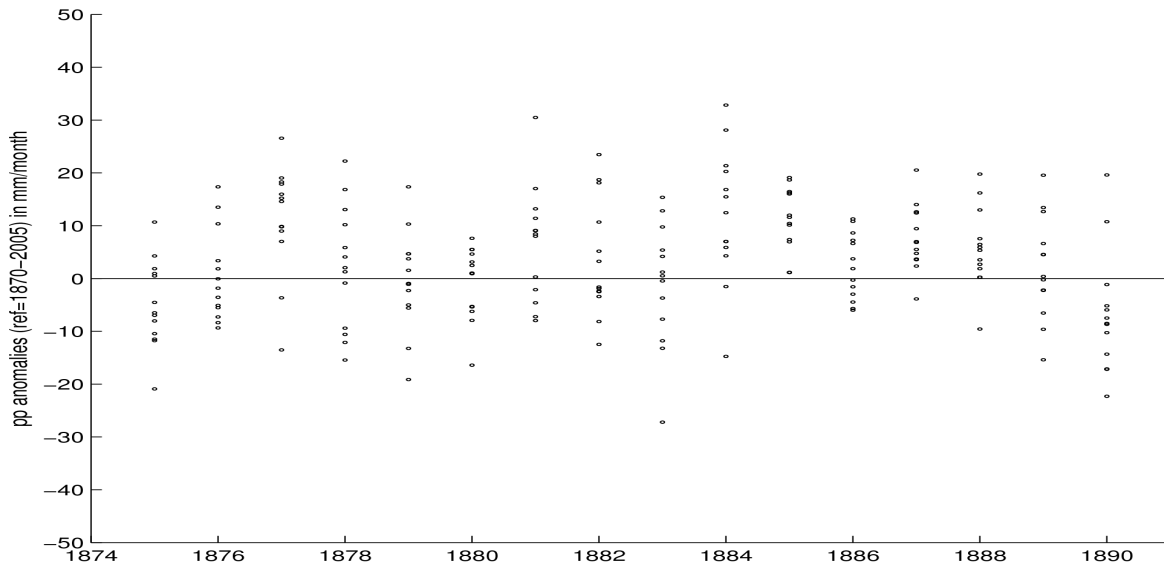


Figure 4.2: Summer (JJASO) precipitation anomalies (ref=1870-2005) simulated for each year between 1875 and 1890, as simulated in the 13 individual members of the CTRL ensemble (mm/month).

Figure 4.3 displays the geographical distribution of the observed and simulated JJASO precipitation anomalies averaged over the 1875-1890 time period. All panels show a dipole pattern with high values in central Europe (2° - 30° E, 44° - 55° N) and low values in Scandinavia. There are, however, significant differences in the spatial details: Casty et al. (2007) reconstruct the precipitation maximum near the Alps and the Adriatic Sea, Compo et al. (2011) find it further to the east, while in our simulations it is located further north. There are also differences in the Mediterranean, with a dry anomaly over Northern Italy and Spain in the reanalysis.

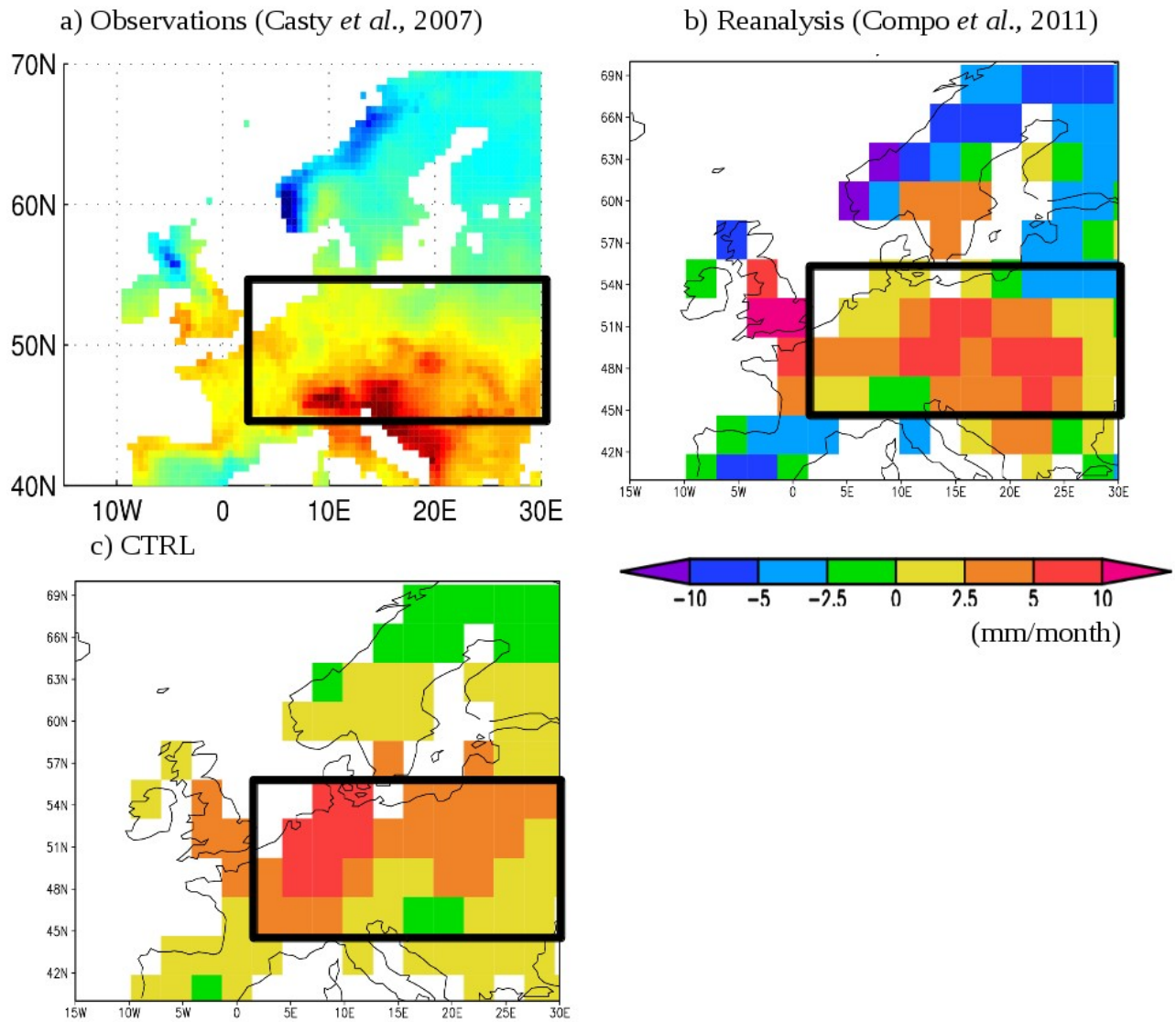


Figure 4.3: Maps of summer (JJASO) land precipitation anomalies (ref=1870-2005) averaged over the 1875-1890 time period (mm/month). Shown are the observations from Casty et al. (2007, a), the reanalysis from Compo et al. (2011, b), and the simulations from the CTRL ensemble mean (c). The area delimited by the black box corresponds to the region referred to as “central Europe” (2°-30°E; 44°-55°N).

4.3.2 Sensitivity of simulated precipitation to forcings

Given the overall satisfactory agreement between the observed and simulated precipitation patterns in the late nineteenth century, we expect that more can be learned on the cause of this wet anomaly from our sensitivity studies. Because the probabilistic nature of our results requires ensembles of simulations, we restrict the sensitivity experiments to the time period 1870-1900. The purpose of these simulations is to assess the sensitivity of the simulated 1870-1900 precipitation anomalies to the main climate forcings, namely SSTs and aerosol emissions.

4.3.2.1 SSTs and aerosol emissions

Figure 4.4 shows the summer land precipitation anomalies (11-year running means, ref=1875) averaged over central Europe (2° - 30° E; 45° - 55° N) as simulated in the CTRL (black curve), SSTC (blue curve), AEC (red curve), and AECVT (green) ensemble means for the time period 1870-1900.

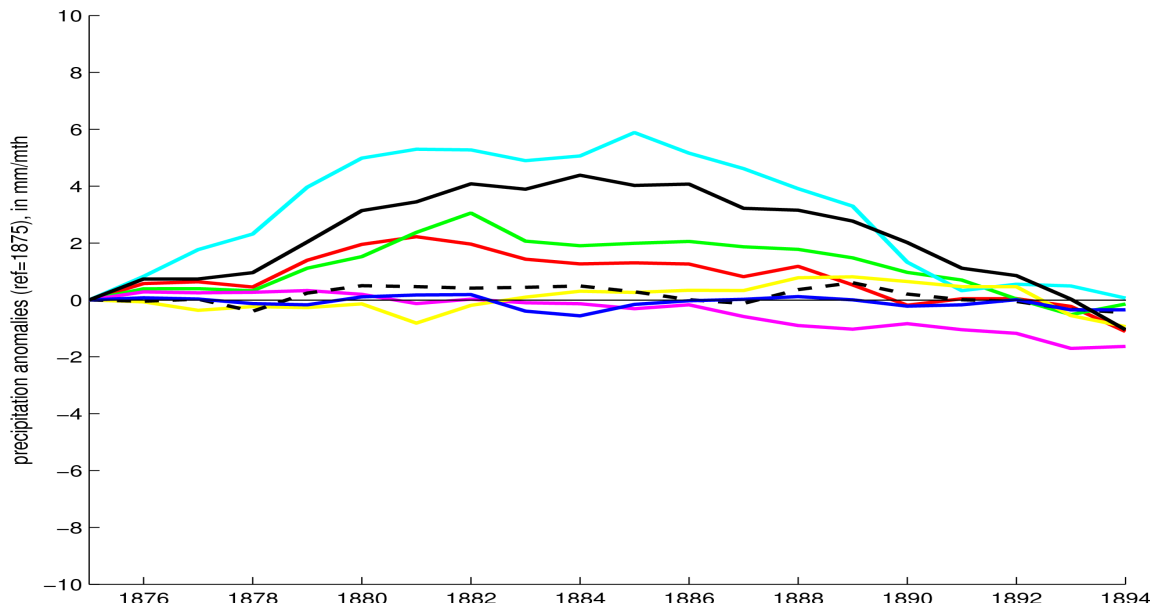


Figure 4.4: Summer (JJASO) land precipitation anomalies (ref= 1875) averaged over central Europe (2° - 30° E; 45° - 55° N), shown as 11-year running means (mm/month). Shown are the ensemble means from CTRL (black), SSTC (blue), AEC (red), AECVT (green), AOT (magenta), AOC (cyan), POC (yellow) and NINOC (dashed black).

The comparison of the black (CTRL) and blue (SSTC) curves in Figure 4.4 shows that transient SSTs, as opposed to climatological SSTs, increase the late nineteenth century summer precipitation in central Europe: The high precipitation anomalies simulated in the CTRL ensemble mean (black curve) in late nineteenth century are no longer simulated in the SSTC ensemble mean (blue curve). A Mann-Whitney test confirms that the median values of the two ensembles indeed differ (p-value < 0.05 for the period 1875 – 1890).

The comparison of the black (CTRL) and red (AEC) curves in Figure 4.4 shows that transient aerosol emissions (anthropogenic and volcanic) contribute to the late nineteenth century summer precipitation in central Europe (p-value from mw-test < 0.05 again). Similar conclusions are drawn when anthropogenic aerosol emissions only are held constant (AECVT, green curves), suggesting that this aerosol contribution is due to anthropogenic (rather than volcanic) emissions. From 1870 to 1900, the main changes in anthropogenic aerosol emissions are mostly located in England and Germany, where sulphate emissions have doubled in some regions (Figure 4.5) from 1870 to 1900 due to the industrialization.

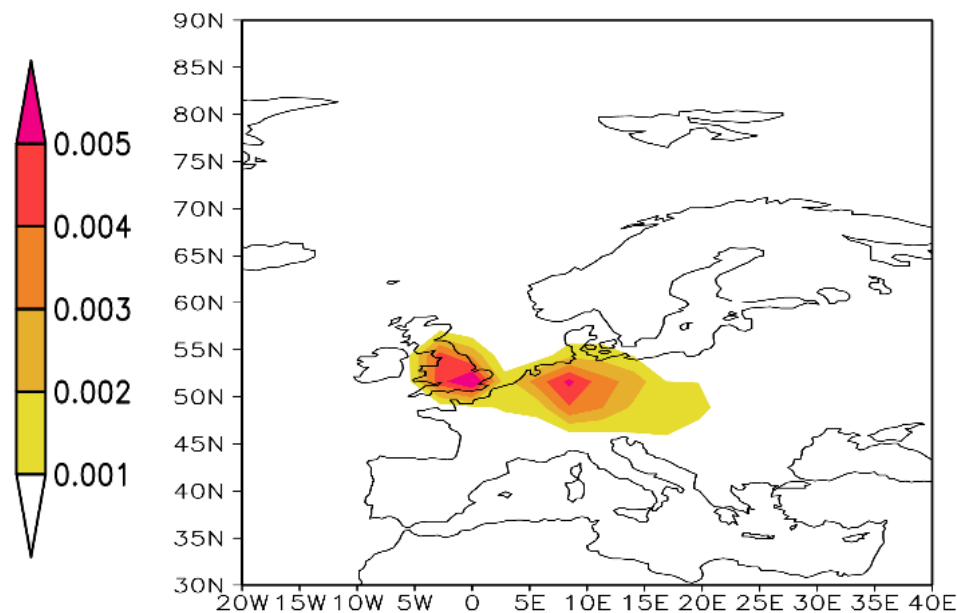


Figure 4.5: Map of sulphate aerosol emissions relative change in Europe: Difference between 1900 and 1870 ($\text{kg(S) /m}^2/\text{year}$).

Finally, even though we do not explicitly test the sensitivity of the European precipitation to greenhouse gas concentrations in the current study, their small relative changes in the late nineteenth century suggest that they do not have a significant impact on European precipitation during this time period (see also Bichet et al., 2011).

We conclude that between 1875 and 1890, transient SSTs are the primary driver for the enhanced summer precipitation in central Europe, and that transient anthropogenic aerosol emissions further enhance this increase by about 50%. Because transient SSTs are the primary driver, the next section further investigates, for the period 1870-1900, the link between transient SSTs and summer precipitation in central Europe, and tries to pinpoint the relevant SST anomalies.

4.3.2.2 Pinpointing the relevant SST anomalies

To understand which SST anomaly pattern(s) drive the high precipitation anomalies observed and simulated in central Europe between 1875 and 1890, Figure 4.6 shows the summer SST anomalies (ref=1870-1900). Panel (a) displays the average SST anomaly over the 1875-1890 period, while the other panels display composites of summer SST anomalies for the 6 wettest summers according to (b) observations and (c) simulated ensemble mean in CTRL. Panels (b) and (c) differ as simulations and observations disagree on the ranking of wet central European summers. Averaged over the 1875-1890 time period (Figure 4.6a), summer SST anomalies include warm conditions in the western Atlantic and eastern Pacific, cold conditions in the eastern Atlantic and western/central Pacific, and slightly warmer than average conditions in the Indian Ocean. Averaged over the simulated (Figure 4.6b) and observed (Figure 4.6c) six wettest summers, recurrent summer SST anomalies include a particularly pronounced warm signature in the eastern central Pacific El Niño region, along with the anomalies mentioned for the 1875-1890 above. In general, these patterns are enhanced from left to right in the panels of Figure 4.6.

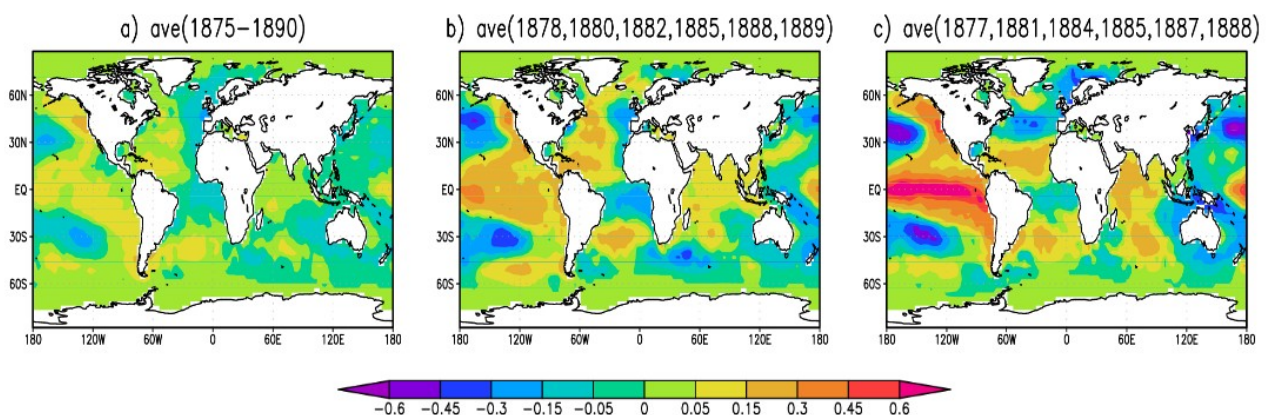


Figure 4.6: Summer (JJASO) SSTs anomalies (ref=1870-1900) in °C, averaged over the 1875-1890 mean (a), averaged over the six wettest years observed in central Europe (2°-30°E; 44°-55°N) between 1875 and 1890 (Casty et al., 2007, b), and averaged over the six wettest years simulated in central Europe between 1875 and 1890 (CTRL, c).

To identify which parts of the ocean drive the high precipitation anomalies, Figure 4.4 includes the summer precipitation anomalies (11-year running means, ref=1875) averaged over central Europe (2° - 30° E; 45° - 55° N), as simulated in the AOT (magenta), AOC (cyan), POC (yellow), and NINOC (dashed black) ensemble means, for the time-period 1870-1900.

As discussed in Section 4.3.2.1, there is no enhancement of the central European summer precipitation in the late nineteenth century when SSTs are globally constant at their 1870-1900 mean values (compare the black (CTRL) and blue (SSTC) curves in Figure 4.4). The comparison between the black (CTRL) and the magenta (AOT) curves from Figure 4.4 shows that when SSTs are transient in the Atlantic Ocean only, there is still no enhancement of central European summer precipitation. This suggests that the SST variability in the Atlantic Ocean is not the primary driver for the central European high summer precipitation anomalies in the late nineteenth century. This is confirmed when comparing the black (CTRL) and the cyan (AOC) curves in Figure 4.4, which shows that even with climatological SSTs in the Atlantic Ocean, there is an enhancement of central European summer precipitation in the late nineteenth century, which is even slightly larger than in the CTRL ensemble. On the other hand, the comparison between the black (CTRL) and the yellow (POC) curves in Figure 4.4 shows that if SSTs are kept at climatological values in the Pacific Ocean, there is no enhancement of central European summer precipitation. Comparing the black solid (CTRL) and black dashed (NINOC) curves in Figure 4.4 shows that this is still the case when SSTs are kept climatological only in the “El Nino region”. This suggests that the SST variability in the “El Nino region” is the primary driver of the central European summer high precipitation anomalies in the late nineteenth century.

4.3.2.3 SST impacts on the atmospheric circulation

To understand the atmospheric circulation patterns associated with the wet summers simulated between 1875 and 1890 in central Europe, Figure 4.7a-b shows composites of the simulated northern hemispheric summer anomalies (ref=1870-1900) of surface pressure and 500hPa geopotential height (gpm500), for the six wettest summers simulated (CTRL) in central Europe between 1875 and 1890. According to Figure 4.7a-b, the wet summers simulated in the CTRL ensemble mean are associated with positive surface pressure and gpm500 anomalies over the North Pole, and negative anomalies over the northern subtropics. This suggests a weakening of the westerlies, and larger meridional fluctuations of the storm track and upper-level westerly flow. In addition, the negative anomalies located over central/southern Europe suggest an increased frequency and/or amplitude of low-pressure systems over Europe, which is expected to enhance the probability for high precipitation in central Europe. Over North America, the gpm500 anomaly resembles the positive phase of the Pacific North American (PNA) pattern (Figure 4.7b), which is expected to affect mostly North America, but also Europe via its non-stationary modulation of the ENSO signal (e.g. Brönnimann et al., 2007a).

Figure 4.7c-d is identical to Figure 4.7a-b, respectively, but is taken from the reanalysis (Compo et al., 2011) and averaged over the six wettest summers observed (Casty et al., 2007) in central Europe between 1875 and 1890. According to Figure 4.7c-d, the trough over Western Europe is also found in the reanalysis, along with the high pressure systems over Greenland. The link to the Pacific on the other hand is weaker than in the model.

Over Europe, the simulated pressure pattern anomalies in CTRL are in line with previous studies. Schmocker-Fackel and Naef (2010b) find that most of the nineteenth century Swiss floods are associated with a westerly flow, Cornes and Jones (2011) link the high frequency of the late nineteenth century summer storms in central Europe to a Greenland-blocking system, and Jacobeit *et al.* (2004) find that in central Europe, the summer floods occur more frequently during circulation modes with troughs over the British Isles. Note also that the simulated pressure pattern anomalies resemble the second principal mode computed by Jacobeit *et al.* (2003a) for the July months since 1659, which was found particularly frequently in the late nineteenth century. The situation over Europe is also reminiscent of circulations with a low North Atlantic Oscillation (NAO) index, an anomaly that has been linked to the variability of European summer precipitation in several studies (e.g. Hurrell and Folland, 2002, Zveryaev, 2005, Folland *et al.*, 2009, and Zveryaev and Allan, 2010).

Doing a similar analysis (in terms of surface pressure and gpm500) with the sensitivity ensembles yields similar anomaly patterns as for CTRL in all cases, except for those where the “El Nino region” has climatological SSTs (SSTC, POC, NINOC, and AOT). This suggests that the SSTs variation in the “El Nino region” is the main driver for the pressure patterns associated with the wet summers simulated in central Europe between 1875 and 1890.

4.4 Discussion

Our results suggest that SST variations in the El Nino region played a crucial role in driving the central European wet summers in the late nineteenth century. We find however that this link is not deterministic, even the probability for above-normal precipitation is very significantly shifted: for five years in the period 1875-1990, at least 11 of the 13 ensemble members simulated above-normal precipitation in the extended summer season (Figure 4.2). The non-deterministic relation is further illustrated in Table 4.2, as observed and simulated wet summers do not correspond on the yearly basis, and as none of the individual wet summers (observed and simulated) systematically occurs after major El Nino or La Nina events (or after known volcanic eruptions).

Years	6 highest precipitation anomalies		Preceding winter NINO3.5 index	Major volcanoes
	CTRL	Casty <i>et al.</i> , 2007	September-February	
1875			-0.9: NINA (Sept 74)	Askja (Iceland)
1876			-0.8: NINA (Sept 78)	
1877	3/ JJASO		0.3	
1878		6/ JJASO	2.3: NINO (Sept 77)	
1879			-0.4	
1880		2/ JJASO	-0.9: NINA (Sept 79)	
1881	5/ JJASO		0.26	
1882		1/ JJASO	-0.4	
1883			-0.6: NINA (Sept 82)	Krakatau (Indonesia)
1884	1/ JJASO		-0.1	
1885	2/ JJASO	4/ JJASO	0.3	
1886			0.6: NINO (Sept 85)	Tarawera (N. Zealand)
1887	4/ JJASO		-1: NINA (Sept 86)	
1888	6/ JJASO	5/ JJASO	0.2	
1889		3/ JJASO	1.6: NINO (Sept 88)	
1890			-1.5: NINA (Sept 89)	

Table 4.2: Chronology of the six wettest simulated (column 2) and observed (column 3) summers (JJASO) between 1875 and 1889, along with the preceding Winter NINO3.4 index (column 4) from observed SSTs (Rayner *et al.*, 2003), and the major volcanic eruptions (column 5) from Ammann and Naveau (2003).

According to our results, the summer pressure patterns associated with the wet central European summers between 1875 and 1890 are triggered by the tropical Pacific SSTs, and resemble the common winter patterns associated with El Nino events. El Nino usually starts developing in summer with warm tropical Pacific SSTs, already accompanied by early Pacific teleconnections. The signal reaches its maximum intensity in winter and fades again around the following spring/summer (e.g. Brönnimann 2007). Therefore, even though the European impact of El Nino is usually stronger in winter and spring, some teleconnections can take place in the summer either preceding, or following the peak of an El Nino event. Note that as mentioned in Section 4.3.2.3, the summer pressure patterns associated with the wet central European summers between 1875 and 1890 also resembles the negative phase of the summer NAO (e.g. Folland *et al.*, 2009). The NAO is one of the leading modes for the summer European climate (e.g. Zveryaev, 2005), and its negative phase is expected to change the position of the storm track and weaken the westerlies, generally leading to a dry northern Europe and a wet southern Europe (e.g. Folland *et al.*, 2009, Miettinen *et al.*, 2011), as well as extended meridional circulations that are known to be conducive to heavy precipitation events in the Alps and Central Europe. It is also worth noting that a strong negative winter NAO pattern is usually associated with the El Nino impact in Europe (Brönnimann, 2007).

According to the NINO3.4 index (Table 4.2), three El Niño events (1877, 1885, and 1888) were recorded between 1875 and 1890, two of them (1877 and 1888) counting amongst the five largest events of the past 140 years (Figure 4.8a). The comparison between the NINO3.4 (Figure 4.8a) and the SOI index (Figure 4.8b) however shows differences, especially in the 1880s. Therefore, the definition of an El Niño event, along with its strength, may vary depending on the index and the underlying data quality. This suggests that the year-to-year comparison between individual wet summers (observed and simulated) as well as with the NINO3.4 index should be taken with caution. We therefore suggest that El Niño played an important role in driving the wet summers in central Europe in the late nineteenth century in a non-deterministic way. The non-deterministic link could be due to the misrepresentation of processes in the model, and/or uncertainties in the precipitation reconstructions (Casty et al., 2007), and/or in the SSTs measurements (e.g. Rayner et al., 2003, Roemmich et al., 2012), and/or to local conditions (e.g. phase of NAO).

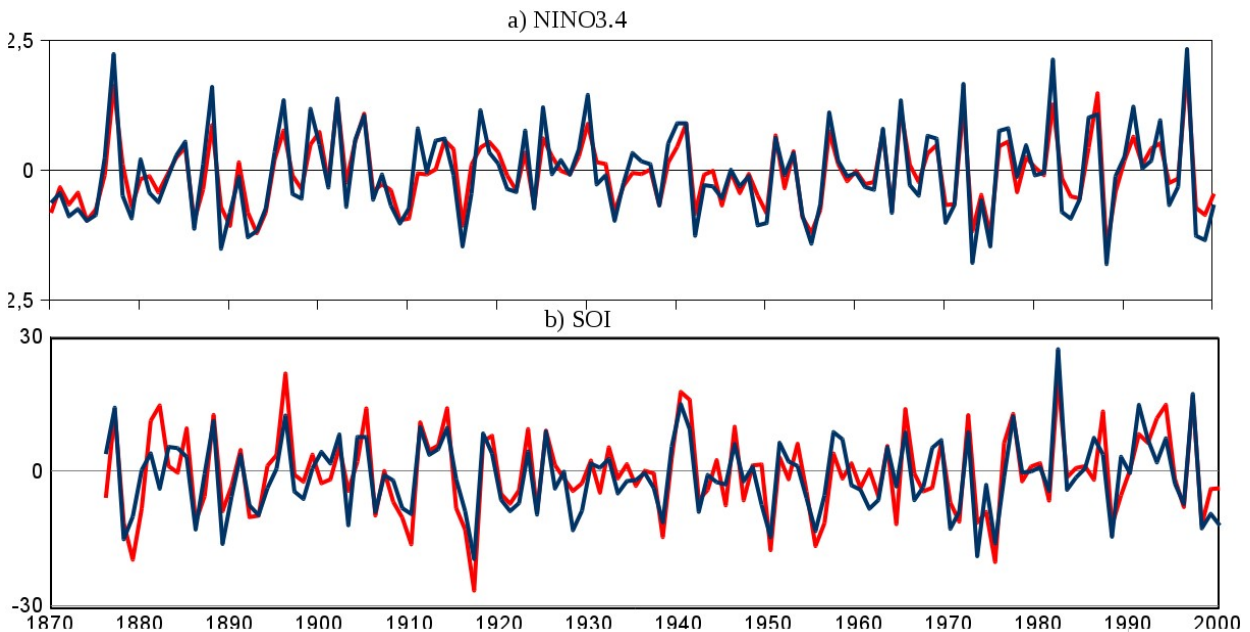


Figure 4.8: Times series of the NINO3.4 index (a) from observed SSTs (Rayner et al., 2003), and the inverse of the SOI index (b) from observed surface pressure (Bureau of Meteorology, National Climate Centre of Australia), shown since 1870, for the summer (JJASO, red curves) and winter half year (SONDJF, blue curves).

To further investigate the link between tropical Pacific SSTs and the late nineteenth century European precipitation, additional simulations should be conducted. In particular, the role of the Indian Ocean should be investigated (e.g. Mariotti et al., 2005). Finally, whereas we find that ECHAM5-HAM is able to satisfactorily reproduce the observed European precipitation since 1870, modelling the European climate with a GCM has limitations. The use of a regional model might be considered, but since our study specifically demonstrates the large scale influence on European precipitation, one must be particularly careful about the choice of input data in case of a regional model study. Also, since SSTs play an important role for European precipitation in the late nineteenth century, there is no guarantee to obtain similar results with a coupled Atmosphere-Ocean GCM. Finally, considering the probabilistic nature of these precipitation anomalies, studying the European climate with a GCM only makes sense with a large ensemble, ideally even larger than the one used in our study.

4.5 Conclusions

Our study shows that ECHAM5-HAM satisfactorily reproduces the high precipitation anomalies observed in the late nineteenth century. Within our modelling framework, we show that between 1875 and 1890, transient SSTs, as opposed to climatological ones, are the primary driver for the enhanced precipitation in central Europe. More specifically, we find that the SST variability in the tropical Pacific Ocean associated and more specifically in the “El Nino region” is the main reason behind these anomalies, most probably via its impact on the atmospheric circulation. The associated pressure patterns simulated during these wet summers include a PNA-like pattern over North America, a substantially weakened mid-troposphere westerly flow, and reduced pressure over southern Europe. In addition, transient anthropogenic aerosol emissions further enhance the increase in precipitation by about 50%. The present study thus further supports the idea that high precipitation anomalies due to large-scale circulation changes played an essential role in the extraordinary number of summer floods in the late nineteenth century.

Acknowledgements

The authors thank the MPI Hamburg for providing access to the ECHAM5-HAM code, colleagues at ETH Zürich and the Centre for Climate System Modelling C2SM who contributed to model development, in particular Ulrike Lohmann, Sylvaine Ferrachat, and Grazia Frontosa. This research has partly been supported by the NCCR Climate funded by the Swiss National Science Foundation. The simulations were done on the CRAY at the Swiss National Supercomputing Centre (CSCS) in Manno, Switzerland.

Chapter 5

Conclusions

In this thesis, extensive transient experiments were performed using the GCM “ECHAM5” coupled to aerosol module “HAM”, which includes a sophisticated treatment of aerosols and cloud microphysics (Stier et al., 2005, Lohmann et al., 2007). In total, 45 experiments clustered in 5 ensembles cover the time periods 1870-2005, and 104 experiments clustered in 9 ensembles cover the time period 1870-1900. The model was forced with prescribed, time-varying observationally based SSTs (Rayner et al., 2003), TSI (Solanki and Krivova, 2003), stratospheric optical depth due to aerosols from explosive volcanoes (Sato et al., 2003), greenhouse gas concentrations (IPCC, 2007), and aerosol emissions (NIES). The sensitivity experiments, which consist in keeping one or more of these climate forcings constant throughout the experiment are then used to assess the time-varying impacts of the mentioned climate forcings on the hydrological cycle. On the global scale, the thesis focusses on the decadal variations of land precipitation (Chapter 2) and 10m wind speed (Chapter 3) during the time period 1870-2005, and on the regional scale, it focusses on the high summer precipitation anomalies observed in central Europe in the late nineteenth century (Chapter 4). Conclusions from each chapter are resumed in the following.

Global land precipitation is investigated in Chapter 2 in order to identify the main climate forcings that drive its decadal variability during the time period 1870-2005. It is shown that when forced with time-varying observed SSTs and major climate forcings, ECHAM5-HAM satisfactorily reproduces the global land temperature and precipitation anomalies observed since 1870 and 1900, respectively. The sensitivity experiments then show that as opposed to their climatological values (1870-1900 mean), transient SSTs (encapsulating other forcings and internal variability) determine the decadal variability of the global land temperature, evaporation, and precipitation between 1870 and 2005. In addition, it is shown that the long-term trends of these variables are driven by atmosphere-only processes: On the one hand, increasing aerosol emissions decreases the global land temperature and precipitation (mostly summer convection) by up to 0.4°C and 30 mm/year, respectively, after about 1930, with large impacts in China and the Amazonian region. On the other hand, increasing greenhouse gas concentrations increases the global land temperature and precipitation by up to 0.25 °C and 10 mm/year, respectively, after about 1950. After about 1950 therefore, increasing aerosol emissions and greenhouse gas concentrations affect the hydrological cycle in opposite ways. In line with previous studies (e.g. Wild et al., 2007 and 2008, Wild and Liepert, 2010), it is also suggested that between about 1950 and 1970, anthropogenic aerosols may have “masked” the greenhouse gas impact on the hydrological cycle, which emphasizes the important impact of aerosol emissions on precipitation.

Global land wind speed is investigated in Chapter 3, motivated by the observational evidence for a substantial wind stilling after about 1970, which can potentially affect the hydrological cycle and industries such as wind powered energy. It is shown that ECHAM5-HAM reproduces the observed decline in 10m land wind speed after 1970, but the simulated amplitude of the decline is considerably smaller than in the observations (a maximum of 20% is reproduced in summer, in China). Such a difference in magnitude was however expected, since previous work (Vautard et al., 2010) suggests that the observed decline primarily results from the recent increase in vegetation roughness length, and that this variable is prescribed as a constant climatological field in the transient experiments performed in this thesis. Additional equilibrium experiments performed within the framework of this thesis show that in ECHAM5-HAM, the totality of the observed wind stilling can be reproduced by “artificially” increasing the vegetation roughness length by a factor between 1.2 and 4.9, depending on the region. Such an increase in roughness length may however not necessarily be realistic everywhere, and the transient simulations show that up to 20% of the observed wind stilling must anyway be explained by the other factors included in the model: According to the sensitivity studies, the realistic increase in aerosol emissions decreases the global land wind speed after about 1950 (atmosphere-only responses), with large impacts in summer, as well as in Asia and India (up to -0.3 m/s in summer in India). The contribution from the realistic increase in greenhouse gas concentrations is however relatively small (atmospheric-only response), and the SST variations are found to affect mostly the decadal variability of land wind speed, as opposed to its long-term trend.

Finally, European precipitation in the late nineteenth century is investigated in Chapter 4 for its potential contribution to the accumulation of large floods that were recorded in central Europe at the time. The results show that ECHAM5-HAM satisfactorily reproduces the summer (JJASO) precipitation anomalies observed in central Europe between 1870 and 2005, and in particular, the high precipitation anomalies observed in the 1800s. Between 1875 and 1890, the sensitivity results show that transient SSTs in the “El Niño region”, as opposed to climatological SSTs (1870-1900 mean), are the primary driver for these high anomalies. In the model, this occurs via their impacts on the atmospheric circulation, the relevant associated atmospheric circulation anomalies showing a PNA-like pattern over North America, a substantially weakened mid-troposphere westerly flow over Europe and the North Atlantic, and reduced pressure over Europe. Finally, it is found that when SSTs are transient in the model, increasing anthropogenic aerosol emissions further enhance the late nineteenth century central European precipitation by about 50%.

General conclusions. To summarize, this thesis shows that when forced with prescribed, observationally based, time-varying SSTs and major climate forcings, ECHAM5-HAM satisfactorily reproduces the decadal variability of the main components of the hydrological cycle observed on the global and to some extent European scales, between 1870 and 2005. The sensitivity experiments highlight the dominant role of the SSTs (encapsulating other forcings) in driving these decadal variations, whereas atmosphere-only processes affect mostly their long-term trends. In particular, it is shown that increasing aerosol emissions decreases the global land temperature, precipitation (mostly summer convection), wind speed and evaporation after about 1950, and may even have “masked” the precipitation increase expected from increasing greenhouse gas concentrations between about 1950 and 1970. Finally, this thesis also illustrates the complex impact of the Pacific Ocean on the European precipitation, with a potential relevance in the late nineteenth century.

Chapter 6

Outlook

On the global scale, open questions remain regarding the impact of anthropogenic aerosols and greenhouse gases on the hydrological cycle. In particular, whereas this thesis shows that prescribed SSTs determine the decadal variability of global land temperature and precipitation between 1870 and 2005 in the model, it does not investigate the impact of anthropogenic aerosols and greenhouse gases on the SSTs. This could be tested by using a coupled ocean-atmosphere model, and would complete the picture by quantifying, since 1870, the “full” (atmosphere-only and via the ocean) time-varying impact of these anthropogenic forcings on the hydrological cycle.

Another unexplored aspect of this thesis regards the time-varying impact of land-use changes on the hydrological cycle since 1870. This has not been addressed in this work because the transient experiments used in this thesis are forced with climatological land-use. However, the thesis shows that increasing the vegetation roughness length considerably reduces the surface land wind speed, with potential consequences for the hydrological cycle. It would therefore be useful to assess the impact of land-use change on the hydrological cycle since 1870, which could be done by using either a time-varying land-use dataset, or a coupled land-atmosphere model.

On the European scale, more work is still needed to fully understand the mechanisms driving the late nineteenth century high precipitation anomalies. The role of individual oceanic basins could further be investigated (e.g. impact of the Indian and South Atlantic Ocean, in depth analysis of the role of El Niño events), and in particular the role of the North Atlantic Ocean: Whereas the thesis shows that as compared to the 1870-1900 climatological mean, transient SSTs in the Atlantic Ocean do not affect the European precipitation, it does not assess the impact of the 1870-1900 climatological mean, as compared for instance to long-term mean (1870-2005). This would however be of prior interest, since the comparison between these two climatological means shows large differences, and in particular, considerably warmer SSTs in the Greenland Sea in the former period (1870-1900). To assess this impact, additional transient experiments could be performed, using for instance the 1870-2005 climatological means.

Furthermore, the extent to which the results from this thesis depend on the chosen model version and/or input data is of major interest, in particular regarding the impact of anthropogenic aerosols. To test this dependency, similar experiments could be performed using a different microphysical scheme in ECHAM5-HAM (Lohmann and Roeckner, 1996, Lohmann et al., 1999, Lohmann, 2002 and Lohmann and Diehl, 2006), or a different aerosol module, GCM, or even observational dataset for aerosol emissions. In addition, note that the role of individual aerosol

species could also be investigated, which would be of particular interest regarding the impact of black carbon on convective precipitation (e.g. Ramanathan et al., 2005).

An attractive way to carry on this work also includes the identification of the role of individual oceanic basins in affecting the global and regional climate, by simply continuing until 2005 the simulations started in the framework of the late nineteenth century European precipitation (Chapter 4).

Without performing additional experiments however, the extensive ensembles performed within the framework of this thesis could also be used for a wide range of scientific applications on various temporal and spatial scales: For instance, the impact of anthropogenic aerosols and/or volcanoes could further be investigated, on the global and regional scales. Note that to investigate the regional climate more into details since 1870, the ensembles realised within the framework of this thesis could also be used to drive a regional climate model.

At last, one could also extend these experiments further back in time and check for instance, if the European high precipitation anomalies observed in the 1850s are also captured by ECHAM5-HAM, and in such case, whether or not they have the same origin as in the 1870s. Covering the twenty-first century with ECHAM5-HAM would also be useful, especially to assess the impact of the projected increase in greenhouse gases and aerosols in Asia and India. Finally, note that the analysis of the recently released NCEP-NCAR CR20 reanalysis (Compo et al., 2011) would shed a light on the results obtained in this thesis, which would be of particular interest for the late nineteenth century.

References

- Ackerman A.S., O.B. Toon, D.E. Stevens, A.J. Heymsfield, V. Ramanathan, and E.J. Welton (2000), Reduction of tropical cloudiness by soot, *Science*, 288, 1042-1047.
- Adler R.F., G. Gu, J.J. Wang, G.J. Huffman, S. Curtis, and D. Bolvin (2008), Relationships between global precipitation and surface temperature on interannual and longer time-scales (1979-2006), *J. Geophys. Res.*, 133, D22104, doi:10.1029/2008JD010536.
- Albrecht B. (1989), Aerosols, cloud microphysics, and fractional cloudiness, *Science*, 245, 1227-1230.
- Allen M.R. and W.J. Ingram (2002), Constraints on future changes in climate and the hydrological cycle, *Nature*, 419, 224-232.
- Ammann, C. M., and P. Naveau (2003), Statistical analysis of tropical explosive volcanism occurrences over the last 6 centuries, *Geophys. Res. Lett.*, 30(5), 1210, doi:10.1029/2002GL016388.
- Andrews T. and P.M. Forster (2009), A surface energy perspective on climate change, *J. Climate*, 22, 2557-2570, doi:10.1175/2008JCLI2759.1.
- Angström A. (1962), Atmospheric turbidity, global illumination and planetary albedo of the earth, *Tellus*, 14, 435-450.
- Avissar R. and D. Werth (2005), Global hydroclimatological teleconnections resulting from tropical deforestation, *J. Hydrometo.* 6, 134-145.
- Bader S. and H. Bantle (2004), *Das Schweizer Klima im Trend Temperatur und Niederschagsentwicklung 1864-2001*, Veröffentlichung 68.
- Baumgartner A. and E. Reichel (1975), *The world water balance: Mean annual global, continental and maritime precipitation, evaporation and run-off* (Amsterdam: Elsevier), 179 pp.
- Begert, M., T. Schlegel, and W. Kirchhofer (2005), Homogeneous temperature and precipitation series of Switzerland from 1864 to 2000, *International J. of Climate* 25, 65-80, doi:10.1002/joc.1118.
- Benito G., A. Diez-Herrero, and M.-F. De Villalta (2004), Magnitude and frequency of flooding in the Tagus Basin (Central Spain) over the last Millennium, *Clim. Change* 58, 171-192, 2003.
- Bichet A., M. Wild, D. Folini and C. Schär (2011), Global precipitation response to changing forcings since 1870, *Atmos. Chem. Phys.*, 11, 9961-9970, doi:10.5194/acp-11-9961-2011.
- Boer G.J. (1993), Climate change and the regulation of the surface moisture and energy budgets, *Clim. Dyn.*, 8, 225-239.

- Boer G.J., G. Flato, M.C. Reader, and D. Ramsden (2000), A transient climate change simulation with greenhouse gas and aerosol forcing: experimental design and comparison with the instrumental record for the twentieth century, *Clim. Dyn.*, 16, 405-425.
- Bonan G.B. (1999), Frost followed the plough: Impacts of deforestation on the climate of the United States, *Ecological App.*, 9(4), 1305-1315.
- Brazdil R., K. Chroma, P. Dobrovolny, and R. Tolasz (2009), Climate fluctuations in the Czech Republic during the period 1961-2005, *Int. J. Climatol.*, 29, 223-242, doi:10.1002/joc.1718.
- Brazdil R., P. Dobrovolny, V. Kako, and O. Kotyza (2006), Historical and recent floods in the Czech Republic: Causes, seasonality, trends, impacts. *Flood Risk Management Hazards, Vulnerability and Mitigation Measures*, edited by: Schanze, J. et al., Springer, 247-259, available online at: <http://www.springerlink.com/content/m386p490132n5334/fulltext.pdf>.
- Brazdil, R., C. Pfister, H. Wanner, H.V. Storch, and J. Luterbacher (2005), Historical climatology in Europe - The state of the art, *Climate change* 70, 363-430., doi:10.1007/s10584-005-5924-1.
- Brohan P., J.J. Kennedy, I. Harris, S.F.B. Tett, and P.D. Jones (2006), Uncertainty estimates in regional and global observed temperature changes: A new data set from 1850, *J. Geophys. Res.*, 111, 12106, doi:10.1029/2005JD006548, 2006.
- Brönnimann S. (2007), Impact of El Nino-Southern Oscillation on European climate, *Rev. Geophys* 45, RG3003, doi:10.1029/2006RG000199.
- Brönnimann S., E. Xoplaki, C. Casty, A. Pauling, and J. Luterbacher (2007), ENSO influence on Europe during the last centuries, *Clim. Dyn.* 28, 181-197.
- Bulic I.H. and C. Brankovic (2007), ENSO forcing of the Northern Hemisphere climate in a large ensemble of model simulations based on very long SST record, *Clim. Dyn.* 28, 231-254.
- Casty C, H. Wanner, J. Luterbacher, J. Esper, and R. Böhm (2005), Temperature and precipitation variability in the European Alps since 1500, *Int. J. of Clim* 25, 1855-1880.
- Casty C., C.C. Raible, T.F. Stocker, H. Wanner and J. Luterbacher (2007), A European pattern climatology 1766-2000, *Clim. Dyn.* 29, 791-805.
- Ciais P., M.J. Schelhaas, S. Zaehle, S.L. Piao, A. Cescatti, J. Liski, S. Luysaert, G. Le-Maire, E.D. Schulze, O. Bouriaud, A. Freibauer, R. Valentini and G.J. Nabuurs (2008), Carbon accumulation in European forests, *Nature Geoscience*, 1, 425-429, doi:10.1038/ngeo233.
- Compo G.P. and P.D. Sardeshmukh (2009), Oceanic influences on recent continental warming, *Clim. Dynam.*, 32, 333-342.
- Compo G.P., J.S. Whitaker, P.D. Sardeshmukh, N. Matsui, R.J. Allan, X. Yin, B.E. Gleason, R.S. Vose, G. Rutledge, P. Bessemoulin, S. Brönnimann, M. Brunet, R.I. Crouthamel, A.N. Grant, P.Y. Groisman, P.D. Jones, M. Kruk, A.C. Kruger, G.J. Marshall, M. Mauerer, H.Y. Mok, Ø. Nordli, T.F. Ross, R.M. Trigo, X.L. Wang, S.D. Woodruff, and S.J. Worley (2011), The Twentieth Century Reanalysis Project, *Quarterly J. Roy. Meteorol. Soc.*, 137, 1-28. doi: 10.1002/qj.776.
- Copeland J.H., R.A. Pielke, and T.G.F. Kittel (1996), Potential climatic impacts of vegetation change: A regional modelling study, *J. Geophys. Res.*, 101, D3, 7409-7418.
- Cornes R.C. and P. Jones (2011), An examination of storm activity in the north-east Atlantic region over the 1851-2003 period using the EMULATE gridded MSLP data series, *J. of Geophys. Res.* 116,

D16110, doi:10.1029/2011JD016007.

Dai A., K.E. Trenberth, and T. Qian (2004), Global Dataset of Palmer Drought Severity Index for 1870–2002: Relationship with Soil Moisture and Effects of Surface Warming, *J. Hydrometeor.*, 5 117-1130.

Dentener F., S. Kinne, T. Bond, O. Boucher, J. Cofala, S. Generoso, P. Ginoux, S. Gong, J. Hoelzemann, A. Ito, L. Marelli, J. Penner, J.-P. Putaud, C. Textor, M. Schultz, G. van der Werf, and J. Wilson (2006), Emissions of primary aerosol and precursor gases in the year 2000 and 1750 prescribed data-sets for AeroCom, *Atmos. Chem. Phys.*, 6, 4321-4344.

Dettinger, M. D., D. R. Cayan, G. J. McCabe, and J. A. Marengo (2000b), Multiscale streamflow variability associated with El Niño/Southern Oscillation. *Oscillation*, in H.F.

Dettinger, M. D. and H.F. Diaz (2000a), Global characteristics of stream flow seasonality and variability. *Journal of hydrometeorology* 1, 289-310.

Diaz H.F. and V. Markgraf (2000), *El Niño and the southern oscillation, multiscale variability and global and regional impacts*. Cambridge University Press, Cambridge, UK, and New York, NY, USA.

Douville H., D. Salas-Melia, and S. Tyteca (2006), On the tropical origin of uncertainties in the global land precipitation response to global warming, *Clim. Dyn.*, 26, 367-385.

Easterling D.R., J.L. Evans, P. Ya. Groisman, T.R. Karl, K.E. Kunkel, and P. Ambenje (2000), Observed variability and trends in extreme climate events: A brief review, *Bull. Amer. Meteor. Soc.*, 81, 417–425.

Feddema, J.J., K.W. Oleson, G.B. Bonana, L.O. Mearns, L.E. Buja, G.A. Meehl, and W.M. Washington (2005), The Importance of Land-Cover Change in Simulating Future Climates, *Science*, 310(5754), 1674-1678.

Feichter J., E. Kjellström, H. Rodhe, F. Dentener, J. Levievel, and G.-J. Roelofs (1996), Simulation of the tropospheric sulphur cycle in a global climate model, *Atmos. Environ.*, 30(10/11), 1963-1707.

Feichter J., E. Roeckner, U. Lohmann, B.G. Liepert (2004), Nonlinear aspects of the climate response to greenhouse gas and aerosol forcing, *J. Climate*, 17, 2384-2398.

Findell K.L., A.J. Pitman, M.H. England, and P.J. Pegion (2009), Regional and global impacts of land-cover changes and sea-surface temperature anomalies, *J. Climate*, 22, 3248-3269.

Fischer E.M., J. Luterbacher, E. Zorita, S.F.B. Tett, C. Casty, and H. Wanner (2007), European climate response to tropical volcanic eruptions over the last half millennium, *Geophys. Res. Lett.*, 34, L05707, doi:10.1029/2006GL027992.

Fischer E.M. and C. Schär (2010), Consistent geographical patterns of changes in high-impact European heatwaves, *Nature geoscience* 3, 398-403, doi:10.1038/NGEO866.

Folini D. and M. Wild (2011), Aerosol Emissions and Dimming / Brightening in Europe: sensitivity studies with ECHAM5-HAM, *J. Geophys. Res.*, 116 (D201104), doi:10.1029/2011JD016227.

Folland C., J. Knight, H.W. Linderholm, D. Fereday, S. Ineson and J.W. Hurrell (2009), The summer North Atlantic Oscillation: Past, present and future. *Journal of climate* 22, 1082-1103.

Foukal P., C. Fröhlich, H. Spruit, and T.M.L. Wigley (2006), Variations in solar luminosity and their effect on the Earth's climate, *Nature*, 443, 161-166, doi:10.1038/nature05072.

- Frei C., H.C. Davies, J. Gurtz, and C. Schär (2000), Climate dynamics and extreme precipitation and flood events in Central Europe, *Integrated Assessment* 1, 281-299.
- Gates W.L. (1992), AMIP: The Atmospheric Model Intercomparison Project, *Bull. Amer. Meteor. Soc.*, 73, 1962-1970.
- Glaser, R. (1998), Historische Hochwässer im Maingebiet-Möglichkeiten und Perspektiven auf der Basis der historische Klimadatenbank Deutschland (HISKLID), in: Aktuelle und historische Hochwasserereignisse, edited by: Pörtgen, K.H. And Deutsch M., *Erfurter Geographische Studien* 7, 93-108.
- Giannini A., R. Saravanan, and P. Chang (2003), Oceanic forcing of Sahel rainfall on interannual to interdecadal time scales, *Science*, 302(5647), 1027-1030.
- Givati A. and D. Rosenfeld (2004), Quantifying precipitation suppression due to air pollution, *J. Appl. Meteor.*, 43, 1038-1056.
- Gilgen H., M. Wild, and A. Ohmura (1998), Means and trends of short-wave irradiance at the surface estimated from GEBA, *J. Geophys. Res.*, 111, D19101, doi:10.1029/2005JD006901.
- Glaser R. (1998), Historische Hochwässer im Maingebiet-Möglichkeiten und Perspektiven auf der Basis der historische Klimadatenbank Deutschland (HISKLID), in: Aktuelle und historische Hochwasserereignisse, edited by: Pörtgen, K.H. And Deutsch M., *Erfurter Geographische Studien* 7, 93-108.
- Gu G., R.F. Adler, G.J. Huffman, and S. Curtis (2007), Tropical Rainfall Variability on Interannual-to-Interdecadal and Longer Time Scales Derived from the GPCP Monthly Product, *J. Climate.*, 20, 4033-4046.
- Guo, H., M. Xu, and Q. Hu (2011), Changes in near-surface wind speed in China: 1969-2005, *Int. J. Climatol.*, 31, 349-358, doi:10.1002/joc.2091.
- Hagemann S. (2002), An improved land surface parameter dataset for global and regional climate models, Report No. 336, Max-Planck-Institute für Meteorologie ISSN 0937-1060: Available online at: https://www.mpimet.mpg.de/fileadmin/publikationen/Reports/max_scirep_336.pdf.
- Hagemann S., K. Arpe, and E. Roeckner, E. (2006), Evaluation of the Hydrological Cycle in the ECHAM5 Model, *J. Climate*, 19, 3810-3827.
- Hansen J., D. Johnson, A. Lacis, S. Lebedeff, P. Lee, and G. Russell (1981), *Science*, 213(4511), 957-966.
- Hansen J., R. Ruedy, M. Sato, M.L. Imhoff, W.T. Lawrence, D.R. Easterling, T.C. Peterson, and T.R. Karl (2001), A closer look at United States and global surface temperature change, *J. Geophys. Res.*, 106, 23947-23963.
- Hartmann D.L. (1994), *Global Physical Climatology*, International Geophysics Series, 56, Smowska, R. and Holton, J.R., Academic Press Limited, London.
- Haywood J. and O. Boucher (2000), Estimates of the direct and indirect radiative forcings due to tropospheric aerosols: A review, *Reviews of Geophys.*, 38(4), 513-543.
- Held I.M. and B.J. Soden (2000), Water vapour feedback and global warming, *annual review of energy and the environment*, 25, 441-475.
- Hegg C. and S. Vogt (2005), Häufigkeiten und Trends von Starkniederschlägen in der Schweiz im

Zeitraum 1864-2002, *Wasser Energy Luft* 97, 209-212.

Hohenegger, C., A. Walser, W. Langhans and C. Schär, 2008: Cloud-resolving ensemble simulations of the August 2005 Alpine flood. *Quart. J. Roy. Meteorol. Soc.*, **134** (633), 889-904

Hoerling M., J. Hurrell, J. Eischeid, A. Phillips (2006), Detection and attribution of 20th century northern and southern African monsoon change, *J. Climate*, 19, 3989-4008.

Hoerling M., A. Kumar, J. Eischeid, and B. Jha (2008), What is causing the variability in global mean land temperature?, *Geophys. Res. Lett.*, 35, 23712, doi10.1029/2008GL035984.

Houghton R.A. (1999), The annual net flux of carbon to the atmosphere from changes in land use 1850-1990, *Tellus B*, 51(2), 298-313.

Huntington T.G. (2006), Evidence for intensification of the global cycle: Review and synthesis, *J. Hydrology*, 319, 83-95.

Hurrell, J.W. and C.K. Folland (2002), A change in the summer atmospheric circulation over the North Atlantic. *CLIVAR Exch* 25, 85-54.

IPCC AR1 (1990), Contribution of Working Group I to the First Assessment Report of the Intergovernmental Panel on Climate Change: Houghton, J.T., G.J. Jenkins, and J.J. Ephraums, Cambridge University Press, Cambridge.

IPCC AR4 (2007), Contribution of Working Group I to the Fourth Assessment Report of the Intergovernmental Panel on Climate Change: Solomon, S., Qin, D., Manning, M., Chen, Z., Marquis, M., Averyt, K.B., Tignor, M and Miller H.L., Cambridge University Press, Cambridge.

Jacobeit J., H. Wanner, J. Luterbacher, C. Beck, A. Philipp, and K. Sturm (2003a). Atmospheric circulation variability in the North-Atlantic-European area since mid-seventeenth century. *Climate Dynamic* 20, pp. 341-352.

Jacobeit J., R. Glaser, M. Nonnenmacher, and H. Stangl H. (2004) Hochwasserentwicklung in Mitteleuropa und Schwankungen der atmosphärisch Zirculation, *Geographische Rundschau*, 56, pp. 26-34.

Kauppi P.E., J.H. Ausubel, J. Fang, A.S. Mather, R.A. Sedjo and P.E. Waggoner (2006), Returning forests analysed with the forest identity, *Proc. Natl. Acad. Sci.*, 103, 17574-17579, doi:10.1073/pnas.0608343103.

Klein Goldewijk K. (2001), Estimating global land use change over the past 300 years: the HYDE database, *Global Biogeochemical Cycles* 15(2), 417-433.

Klein Goldewijk K. and N. Ramankutty (2004), Land cover change over the last three centuries due to human activities: The availability of new global data sets, *GeoJournal*, 61, 335-344.

Klink K. (1999), Trends in monthly maximum and minimum surface wind speeds in the coterminous United States, 1961 to 1990, *Clim. Res.*, 13, 193-205.

Koch D. and A. Del Genio (2010), Black carbon semi-direct effects on cloud cover: review and synthesis, *Atmos. Chem. Phys.*, 10, 7685-7696.

Koch D., S. Menon, A. Del Genio, R. Ruedy, I. Alienov, and G.A. Schmidt (2009), Distinguishing aerosol impacts on climate over the past century, *J. Climate*, 22, 2659-2677.

Koster R.D. and M.J. Suarez (1995), Relative contributions of land and ocean processes to

- precipitation variability, *J. Geophys. Res.*, 100, 13775-13790.
- Kundzewicz Z.W., U. Ulbrich, T. Brücher, D. Graczyk, A. Krüger, G.C. Leckebusch, L. Menzel, I. Pinskawar, M. Radziejewski, and M. Szwed (2005), Summer floods in Central Europe – climate change track?, *Nat. Hazard* 36, 165-189.
- Labitzke K. and K. Matthes (2003), Eleven-year solar cycle variations in the atmosphere: Observations, mechanisms and models, *The Holocene*, 13(3), 311-317.
- Lamarque J.-F., T.C. Bond, V. Eyring, C. Granier, A. Heil, Z. Klimont, D. Lee, C. Liousse, A. Mieville, B. Owen, M.G. Schultz, D. Shindell, S.J. Smith, E. Stehfest, J. Van Aardenne, O.R. Cooper, M. Kainuma, N. Mahowald, J.R. McConnell, V. Naik, K. Riahi, and D.P. van Vuuren (2010), Historical (1850–2000) gridded anthropogenic and biomass burning emissions of reactive gases and aerosols: methodology and application, *Atmos. Chem. Phys.*, 10, 7017-7039.
- Liepert B.G. (2010), The physical concept of climate forcing, *John Wiley&Sons* 1, 786-802.
- Liepert B.G., J. Feichter, U. Lohmann, and E. Roeckner (2004) Can aerosols spin down the water cycle in a warmer and moisture world?, *Geophys. Res. Lett.*, 31, 06207, doi10.1029/2003GL019060.
- Liepert B.G. and M. Previdi (2009), Do models and observations disagree on the rainfall response to global warming? *J. Climate*, 22, 3156-3166.
- Lin S.J. and R.B. Rood (1996), Multidimensional Flux-Form Semi-Lagrangian Transport Scheme, *Monthly Weather Review*, 124, 2046, doi:10.1175/1520-04931996.
- Lohmann U. (2002), Possible aerosol effects on ice clouds via contact nucleation, *J. Atmos. Sc.*, 59, 647-656.
- Lohmann U. and K. Diehl (2006), Sensitivity studies of the importance of dust ice nuclei for the indirect aerosol effect on stratiform mixed-phase clouds, *J. Atmos. Sci.*, 63, 968-982.
- Lohmann U. and J. Feichter (2005), Global indirect aerosol effects: A review, *Atmos. Chem. Phys.*, 5, 715-737.
- Lohmann U., J. Feichter, C.C. Chuang, and J.E. Penner (1999), Predicting the number of cloud droplets in the ECHAM GCM, *J. Geophys. Res.*, 104, 91-9198.
- Lohmann U. and E. Roeckner (1996), Design and performance of a new cloud microphysics scheme developed for ECHAM general circulation model, *Clim Dyn.*, 12, 557-572.
- Lohmann U., P. Stier, C. Hoose, S. Ferrachat, S. Kloster, E. Roeckner and J. Zhang (2007), Cloud microphysics and aerosol indirect effects in the global climate model ECHAM5-HAM, *Atmos. Chem. Phys.*, 7, 3425-3446.
- Lugina K.M., P.Y. Groisman, K.Y. Vinnikov, V.V. Koknaeva, and N.A. Speranskaya (2006) Monthly surface air temperature time series area-averaged over the 30-degree latitudinal belts of the globe, 1881–2005. In *Trends: A Compendium of Data on Global Change*. Carbon Dioxide Information Analysis Centre, Oak Ridge National Laboratory, U.S. Department of Energy, Oak Ridge, Tenn., U.S.A. doi: 10.3334/CDIAC/cli.003, 2005. Available online at: <http://cdiac.esd.ornl.gov/trends/temp/lugina/lugina.html>.
- Mariotti, A., J. Ballabrera-Poy, and N. Zeng (2005), Tropical influence on Euro-Asian autumn rainfall variability, *Climate Dynamics*, 24, 511-521, doi:10.1007/s00382-004-0498-6.

- Mason B.J. (1962), *Clouds, rain and rainmaking*, Cambridge University Press, London.
- McCornic R.A. and J.H. Ludwig (1967), Climate modification by atmospheric aerosols, *Science*, 156(3780), 1358-1359, doi:10.1126/science.156.3780.1358.
- McVicar, T.R., T.G. Van Niel, L. Tao Li, M.L. Roderick, D.P. Rayner, L. Ricciardulli, and R.J. Donohue (2008), Wind speed climatology and trends for Australia, 1975-2006: Capturing the stilling phenomenon and comparison with near-surface reanalysis output, *Geophys. Res. Lett.*, 35, L20403, doi:10.1029/2008GL035627.
- McVicar T.R. and M.L. Roderick (2010), Atmospheric science: Winds of change, *Nature Geoscience*, 3, 747-748, doi:10.1038/ngeo1002.
- McVicar T.R. and M.L. Roderick, R. Donohue, L.T. Li, T.G. Van Niel, A. Thomas, J. Grieser, D. Jhajharia, Y. Himri, N.M. Mahowals, A.V. Mescherskaya, A.C. Kruger, S. Rehman, Y. Dinpashoh (2012), Global review and synthesis of trends in observed terrestrial near-surface wind speed: Implications for evaporation, *J. of Hydrol.* 416-417, 182-205, doi: 10.1016/j.jhydrol.2011.10.024.
- Meehl G.A., T.F. Stocker et al. (2007): Global Climate Projections. In: *Climate Change 2007: The Physical Science Basis. Contribution of Working Group I to the Fourth Assessment Report of the Intergovernmental Panel on Climate Change (IPCC)*.
- Meehl G.A., W.M. Washington, W.D. Collins, J.M. Arblaster, A. Hu, L.E. Buja, W.G. Strand, and H. Teng (2005), *Science*, 307(5716), 1769-1772, doi:10.1126/science.1106663.
- Miettinen A., N. Koc, I.R. Hall, F. Godtlielsen and D. Divine (2011), North Atlantic sea surface temperatures and their relation to the North Atlantic Oscillation during the last 230 years., *Clim. Dyn.*, 36, 533-543.
- Milly P.C.D., R.T. Weatherals, K.A. Dunne, and T. L. Delworth (2002), Increasing risk of great floods in a changing climate, *Nature*, 415, 514-517.
- Mitchell J.F.B. (1983), The seasonal response of a general circulation model to change in CO₂ and sea temperatures, *Quat. J. Res. Meteor. Soc.*, 109, 113-152.
- Mitchell T.D. and P.D. Jones (2005), An improved method of constructing a database of monthly climate observations and associated high resolution grids, *Int. J. Climatol.*, 25, 693–712.
- Mudelsee M., M. Börngen, G. Tetzlaff, and U. Frunewald (2004), Extreme floods in central Europe over the past 500 years: Role of cyclone pathway “Zugstrasse Vs”, *Journal of Geophysical Research* 109, D23101, doi:101029/2004JD005034.
- Mudelsee, M., M. Deutsch, M. Börngen, and G. Tetzlaff (2006), Trends in flood risk of the River Werra (Germany) over the past 500 years / Tendances du risqué d’inondation dans le vallée de la rivière Werra (Allemagne) Durant les 500 dernières années, *Hydrological Sciences Journal* 51 (1), 818-833.
- New M., M. Hulme, and P.D. Jones (2000), Representing Twentieth-Century Space–Time Climate Variability. Part II: Development of 1901–96 Monthly Grids of Terrestrial Surface Climate, *J. Climate*, 13, 2217-2238.
- New M., M. Todd, M. Hulme, and P.D. Jones (2001), Precipitation measurements and trends in the twentieth century, *Int. J. Climatol.*, 21, 1899-1922.
- Nienhui, P.P. (2008), *Environmental history of the Rhine-Meuse Delta: An ecological story on*

evolving human-environmental relations coping with climate change and sea-level rise, Springer Science & Business Media B.V., ISBN 978-1-4020-8211-5.

Nozawa T., T. Nagashima, T. Ogura, T. Yokohata, N. Okada, and H. Shiogama (2007), Climate Change Simulations with a Coupled Ocean-Atmosphere GCM Called the Model for Interdisciplinary Research on Climate: MIROC. CGER's Tech. Rep., Natl. Inst. For Environ. Stud., Japan, available at: <http://www.cger.nies.go.jp/publications/report/i073/I073.pdf>.

Oguntunde P.G., B.J.Abiodun, O.J. Olukunle, A.A. Olufayoa (2011), Trends and variability in pan evaporation and other climatic variables at Ibadan, Nigeria, 1973-2008. *Meteorol. Appl.*, doi:10.1002/met.281.

Ohmura A. (2009), Observed decadal variations in surface solar radiation, *J. Geophys. Res.*, 114, D00D05, doi:10.1029/JD011290.

Pauling A., J. Luterbacher, C. Casty and H. Wanner (2006), Five hundred years of gridded high-resolution precipitation reconstructions over Europe and the connection to large-scale circulation, *Clim. Dyn* 26, 387-405.

Pauling A. and H. Paeth (2007), On the variability of return periods of European winter precipitation extremes over the last three centuries, *Clim. Past* 3, 65-76.

Penman H.L. (1950), The dependence of transpiration on weather and soil conditions, *J. Soil. Sci.*, 1, 74-89.

Peterson T.C., M.A. Taylor, R. Demeritte, D.L. Ducombe S. Burton, F. Thompson, A. Porter, M. Mercedes, E. Villegas, R. Semexant Fils, A. Klein Tank, A. Martis, R. Warner, A. Joyette, W. Mills, L. Alexander, and B. Gleason (2002) Recent changes in climate extremes in the Caribbean region, *J. Geophys Res.*, 107(D21,4601), doi:10.1029/2002/JD002251.

Peterson T.C. and R.S. Vose (1997), An Overview of the Global Historical Climatology Network temperature database, *B. Am. Meteorol. Soc.*, 78, 2837-2849.

Pfister, C. (1999), *Wetternachhersage 500 Jahre Klimavariationen und Naturkatastrophen (1496-1995)*, published by P. Haupt, Bern. ISBN 325805696X, p 304.

Pfister, C. (2003), The lessons learned from the past natural catastrophes, Environmental documentation number 165, Forests. 23rd session of the working Party on Mountain Watershed Management, Davos, Ch, published by the Swiss Agency for the Environment, Forests and Landscape SAEFL, Bern, p. 204.

Pfister, C. (2009), Die "Katastrophenlücke" des 20. Jahrhunderts und der Verlust traditionellen Risikobewusstseins, *GAIA* 18/3, 239-246.

Pielke R.A. (2005), Land use and climate change, *Science*, 310(5754), 1625-1626.

Pirazzoli P.A. and A. Tomasin (2003), Recent near-surface wind changes in the Central Mediterranean and Adriatic areas, *Int. J. Climatol.*, 23, 963-973, doi:10.1002/joc.925.

Pryor S.C., R.J. Barthelmie, D.T. Young, E.S. Takle, R.W. Arritt, D. Flory, W.J. Gutowski Jr., A. Nunes, and J. Roads (2009), Wind speed trends over the contiguous United States, *J. Geophys. Res.*, 114(D14105), doi:10.1029/2008JD011416.

Ramanathan V., C. Chung, D. Kim, T. Bettge, L. Buja, J.T. Kiehl, W.M. Washington, Q. Fu, D.R. Sikka and M. Wild (2005), Atmospheric brown clouds: Impacts on South Asian climate and

hydrological cycle, PNAS 102(15), 5326-5333.

Ramanathan, V., P.J. Crutzen, J.T. Kiehl, and D. Rosenfeld (2001), Aerosols, Climate, and the Hydrological Cycle, *Science*, 294, 2119-2124.

Ramankutty N. and J.A. Foley (1998), Characterizing patterns of global land use: An analysis of global croplands data, *Global Biogeochemical cycles*, 12(5), 667-685, doi:10.1029/98GB02512.

Rayner N.A., D.E. Parker, E.B. Horton, C.K. Folland, L.V. Alexander, D.P. Rowell, E.C. Kent, and A. Kaplan (2003), Global analyses of sea surface temperature, sea ice, and night marine air temperature since the late nineteenth century, *J. Geophys. Res.*, 108, 4407, doi:10.1029/2002JD002670.

Robock A. (2000), Volcanic eruptions and climate, *Reviews of Geophys.*, 38(2), 191-219.

Roderick M.L., L.D. Rotstayn, G.D. Farquhar, and M.T. Hobbins (2007), On the attribution of changing pan evaporation, *Geophys. Res. Lett.* 34, L17403, doi:10.1029/2077GL031166.

Roeckner E., L. Bengtsson, and J. Feichter (1999), Transient climate change simulations with a coupled atmosphere-ocean GCM including the tropospheric sulphur cycle, *J. Climate*, 12, 3004-3032.

Roeckner E., G. Baeuml, L. Bonventura, R. Brokopf, M. Esch, M. Giorgetta, S. Hagemann, I. Kirchner, L. Kornblueh, E. Manzini, A. Rhodin, U. Schlese, U. Schulzweida, and A. Tompkins (2003), The atmospheric general circulation model ECHAM5. PART I: Model description, Report 349, Max-Planck-Institute für Meteorologie, available online at: http://www.mpimet.mpg.de/fileadmin/models/echam/mpi_report_349.pdf/.

Roeckner E., P. Stier, J. Feichter, S. Kloster, M. Esch, and I. Fischer-Bruns (2006), Impact of carbonaceous aerosol emissions on regional climate change, *Clim. Dyn.*, 27, 553-571.

Röthlisberger, G. (1991), *Chronik der Unwetterschäden in der Schweiz*, Eidgenössische Forschungsanstalt für Wald Schnee und Landschaft Birmensdorf.

Sato M., J.E. Hansen, M.P. McCormick, and J.B. Pollack(1993), Stratospheric Aerosol Optical Depths, 1850–1990, *J. Geophys. Res.*, 98, 22987-22994.

Schär C., P.L. Vidale, D. Lüthi, C. Frei, C. Häberli, M.A. Liniger, and C. Appenzeller (2004), The role of increasing temperature variability in European summer heatwaves, *Nature* 427, 332-336, doi:10.1038/nature02300.

Schmocker-Fackel P. and F. Naef (2010a), More frequent flooding? Changes in flood frequency in Switzerland since 1850. *J. Hydrology* 381, 1-8.

Schmocker-Fackel P. and F. Naef (2010b), Changes in flood frequencies in Switzerland since 1500. *Hydrology and Earth System Sciences*, 14, 1581-1594.

Shuttleworth, W.J, A. Serrat-Capdevila, M.L. Roderick and R.L. Scott (2009), On the theory relating changes in area-average and pan evaporation, *Q. J. R. Meteorol. Soc.* 135, 1230-1247, doi:10.1002/qj.434.

Smith T.M. and R.W. Reynolds (2005) A Global Merged Land–Air–Sea Surface Temperature Reconstruction Based on Historical Observations (1880–1997), *J. Climate*, 18, 2021-2036.

Sodemann, H., Wernli and C. Schwierz, 2009: Sources of water vapour contributing to the Elbe flood in August 2002-A tagging study in a mesoscale model. *Quart. J. Roy. Meteorol. Soc.*, 135

(638), 205-223.

Solanki S.K. and N.A. Krivova (2003), Can solar variability explain global warming since 1970? *J. Geophys. Res. (Space Physics)*, 108, 1200, doi: 10.1029/2002JA009753.

Stanhill G. and S. Cohen (2001), Global dimming: A review of the evidence for a widespread and significant reduction in global radiation, *Agric. For. Meteorol.*, 107, 255-278.

Stier P., J. Feichter, S. Kinne, S. Kloster, E. Vignati, J. Wilson, L. Ganzeveld, I. Tegen, M. Werner, Y. Balkanski, M. Schulz, O. Boucher, A. Minikin, and A. Petzold (2005), The aerosol-climate model ECHAM5-HAM, *Atmos. Chem. Phys.*, 5, 1125-1156.

Stier P., J. Feichter, E. Roeckner, S. Kloster, and M. Esch (2006a), The evolution of the global aerosol system in a transient climate simulation from 1860 to 2100, *Atmos. Chem. Phys.*, 6, 3059-3076.

Stier P., J. Feichter, S. Kloster, E. Vignati, and J. Wilson (2006b) Emission-induced non-linearities in the global aerosol system: Results from the ECHAM5-HAM aerosol-climate model, *J. Climate*, 19, 3845-3862.

Streets D.G., F. Yan, M. Chin, T. Diehl, N. Mahowald, M. Schultz, M. Wild, Y. Wu, and C. Yu (2009), Discerning human and natural signatures in regional aerosol trends, 1980-2006, *J. Geophys. Res.*, 114, D00D18.

Thompson D.W.J, J.J. Kennedy, J.M. Wallace, and P.D. Jones (2008), A large discontinuity in the mid-twentieth century in observed global-mean surface temperature, *Nature*, 453, 646-649.

Trenberth, K. E. (1997), The definition of El Nino, *Bull. Amer. Meteor. Soc.*, 78, 2771-2777.

Trenberth, K.E. (1999), Conceptual Framework for Changes of Extremes of the Hydrological Cycle with Climate Change, *Climatic Change*, 42, 327-339.

Trenberth, K.E. (2011), Changes in precipitation with climate change, *Clim. Res.*, in press, doi:10.3354/cr00953.

Trenberth K.E. and J.M. Caron (2000), The Southern Oscillation revisited: Sea level pressures, surface temperatures and precipitation, *J. Climate*, 13, 4358-4365.

Trenberth K.E. and A. Dai (2007), Effects of Mount Pinatubo volcanic eruption on the hydrological cycle as an analogue of geoengineering. *Geophys. Res. Lett.*, 34, L15702, doi:10.1029/2007GL030524.

Trenberth K.E., J.T. Fasullo, and K. Kiehl (2009), Earth's global energy budget, *Am. Meteor. Soc.*, 311-323, doi:10.1175/2008BAMS2634.1.

Trenberth K.E. and C.J. Guillemot (1998), Evaluation of the atmospheric moisture and hydrological cycle in the NCEP/NCAR reanalysis, *Clim. Dyn.*, 14, 213-231.

Trenberth K.E., L. Smith, T. Qian, A. Dai and J. Fasullo (2007), Estimates of the global water budget and its annual cycle using observational and modelled data. *J. Hydrometeor.*, 8, 758-769.

Troccoli A., K. Muller, P. Coppin, R. Davy, C. Russel and A.L. Hirsch (2011), Long term wind trends over Australia. *J. Climate.*, 25, 170-183, doi: 10.1175/2011JCLI4198.1.

Tuller S.E. (2004), Measured wind speed trends on the west coast of Canada, *Int. J. Climatol.*, 24, 1359-1374, doi:10.1002/joc.1073.

- Twomey S.A. (1977), The influence of pollution on the shortwave albedo of clouds, *J. Atmos. Sci.*, 34, 1149-1152.
- Van der Ent R.J., H.H.G. Savenije, B. Schaefli, and S.C. Steele-Dunner(2010), Origin and fate of atmospheric moisture over continents, *Water Resour. Re.*, 46, W09525, doi:10.1029/2010WR009127.
- Vautard R., J.Cattiaux, P. Yiou, J. N. Thepaut and P. Ciais (2010), Northern Hemisphere atmospheric stilling partly attributed to an increase in surface roughness, *Nature Geoscience*, 3, 756-761, doi:10.1038/ngeo979.
- Wang C., S.-P. Xie, and J. A. Carton (2004), A global survey of ocean atmosphere interaction and climate variability, in *Earth's climate : The ocean-atmosphere interaction* , *Geophys. Monogr. Ser.*, 147, edited by C. Wang et al., 1-19, AGU, Washington, D. C.
- Wanner H., C. Beck, R. Brazdil, C. Casty, M. Deutsch, R. Glaser, J. Jacobeit, J. Luterbacher, C. Pfister, S. Pohl, K. Sturm, P.C. Werner and E. Xoplaki (2004), Dynamic and socioeconomic aspects of historical floods in Central Europe, *Erdkunde* 58, 1-16.
- Wentz F.J., L. Ricciardulli, K. Hilburn, and C. Mears (2007), How much more rain will global warming bring? *Science*, 317, 233-235, doi: 10.1126/science.1140746.
- Werth D. and R. Avissar (2002), The local and global effects of Amazon deforestation, *J. Geophys. Res.*, 107, D20, 8087, doi:10.1029/2001JD000717.
- Wetter, O., C. Pfister, R. Weingartner, J. Luterbacher, T. Reist, and J. Trösch (2011), The largest floods in the High Rhine basin since 1268 assessed from documentary and instrumental evidence, *Hydrology Sciences Journal* 56, 733-758.
- Whitaker, J. S., and T.M. Hamill (2002), Ensemble data assimilation without perturbed observations. *Mon. Wea. Rev.*, 130, 1913-1924.
- Wild M. (2009), Global dimming and brightening: A review, *J. Geophys. Res.*, 114, D00D16.
- Wild M., J. Grieser, J., and C. Schär (2008), Combined surface solar brightening and increasing greenhouse effect support recent intensification of the global land-based hydrological cycle, *Geophys. Res. Lett.*, 35, 17706, doi:10.1029/2008GL034842.
- Wild M. and B.G. Liepert (2010), The Earth radiation balance as driver of the global hydrological cycle, *Environ. Res. Lett.*, 5, 025203, doi:10.1088/1748-9326/5/2/025203.
- Wild M., A. Ohmura, and K. Makowski (2007), Impact of global dimming and brightening on global warming, *Geophys. Res. Lett.*, 34, 04702, doi:10.1029/2006GL028031.
- Wild M., H. Gilgen, A. Roesch, A. Ohmura, C.N. Long, E.G. Dutton, B. Forgan, A. Kallis, V. Russak, and A. Tsvetkov (2005), From Dimming to Brightening: Decadal Changes in Solar Radiation at Earth's surface, *Science*, 308, 847-850.
- Xu M., C.P. Chang, C. Fu, Y. Qi, A. Robock, D. Robinson and H.M. Zhang (2006), Steady decline of east Asian monsoon winds, 1969-2000: Evidence from direct ground measurements of wind speed, *J Geophys. Res.*, 111(D24111), doi:10.1029/2006JD007337.
- Yu L. and R.A. Weller (2007), Objectively analysed air-sea heat fluxes for the global ice-free oceans (1981-2005), *Bull Am. Meteor. Soc.*, 88, 527-539, doi:10.1175/bams-88-4-527.
- Zvervaec I.I. (2006), Seasonally varying modes in long-term variability of European precipitation

during the 20th century, J. Geophys. Res., 111, D21116, doi:10.1029/2005JD006824.

Zveryaev, I.I. and R.P. Allan (2010), Summertime precipitation variability over Europe and its links to atmospheric dynamics and evaporation, Journal of Geophysical Research 115, D12102, doi:10.1029/2008JD011213.

Curriculum Vitae

Adeline Bichet, Kalkbreitestrasse 43, 8003 Zürich, Switzerland;
born on 27 September 1983 in Besancon, France; French citizen.

Education and professional training

- | | |
|-----------|---|
| 2008-2012 | PhD student at the institute for Atmospheric and Climate Science, ETH Zurich (Switzerland). Group: Climate and Water Cycle, Prof. Dr. C. Schär.
PhD defence: 05 April 2012 |
| 2006-2008 | Master student at the Free University, Amsterdam (Netherlands) in Paleoclimatology and Geo-Ecosystem. Graduation: Master of Science |
| 2004-2006 | Bachelor student at Kingston University, London (UK) in Earth System Sciences. Graduation: Bachelor of Science with Honours, lower second class. |
| 2002-2004 | Student at the University of Perpignan (France) in Biology and Environmental Engineering. Graduation: Technical and Academic Diploma in Sciences. |
| 1998-2001 | High school education at Lycée Louis Pasteur, Besancon (France), specialized in Earth Sciences. Graduation: Scientific Baccalaureate, distinction “Bien”. |

International conferences and Workshops

AAAR 30th Annual Conference, 2011, Orlando, USA; XXV IUGG General Assembly, 2011, Melbourne, Australia; 8th EGU General Assembly, 2011, Vienna, Austria; 9th international NCCR Climate Summer School, 2010, Grindelwald, Switzerland; 7th EGU General Assembly, 2010, Vienna, Austria; 8th international NCCR Climate Summer School, 2009, Grindelwald, Switzerland; 6th EGU General Assembly, 2009, Vienna, Austria ECMWF Computer User Training course, Reading, UK.